INVESTIGATION OF THE EFFECT OF DISSIMILAR CHANNEL ANGULAR PRESSING METHOD TO THE MECHANICAL AND MICROSTUCTURAL PROPERTIES OF 6061 ALUMINUM ALLOY SHEETS

A THESIS SUBMITTED TO
THE GRADUATE SCHOOL OF NATURAL AND APPLIED SCIENCES
OF
MIDDLE EAST TECHNICAL UNIVERSITY

BY

ALP AYKUT KİBAR

IN PARTIAL FULFILLMENT OF THE REQUIREMENTS
FOR
THE DEGREE OF MASTER OF SCIENCE
IN
METALLURGICAL AND MATERIALS ENGINEERING

JULY 2010

Approval of the thesis:

INVESTIGATION OF THE EFFECT OF DISSIMILAR CHANNEL ANGULAR PRESSING METHOD TO THE MECHANICAL AND MICROSTUCTURAL PROPERTIES OF 6061 ALUMINUM ALLOY SHEETS

submitted by **ALP AYKUT KİBAR** in partial fulfillment of the requirements for the degree of **Master of Science in Metallurgical and Materials Engineering Department, Middle East Technical University** by

Prof. Dr. Canan Özgen _____
Dean, Graduate School of Natural and Applied Sciences

Prof. Dr. Tayfur Öztürk _____
Head of Department, Metallurgical and Materials Eng.

Prof. Dr. C. Hakan Gür _____
Supervisor, Metallurgical and Materials Eng. Dept., METU

Prof. Dr. Bilgehan Ögel _____
Co-Supervisor, Metallurgical and Materials Eng. Dept., METU

Examining Committee Members

Prof. Dr. Tayfur Öztürk _____
Metallurgical and Materials Eng. Dept., METU

Prof. Dr. C. Hakan Gür _____
Metallurgical and Materials Eng. Dept., METU

Prof. Dr. Macit Özenbaş _____
Metallurgical and Materials Eng. Dept., METU

Prof. Dr. Rıza Gürbüz _____
Metallurgical and Materials Eng. Dept., METU

Assist. Prof. Dr. Besim Baranoğlu _____
Manufacturing Eng. Dept., Atılım University

Date: 02 /07/2010

I hereby declare that all information in this document has been obtained and presented in accordance with academic rules and ethical conduct. I also declare that, as required by these rules and conduct, I have fully cited and referenced all material and results that are not original to this work.

Name, Last name: Alp Aykut KİBAR

Signature :

ABSTRACT

INVESTIGATION OF THE EFFECT OF DISSIMILAR CHANNEL ANGULAR PRESSING METHOD TO THE MECHANICAL AND MICROSTUCTURAL PROPERTIES OF 6061 ALUMINUM ALLOY SHEETS

Kibar, Alp Aykut

M.Sc.,Department of Metallurgical and Materials Engineering

Supervisor : Prof. Dr. C. Hakan Gür

Co-supervisor: Prof. Dr. Bilgehan Ögel

July 2010, 121 Pages

Dissimilar Channel Angular Pressing (DCAP) method is an effective Severe Plastic Deformation (SPD) technique to improve the mechanical properties of sheets or strips by producing ultrafine grains. The aim of this study is to investigate the evolution of the microstructure and the improvement in mechanical properties of 6061 Al-alloy strips deformed by DCAP up to 5 passes. Mechanical properties such as hardness and strength have been observed to increase up to a certain strain level depending on the microstructural evolution. These microstructural changes were investigated by the characterization studies of XRD, SEM and TEM analysis of the DCAPed samples indicating the subgrain formation, changes in the dislocation density and dislocation behaviors.

Keywords: Severe Plastic Deformation, DCAP, Ultra fine grains, 6061 Al-alloy

ÖZ

DEĞİŞİK KANALLI AÇISAL PRESLEME YÖNTEMİNİN 6061 ALUMİNYUM ALAŞIMI PLAKALARIN MEKANİK VE İÇ YAPISAL ÖZELLİKLERİNE ETKİLERİNİN İNCELENMESİ

Kibar, Alp Aykut

Yüksek Lisans, Metalurji ve Malzeme Mühendisliği Bölümü

Tez Yöneticisi : Prof. Dr. C. Hakan Gür

Ortak Tez Yöneticisi : Prof. Dr. Bilgehan Ögel

Temmuz 2010, 121 Sayfa

Değişik Kanallı Açısal Presleme (DKAP) yöntemi plaka veya şerit malzemelerde çok ince taneli yapı oluşturulmasıyla üstün mekanik özellikler sağlayan bir Aşırı Plastik Deformasyon tekniğidir. Bu çalışmanın amacı, DKAP yöntemi ile 5 pasoya kadar deforme edilmiş 6061 Al alaşımı şeritlerin mekanik özelliklerindeki iyileşmenin ve mikroyapısal değişimlerin incelenmesidir. Sertlik ve mukavemet gibi mekanik özelliklerde belli bir gerinim miktarına kadar mikroyapısal değişimlere bağlı olarak iyileşme gözlenmiştir. Bu mikroyapısal değişimler DKAP işlemi görmüş numunelerin X-ışını kırınımı, tarama ve geçirim electron mikroskopları (SEM ve TEM) analizleri ile karakterize edilmiş ve tanecik oluşumu, dislokasyon yoğunluğunda ve davranışlarında değişimler gözlenmiştir.

Anahtar Kelimeler: Aşırı plastic deformasyon, DKAP, çok ince taneli yapı, 6061 Al alaşımı

To my family

ACKNOWLEDGEMENTS

I would like to express my deepest gratitude to my supervisor Prof. Dr. C. Hakan Gür and co-supervisor Prof. Dr. Bilgehan Ögel for their guidance, criticism and continuous support throughout the thesis.

I am grateful to Evren Tan for his endless guidance and support throughout my thesis study and Göktürk Emre Uzunçakmak for his helps during my starting studies.

I wish to thank Doç. Dr. Sunullah Özbek, Doç. Dr. Tarık Baykara and Doç. Dr. Volkan Günay for providing opportunities in TÜBİTAK MAM for TEM analysis studies and my special thanks go to Dr. Özgür Duygulu for his efforts during TEM analysis of this study and critical contribution to this research.

I would also like to thank Doç. Dr. Özgül Keleş and Sedat İhvan by their supports during the optical investigation of the samples.

For their sincere helps; Dr. İbrahim Çam during resistivity measurements, Göksu Gürer during Mechanical Tests, Murat Tolga Ertürk during optical investigation of the samples, Necmi Avcı and Onur Rauf Bingol during XRD analysis and Yusuf Yıldırım during metallographic preparations are gratefully acknowledged.

I am grateful to my employer TÜBİTAK, to my superiors N. Nur Tümok and Olay Salcan and to my colleagues for providing convenience during my M.S. studies.

Furthermore, I would like to thank to my friends Doğukan Doğan, Emre Taşkıran, Aytaç Şengül, Yeşim Kümbet, Meltem Yılmaz, Fatih Sinan Esen, Seyit Tunç, Mert Akkuş, Göksu Gürer, Sadık Bayramoğlu, Serdar Savaş, Murat Tolga Ertürk and others for their moral support and friendship.

Finally, I would like to dedicate this study to my sweet niece Deniz, to my parents Ruhat Kibar and Mehmet Sadık Kibar, to my brothers Arif Alperen Kibar, Mustafa Alptekin Kibar and his wife Sibel Kibar for supporting me throughout all my life.

This study was supported by the TÜBİTAK project 105M174.

TABLE OF CONTENTS

LIST OF TABLES

TABLES

LIST OF FIGURES

FIGURES

CHAPTER I

INTRODUCTION

1.1 General

Materials are desired to have enhanced mechanical properties for practical and industrial applications. Many strengthening techniques are tried and used in the industry throughout the history. Many of these techniques are based on the mechanism of microstructural refinement by plastic deformation. Conventional metal working techniques such as rolling, extrusion or drawing take a significant part in the industry for strengthening of metals. However, these techniques may not be sufficient every time for producing materials with desired properties and/or geometry. Therefore new processing techniques are developed to overcome these problems called Severe Plastic Deformation (SPD) techniques. The most important return of this technique is the ability of producing Ultra Fine Grained (UFG) microstructures. Ultra-Fine Grained materials are defined as polycrystals having very small grain sizes of less than ~1μm with equiaxed microstructures having high fraction of grain boundaries with high misorientation angles and high dislocation density [1]. UFG structure brings many advantages to the materials in terms of mechanical properties such as; high strength and hardness, long fatigue life and good ductility.

Severe Plastic Deformation methods are firstly developed in the early 1990s and many laboratory studies are made about them so far to achieve industrial applications of those techniques. There are many different SPD techniques developed for different purposes. Equal Channel Angular Pressing (ECAP) technique is one of these popular SPD methods to obtain UFG structured materials of billet or rod shape without changing the initial geometry. However, ECAP method has some

disadvantages of being a discontinuous process and impossibilities in applicability to sheet products. Therefore, a new deformation technique is developed for continuous production of UFG structured sheet or strip products called Dissimilar Channel Angular Pressing (DCAP) method. Being a continuous process brings many advantages for industrial processes to DCAP method over other SPD techniques and conventional cold rolling processes. For example; strengthening of the thin products obtained in the final thickness by continuous slab casting process would be possible. In this scope, DCAP technique shows a great potential for industrial processes especially for some metals like aluminum alloys which are promising structural materials for many industrial fields.

1.2 Aim of the Study

A master thesis study is held by Göktürk Emre UZUNÇAKMAK [2] which is entitled as "Design and production of a dissimilar channel angular pressing system to obtain high strength aluminum alloy sheets". This study is a continuation of that thesis in terms of development of the mechanical properties of 6061 Al alloy sheets by DCAP method. Aim of this thesis is described of two main parts which can be considered as theoretical understanding of the mechanism behind DCAP method by generally considering SPD techniques and the evaluation of experimental results about DCAP studies. In this context; aim of the study can be listed as;

Theoretical Part:

- Representation of the descriptions and explanations about DCAP technique and other SPD techniques
- Theoretical understanding of the evolution of UFG structure and grain refinement mechanism during DCAP technique
- Theoretical understanding of the mechanical strengthening mechanism by the formation of UFG structure during DCAP technique by literature studies

- Make a comparison of SPD methods mainly DCAP method with conventional deformation techniques in terms of grain refinement and strengthening mechanisms

Experimental Part:

- Severe Plastic Deformation of 6061 Al alloy by DCAP method
- Observing the evolution of UFG structure of 6061 Al alloy after DCAP processing by evaluating the X-Ray data and microstructural investigation of optical and electron microscopes (SEM and TEM)
- Observing the changes in mechanical and physical properties of 6061 Al alloy after DCAP process by different tests and analyses
- Comparing the mechanical properties for different processing parameters like processing route
- Comparing the mechanical properties for different post annealing operations
- Comparing the results obtained by experiments with literature data

CHAPTER II

THEORY AND LITERATURE REVIEW

2.1 Severe Plastic Deformation

It is known that grain size refinement brings many advantages to many properties of the materials. Conventionally many metal working techniques have been used in refining the grain size of the metals such as; cold rolling, drawing, extrusion etc. However, these techniques are not sufficient for producing materials having submicrometer grain sizes due to their insufficient straining capacity [1] and inability of producing substructures having high angles of misorientations. Consequently, new techniques were required to overcome these problems and produce submicrometer grain sizes so called Ultra-Fine Grained (UFG) materials. Ultra-Fine Grained materials are defined as polycrystals having very small grain sizes of less than ~1μm with equiaxed microstructures having high fraction of grain boundaries with high misorientation angles and high dislocation density [1]. Materials having grain sizes of about 100 nm or smaller are described as nanocrystalline materials [3]. Zhu, Lowe and Langdon [4] suggested two basic approaches which are developed for the synthesis of UFG or nanocrystalline materials as; 'bottom-up' and 'top-down' approaches. 'Bottom up' approach is based on the assembling from individual atoms or from nanoscale building blocks such as nano-particles including inert gas condensation, electrodeposition, chemical and physical deposition whereas 'top down' approach is based on the grain refinement process of coarse grained materials [4].

In this manner; Valiev and his co-workers firstly developed and investigated UFG and Nanostructured materials by using methods called Severe Plastic Deformation (SPD) methods in the early 1990s [5]. Severe Plastic Deformation is a process of producing UFG materials having grain sizes of 100-1000 nm including subgrains

smaller than 100 nm satisfying the nanostructured material term by imposing very large strains on the material.

Many research and development studies were conducted about severe plastic deformation subject in recent years and many severe plastic deformation techniques are developed such as; High Pressure Torsion (HPT), Accumulative Roll-Bonding (ARB), Multiple Forging, Equal Channel Angular Pressing (ECAP), Dissimilar Channel Angular Pressing (DCAP) etc. Some of these SPD techniques are passing through the way from laboratory-scale research to commercial production of UFG materials nowadays [6].

There are some requirements of severe plastic deformation methods that should be accounted in order to produce UFG or nanostructured materials [5], these are;

- Producing UFG structures with grain boundaries having large misorientation angles.
- Formation of uniform nanostructures to provide stable properties throughout the sample.
- Deformed samples should not include any mechanical damage or cracks.

The reason behind why conventional deformation mechanisms are not able to produce nanostructures in bulk samples is that they cannot meet all these requirements [5].

2.2 Grain Refinement by SPD and UFG Materials

Formation of Ultra Fine Grain structures or even nanostructures is possible by severe plastic deformation methods. Type of these structures and grain sizes depends on many parameters such as method itself, processing parameters, total accumulated strain exerted, material type and composition, initial microstructure, temperature and pressure, etc. Depending on these factors, attaining grain sizes of even 100 nm is possible by SPD processing. The mean grain size typically saturates about 300 - 400 nm in case of ECAP [6].

Cell structures are characterized by the size of the grains. Grain interiors can be free from dislocations or consisting of cells shown in Figure 2.1 (a) and (d) respectively [7]. The study of Liu, Roven, Yu, Werenskiold [7] mentioned that grains with 100 nm size have sharp grain boundaries and the grain interiors are free of dislocations, subgrains or dislocation cells (Figure 2.1(a)). Their boundaries are described as in equilibrium state and are high-angle grain boundaries (HAGBs). However, dislocation cell structures are observed in larger grains with ~400 nm size as seen in Figure 2.1 (c) and the misorientation of these non-equilibrium boundaries are said to increase with plastic straining, and eventually becomes large enough to transform through low-angle grain boundaries (LAGBs) to HAGBs [7]. In brief grain refinement is represented as formation of dislocation cell structures and subgrain boundaries with low misorientation and with deformation straining; subgrain boundaries transform into LAGBs and finally HAGBs. Poor and non-homogeneous diffraction contrast of the inside grains by TEM analysis indicates that a high level of internal stresses and elastic distortions of the crystal lattice attributed to long range stresses from non-equilibrium grain boundaries [5].

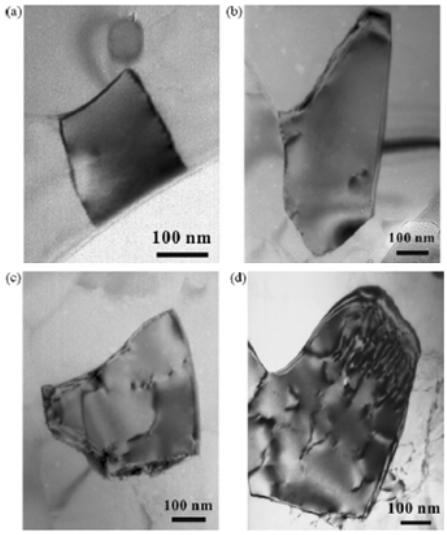

Figure 2.1: TEM images of 2 ECAP passed alloy [7] (a) Dislocation free grain with sharp boundaries (b) Grain with non-equilibrium boundaries (c) Dislocation cell structures inside a larger grain (d) large grain with high dislocation density

Valiev et al. [5] stated that the main idea behind the model of the evolution of the defect structure during SPD is based on transformation of a cellular structure to a granular one and occurring of partial annihilation of dislocations of different signs at the cell boundaries as shown in Figure 2.2. They conclude that remaining of excess dislocations of single sign at the cell boundaries result in misorientation increase by the dislocations with Burgers vectors perpendicular to the boundary and causing the transformation to a granular structure with increasing density of dislocations.

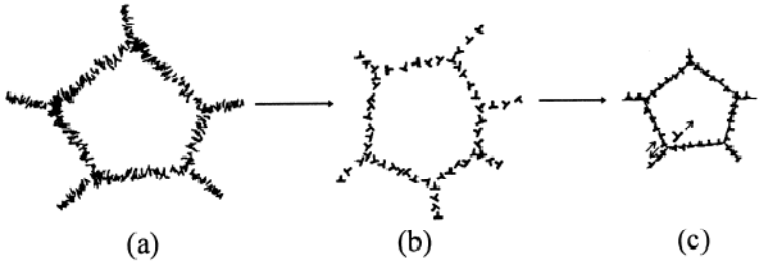

Figure 2.2: Model of dislocation structure evolution at different stages during SPD [5]

According to Valiev et al. [5] the high internal stresses and elastic strains near grain boundaries while lower lattice dislocation density and lower elastic strains inside the grains and distortions of the crystal lattice is the common feature for nanostructured materials processed by SPD. By their HREM observations, they conclude that these grain boundaries are not perfect by their structure since they contain many defects such as steps, facets and dislocations leading to elastic distortions near grain boundaries and this testifies that those are non-equilibrium boundaries which are the sources of the internal stresses.

Kozlov, Zhdanov and Koneva [8] investigated the deformation mechanisms observed in nanosized grains with different sizes remarking the grain boundary processes. They mentioned that; at grain sizes in the neighborhood of 10 nm, both diffusive and dislocation types of grain boundary shear is taking place whereas for grain sizes larger than 1μm, dislocation mechanisms of deformation is mentioned. Finally at

grain sizes between 1000-10 nm, it is told that an interaction between the grain boundary shear and dislocation glide is taking place as shown by the Figure 2.3 which is representing the grain boundary sliding activating the intragranular slip, dislocation glide initiating the grain boundary migration and climb of dislocations triggering the formation of dislocation walls.

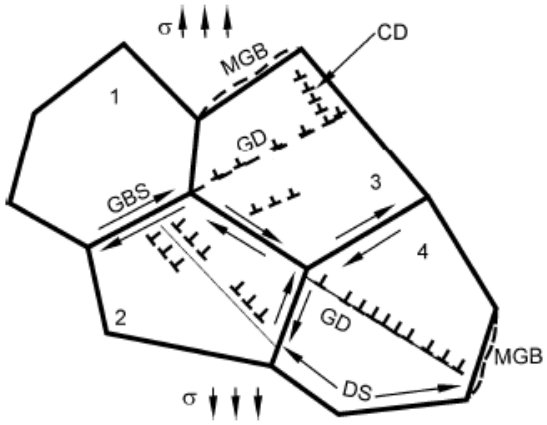

Figure 2.3: Schematic representation of grain boundary sliding accommodated by intragranular dislocation processes [8] (GD: Glide of Dislocations, CD: Climb of Dislocations, MGB: Migrating Grain Boundary, DS: Dislocation Sink, GBS: Grain Boundary Sliding)

Grain refinement mechanisms particularly in Al alloys by Equal Channel Angular Pressing (ECAP) and Dissimilar Channel Angular Pressing (DCAP) methods will be discussed in section 2.5.

2.3 Severe Plastic Deformation Methods

Several types of Severe Plastic Deformation methods are developed to attain ultra-fine grained structure for metallic materials. Most common examples of these methods are going to be discussed in this part:

2.3.1 High Pressure Torsion (HPT) Process

High Pressure Torsion (HPT) is one of the most popular techniques of SPD methods. In this technique, disc-shaped samples having typically 10 to 20 mm diameter and 0.2 to 0.5 mm thickness are compressed between a fixed and a rotating anvil under high pressures as shown in Figure 2.4. It is possible to obtain nanostructures of about 100 nm or even smaller grains with high-angle boundaries by imparting very high shear strains on the sample through the friction between the anvil and the surface of the sample without changing the initial shape [6].

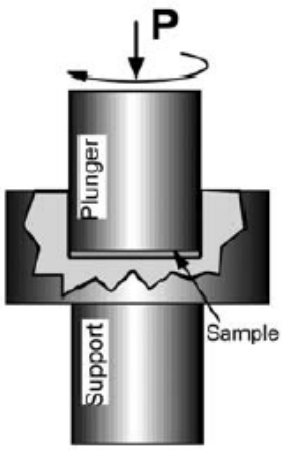

Figure 2.4: Schematic illustration of HPT Process [6]

2.3.2 Accumulative Roll Bonding (ARB) Process

Accumulative Roll Bonding (ARB) is a continuous process that two sheets of the same thicknesses are simultaneously rolled as shown in Figure 2.5 and the sheets are bonded together meanwhile the total thickness is reduced to the original sheet thickness with one pass. With similar several passes of combined rolling; significant amount of grain refinement is possible. The final microstructure is non-uniform through the thickness due to the characteristics of the process.

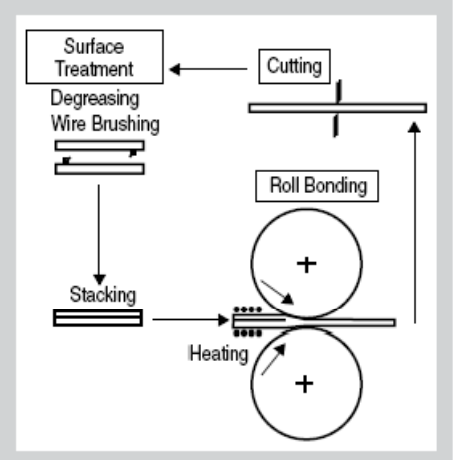

Figure 2.5: Schematic illustration of Accumulative Roll Bonding Process [6]

2.3.3 Con Shearing Process

It is a continuous process of which a sheet material is fed through a die similar to the ECAP die by a large center roll, small satellite rolls and a guide shoe as shown in Figure 2.6. The thickness of the sheet material does not change during the deformation process that is why the process can be repeated several times enabling to impose high strains.

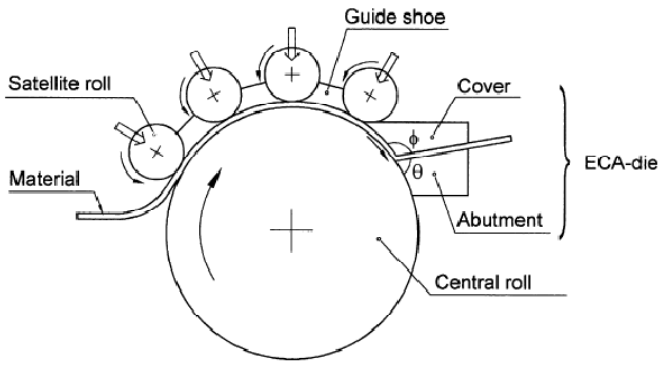

Figure 2.6: Schematic illustration of the con shearing process [9]

2.3.4 Repetitive Corrugation and Straightening (RCS) Process

It is another type of continuous processes that the work piece undergoes repetitive bending and straightening as shown in Figure 2.7 where the initial shape is maintained after deformation process. It relies upon combinations of shear and bending that are imposed under constraining pressure in specially designed rolling surfaces [6].

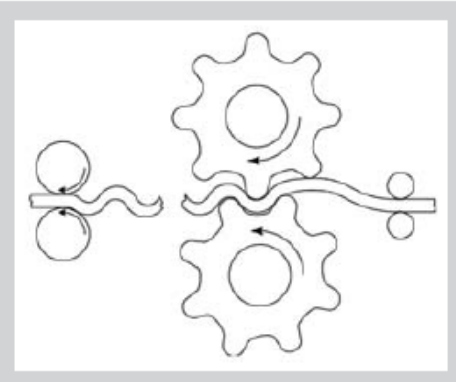

Figure 2.7: Schematic illustration of the RCS process [9]

2.3.5 ECAP Conform Process

This process is a combination of continuous extrusion of wire products and the ECAP process. It is based on the principle of pushing the work-piece into a die by generating a frictional force by a rotating shaft in the center containing a groove where the work-piece is fed into as shown in Figure 2.8 [1]. At the end of the groove, a stationary ECAP like die is constrained that the work-piece passes through the angular region enabling a shear deformation.

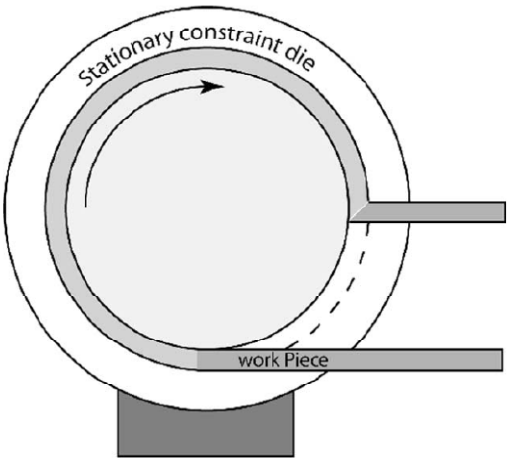

Figure 2.8: Schematic illustration of the ECAP Conform process [1]

2.3.6 Equal Channel Angular Pressing (ECAP) Process

2.3.6.1 Principles of ECAP Process

Equal Channel Angular Pressing (ECAP) Method is the most studied Severe Plastic Deformation technique in the literature which is firstly introduced by Segal and his co-workers in the early 1980s [1]. Valiev and his co-workers firstly applied ECAP as an SPD technique for producing nanostructures [6]. Simple shear is the dominant mechanism of ECAP to obtain high strains inside the material. Primary objective of the ECAP process is to obtain desired properties by producing UFG structure and special textures. The properties and the microstructural features obtained by ECAP will be discussed in subsequent chapters.

The basic principle of the ECAP method is the pressing of the sample in the form of a rod or a bar through a channel which is bent through an abrupt angle inside a die as shown in Figure 2.9.

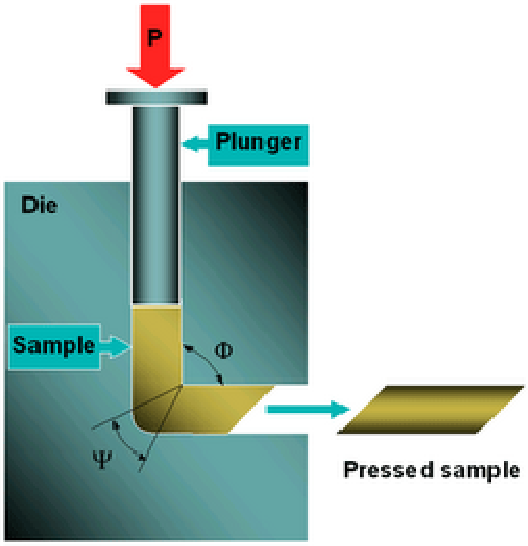

Figure 2.9: Schematic illustration of the ECAP process

Illustration of the relationship between the theoretical shear and the slip planes with resolved shear stresses for a slip system in the single crystal is shown in Figure 2.10 in X-Y-Z coordinates where the pressing is in the -Z direction [10]. The theoretical shear plane lies at 45° to the X-direction just at the intersection of two channels whereas the slip occurs at the most favorite slip systems for that type of crystal.

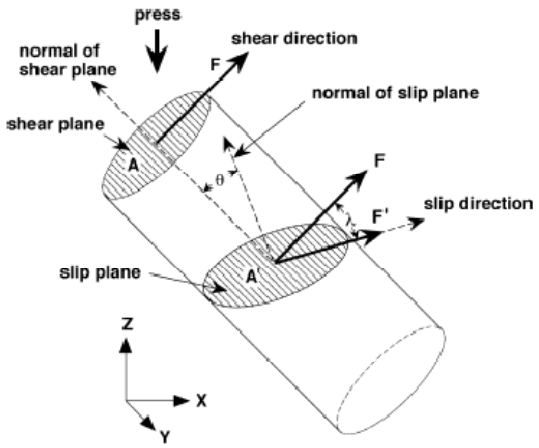

Figure 2.10: Illustration of the relationship between theoretical shear and slip planes [10]

Segal [11] suggested an equation for ECAP to calculate the equivalent shear strain by;

$$\gamma_{xy} = 2Ncot\frac{\phi}{2} \quad (2.1)$$

Where γ_{xy} is the equivalent shear strain, N is the number of ECAP passes and Φ is the die channel angle of the intersecting channels as shown in Figure 2.9.

This equation can be transformed into effective strain formulation of Equation 2.3 based on von-Mises criterion of Equation 2.2 and assuming γ_{xy}shear component is dominant and all of the normal strain components are negligible.

$$\varepsilon_{eff} = \left[\frac{2}{3}\left(\varepsilon_x^2 + \varepsilon_y^2 + \varepsilon_z^2 + \frac{\gamma_{xy}^2+\gamma_{yz}^2+\gamma_{xz}^2}{2}\right)\right]^{0.5} \quad (2.2)$$

$$\varepsilon_{eff} = \frac{1}{\sqrt{3}}\gamma_{xy} = \frac{2N}{\sqrt{3}}cot\frac{\phi}{2} \quad (2.3)$$

Where ε_x, ε_y, ε_z, are the normal strain components and ε_{eff} is the total equivalent strain.

It is assumed in this equation that the die corner curvature (Ψ) angle is 0. Iwahashi et al. [12] modified this equation including the effect of this angle and number of passes as;

$$\varepsilon_N = \frac{N}{\sqrt{3}}\left[2\cot\left(\frac{\phi}{2}+\frac{\psi}{2}\right) + \psi\,\mathrm{cosec}\left(\frac{\phi}{2}+\frac{\psi}{2}\right)\right] \quad (2.4)$$

where Ψ is the die corner curvature angle.

One of the most important principles in ECAP is that the cross-sectional area does not change after ECAP process as many other SPD techniques. This provides the sample can be pressed repetitively several times to obtain very high strains. Simply, with increasing number of ECAP passes, the strain accumulated in the material can be increased.

2.3.6.2 ECAP Routes:

Easy sliding of the grains accompanied by grain rearrangement along the shear plane and shear direction is known to be the main reason of grain deformation [11]. This grain rearrangement, the degree of deformation homogeneity and the types of textures formed depends on the character of the deformation. Therefore, different types of deformation routes are developed for ECAP. Mainly, there are four different ECAP routes called; route A, route B_A, route B_C and route C as shown in Figure 2.11. In route A; the sample is pressed in the same route within the consequent passes. The sample is rotated by 90° in alternative directions between consecutive passes in route B_A, whereas the sample is rotated in the same direction by 90° within consequent passes in route B_C. In route C; the sample is rotated by 180° between the passes.

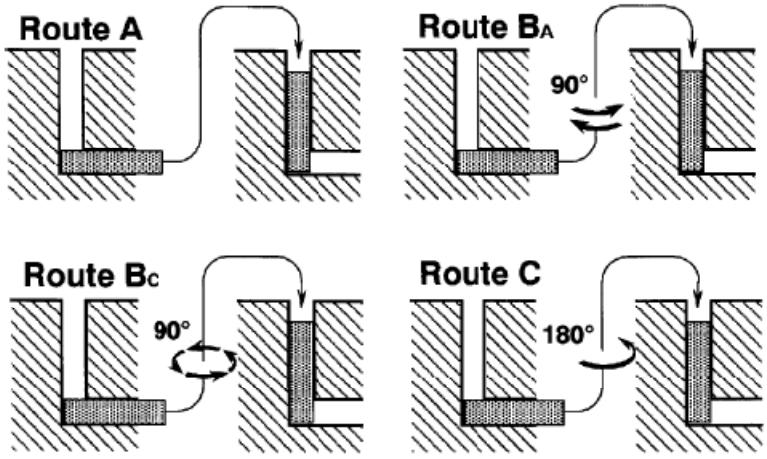

Figure 2.11: The four main processing routes in ECAP [1]

These routes have an important effect on refinement of microstructure and texture evolution. According to Valiev et al. [5] a change in a theoretical spherical cell within the billet body occurs at the intersection of channels differently by these routes. At the first pass, the cell takes an ellipsoidal shape due to pure shear deformation. It is discussed that there occurs an elongation of the ellipsoidal shape in

route A whereas recovery of the spherical shape occurs in route C as shown in Figure 2.11. Finite Element Modeling studies shows that [13] route B_C is the most effective route for deformation homogeneity after many ECAP passes (at the number multiples of four due to the characteristics of the route B_C) meaning that it is the most favorable route in producing UFG materials having homogeneous microstructure. Also it is known that route A is the most inhomogeneous deformation route for ECAP. It is suggested by Segal et al. [11] that a considerable permanent rotation of grains and subgrains occurs as they are deformed back and forth in route C that provides a strong texture formation by rearrangement of crystallographic systems.

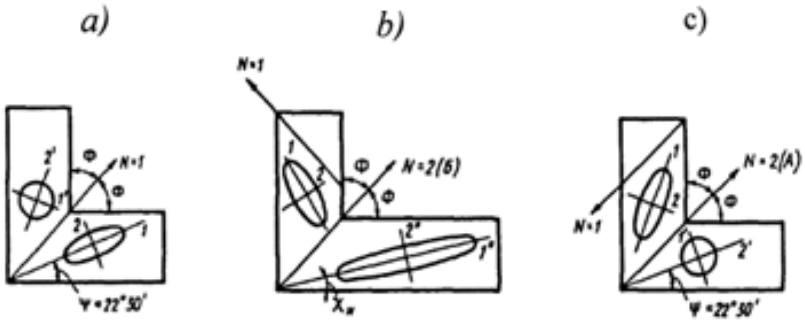

Figure 2.11: Evolution of the spherical cell (a) with first pass and subsequent passes with (b) route A (c) route C [5]

2.3.6.3 Advantages of ECAP Process:

Equal Channel Angular Pressing is an attractive processing method for industrial processes besides the scientific researches. Segal [11], Valiev and Langdon [1] suggested the reasons of this concern as;

- Uniform structure and properties can be developed for many different materials.

- An extremely large total effective deformation can be obtained with multiple passing without changing the billet shape.
- Special textures and structures can be created by controlling the parameters of the process.
- It is relatively simple procedure that is easily performed on a wide range of alloys with inexpensive and available equipment.
- Relatively low pressures and loads are sufficient for extrusion.

2.3.7 Dissimilar Channel Angular Pressing (DCAP) Process

It is discussed in the previous part that producing UFG materials with desired physical and mechanical properties is possible with ECAP process. Industrial applications require continuous processes for massive production of sheet materials. Rolling has been used for producing sheet materials from cast slabs by reducing the thickness by 80-90% [14] through repeated rolling operations which would not be so cost effective. Due to this high production costs, thin slab casting for many materials especially steel and aluminum products is developed to obtain thin sheets of desired thickness. However, it is not possible to obtain desired mechanical and physical properties in thin slab casting process because reduction in thickness by further rolling is limited or impossible anymore. Therefore, it is required to develop a new technique to enhance the mechanical and physical properties by controlling the microstructure without changing the geometry of the material such as ECAP. As a result, a new continuous technique is developed by Lee et al. [14] based on a rolling facility combined with the principles of ECAP [1] called continuous confined strip shearing (C2S2) or Equal Channel Angular Rolling (ECAR). Further FEM studies show that the inlet and outlet channels of the ECAP like die is required to be dissimilar to each other in order to be an effective process which will be discussed later in detail. Because of this characteristic of the method, this technique is frequently called as Dissimilar Channel Angular Pressing (DCAP) method. DCAP process will particularly be discussed in the next part.

2.4 DCAP

2.4.1 Principles of DCAP Method

Dissimilar Channel Angular Pressing (DCAP) method is a Severe Plastic Deformation Technique to obtain desired mechanical and physical properties by producing UFG structure for metals in the form of a sheet or strip. The technique is developed by Lee et al. [14] by modifying the ECAP technique. Thin metal strip or sheet is fed through the feeding rolls into the inlet channel which have a slightly thinner cross-section than the material thickness in order to prevent material to escape from the roll gap, then the material flows into the forming zone where the inlet and the outlet channels intersects at a specific angle. The material then flows into the outlet channel which has the original thickness of the sheet allowing the sheet metal recovers its initial thickness and leaves the DCAP die with its original shape. Recovery of the thickness allows multiple passages providing the continuous process. Figure 2.12 shows the illustration of the DCAP process with an initial strip thickness of 1.55 mm, inlet channel thickness of 1.45 mm and outlet channel thickness of 1.55 mm, an oblique angle of ~120° and 0° of curvature angle from the study of Lee et al. [14].

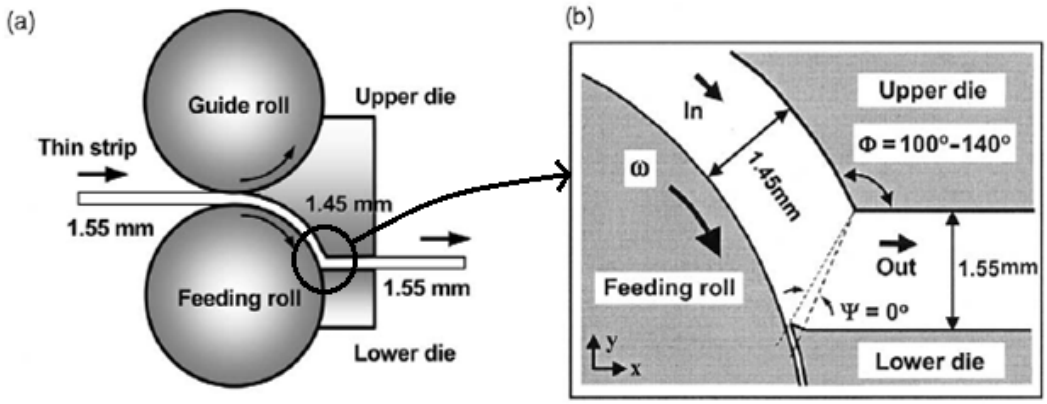

Figure 2.12: Schematic illustration of the DCAP process [14]

It is assumed by many researchers [14,15,16,17] that the dominant mode of deformation during DCAP is pure shear. Actually it is found by the texture analysis of deformation history that the deformation during ECAP or DCAP takes place not exactly on the shear plane where the inlet and the outlet channels intersect. There also found that minor tension and compression modes takes place during deformation. As a result, the deformation behavior of DCAP can be characterized predominantly as shear deformation with minor tension and compression modes. But the amount of these minor components can be considered to be insignificant that it is also possible to assume that the deformation mode of DCAP is perfect simple shear [15].

Han et al. [15] carried out a Finite Element Modeling (FEM) study of DCAP to analyze the deformation history by taking into account of this continuous complex mode of deformation during DCAP. It is shown in Figure 2.13 that the evolution of an initially square cell grid with deformation by increasing time steps obtained by their FEM study. They ended up with the result that deformation behavior in DCAP is different from that in ECAP that starting from the step 2, grid height becomes elongated along the normal direction by the compression mode along tangential direction up to step 11 and the deformation mode changes after this step that a decrease in the grid height occurs due to the tension mode along tangential direction. However, the final grid height does not return its initial value that the final height of the grid is slightly higher than its original value [15]. This difference in the grid height leads to an increase in the thickness of the deformed sheet necessitating a thickness difference between the inlet and outlet channels [18]. As a result the inlet and the outlet channels of the DCAP die are dissimilar to each other. As mentioned earlier, the inlet channel is slightly thinner than the material thickness in order to prevent material to escape from the roll gap. To conclude, the final thickness of the deformed sheet material is recovered to its original value due to these reasons enabling multipass operation.

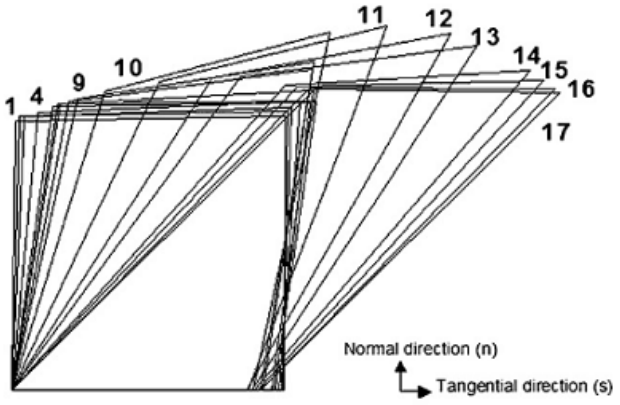

Figure 2.13: Evolution of an initially square cell grid with DCAP deformation by increasing time steps [15]

Calculation of the equivalent strain for ECAP method developed by Segal and Iwahashi were given in Equation 2.3 and 2.4 in the previous section. However, it is not possible to use the same equations for DCAP because of having different cross-sectional areas between inlet and outlet channels. Therefore, Segal model is modified by Lee et al. [14] as shown in Equation 2.5 to calculate the total equivalent strains for DCAP process introducing a new parameter called thickness ratio (K) which is defined as the ratio between the thickness values of inlet and outlet channels. If the die corner curvature angle is not considered as 0° the equation of Iwahashi et al. [12] transforms into the Equation 2.6 for DCAP process [15]:

$$\varepsilon = \frac{2N}{\sqrt{3}} K^2 cot\frac{\phi}{2} \tag{2.5}$$

$$\varepsilon = \frac{N}{\sqrt{3}} K^2 \left[2\cot\left(\frac{\phi}{2}+\frac{\psi}{2}\right) + \psi\, cosec\left(\frac{\phi}{2}+\frac{\psi}{2}\right)\right] \tag{2.6}$$

where; K is the thickness ratio of the inlet and outlet channels.

2.4.2 Advantages of the DCAP Method

DCAP method brings many advantages over other Severe Plastic Deformation (SPD) techniques in many fields. These advantages can be sequenced as;

- Obtaining the original shape after deformation and feeding the workpiece by using rollers instead of a hydraulic press as in the ECAP process makes process continuous allowing DCAP to be applicable to industrial processes.
- Many advanced mechanical properties such as high strength and hardness, long fatigue life, high toughness, good formability with moderate ductility and other desired physical properties can be obtained in sheet products by controlling the texture and microstructure with required DCAP parameters and strain level. (These topics will be discussed in subsequent chapters in detail)
- Strengthening of the thin products obtained in the final thickness by continuous slab casting process is possible as an alternative method for conventional strengthening methods of thin products.
- Applications of light materials such as Aluminum would become more widespread with required strengthening of these products in case of using DCAP method in related industrial processes.
- Spreading of usage of aluminum alloys instead of steels in industrial applications brings great improvements in energy saving, recyclability and life-cycle cost.

2.4.3 Parameters Affecting DCAP

It is stated before that mechanical and physical properties of the sheet metals can be enhanced by producing UFG structure with DCAP method. However; the extend and the nature of UFG structure formation is affected by various factors and parameters of the process such as; the strain imposed, process route, processing speed, die channel angle, die outer corner angle, friction, processing temperature and the type of the material.

2.4.3.1 Strain Imposed on the Material

It is known that formation of UFG structure and strengthening of the materials is directly related with accumulative strain imposed on the material. Related

dependency of these properties to strain will be given in following chapters. Estimation of the magnitude of the strain imposed on the material during DCAP is given by Equation 2.6 in the previous part. According to this equation, it is obvious that the strain is accumulated linearly with increasing number of DCAP passes (N). As a result, larger strain values can be obtained with multipassages of DCAP. It is also inferred by the Equation 2.6 that die channel angle and the outer corner angle is effective in determining the amount of the strain and these parameters will be discussed separately. Finally, the accumulative strain is directly proportional with the square of the thickness ratio between the inner and outer channels of the DCAP die.

2.4.3.2 Possible Routes for DCAP

It is previously mentioned that the final properties is affected by the grain rearrangement, the degree of deformation homogeneity and the types of textures formed which depends on the character of the deformation in ECAP and it is mainly affected by ECAP routes. Due to the geometrical characteristics of the DCAP process, all ECAP routes are not applicable to this method. Only route A and route C can be applicable for DCAP process where the sheet material is fed through the rollers in the same direction in consequent passes and the sheet is rotated 180° between the DCAP passes respectively. There is no any study in the literature about the differences in the properties of the metals deformed by these two different routes of DCAP. However; FEM studies of Xu, Zhao, Ren and Guan [19] shows that distribution of the effective strain is uniform through the thickness of the DCAPed sheet Al marked by the C-D line shown in Figure 2.14. This data leads the result that there would be no big difference between route A and route C in terms of strain distribution along the thickness of the sheet pressed through the 90° angle of DCAP die.

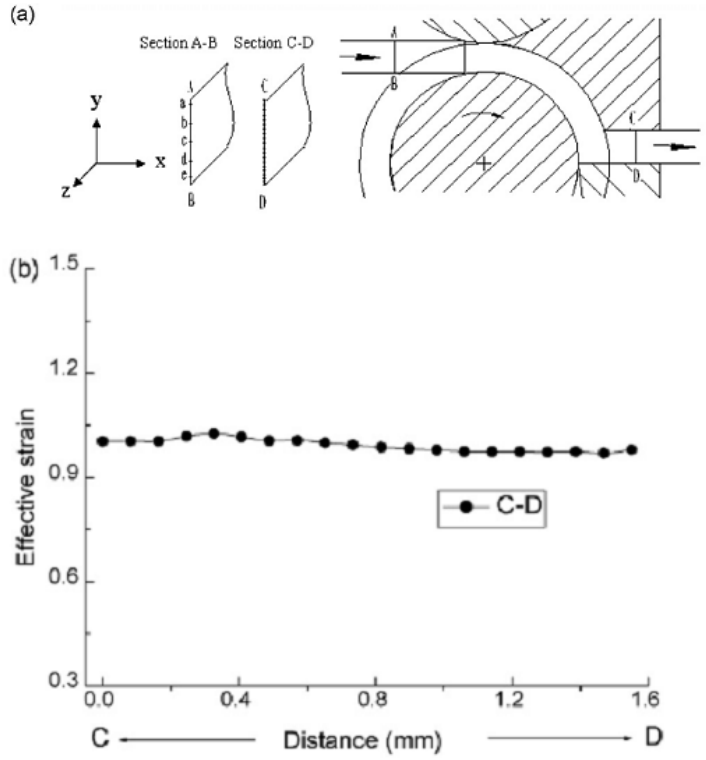

Figure 2.14: (a) Schematic of DCAP process indicating the sections before and after deformation (b) Effective strain distribution along C-D line shown in (a) [19]

2.4.3.3 Friction

Effect of the friction between the sheet material, the surfaces of the feeding rollers and the DCAP die is investigated by Xu et al. [19] for DCAP process. Because the driving force for the passage of the sheet through the DCAP die is the friction between the sheet and the feeding rollers, it should be high enough to reach this driving force and prevent slipping of the sheet at the rollers. However, the friction between the die and the sheet should not be so high to resist the material against deformation and this necessitates lubrication of the die channels. As a result, the friction of the rollers is proposed by Xu et al. [19] to be three times of the resistant friction of the die channel in DCAP process. They also show the effective strain distribution of DCAP processed sheet with time and across sheet thickness by Figure 2.15 for different friction values between sheet and the rollers by FEM studies. It is obtained by the results that the total rolling time is increased with a decrease of the

friction factor as an indication of the dragging at the intersection of the die channels. They also ended up the result that the distribution of the effective strain does not show any significant change along the sheet thickness for different friction conditions. To conclude, optimum friction condition for the DCAP process should be adjusted in order to balance the slipping of sheet at the feeding stage and the dragging at the intersection of the die channels [19].

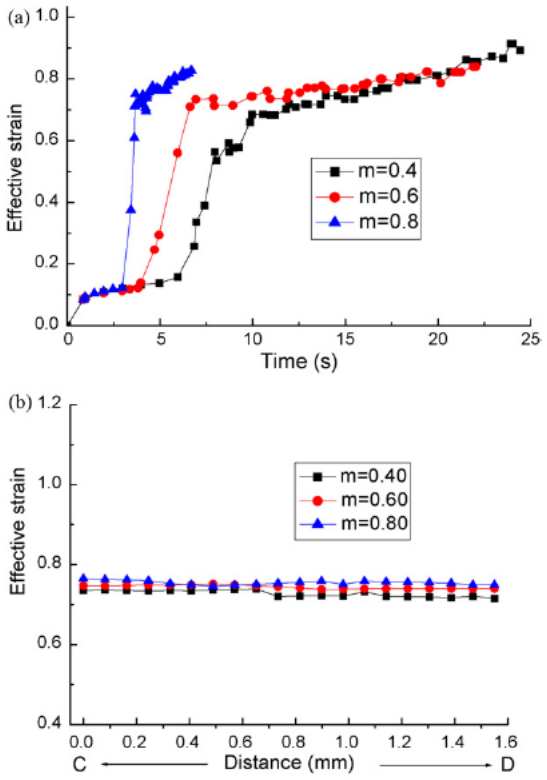

Figure 2.15: Distribution of effective strain (a) with time (b) along the C-D section of the sheet [19]

2.4.3.4 Die Channel Angle

Accumulative strain per each DCAP passes decreases with an increase in the die channel angle according to the Equation 2.6. Generation of the UFG structure and the variation in the mechanical properties of the material during DCAP is directly

dependent on the accumulative strain imparted during each DCAP passes. As a result, the critical strain value and the number of DCAP passes which is required to produce UFG structure varies with the die channel angle. By the Figure 2.16 obtained by Xu et al. [19] it is seen that the accumulation of the effective strain would be faster for smaller die angles meaning higher strain values can be obtained with less passes of DCAP. Also Lee et al. [14] show the variation in the hardness values of Al-1050 alloy DCAP processed at three different die channel angles of 120º, 130º and 140º as shown in Figure 2.17. It can be inferred by this figure that higher hardness values can be obtained with higher die channel angles at a certain strain level, but it is obvious that to obtain this strain level with lower angles, higher numbers of DCAP passes are needed. As a result, die angle should be selected moderately by considering both the total number of DCAP passes to obtain critical strain level and the final microstructural features.

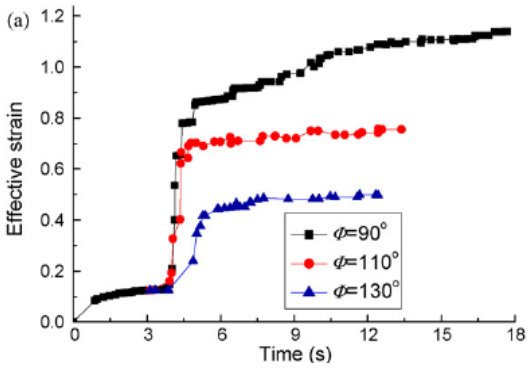

Figure 2.16: Variation of the effective strain with deformation time for three different die channel angles [19]

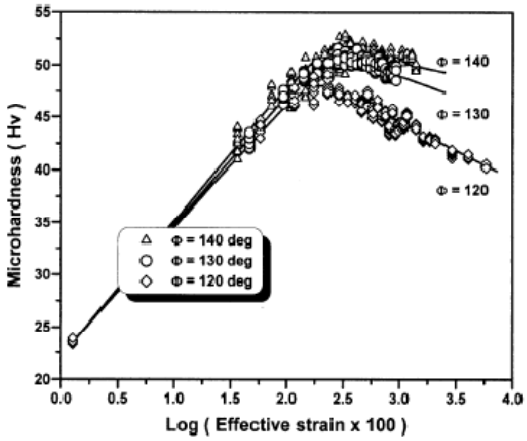

Figure 2.17: Variation in hardness of DCAPed samples for three different die channel angles [14]

2.4.3.5 Die Outer Corner Angle

Die outer corner is also an important factor affecting the total accumulative strain. According to the Equation 2.6; total strain imparted on the sample per each DCAP passes increases with a decrease in die outer corner angle as shown by Figure 2.18 from the study of Xu et al. [19]. The dragging at the intersection of the die channel also depends on the value of the die outer corner angle that the lower angles increases the amount of the dragging.

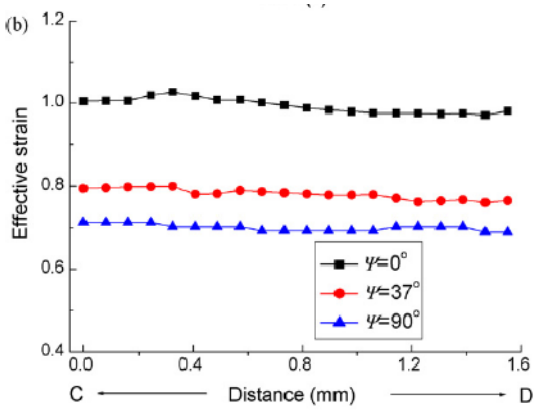

Figure 2.18: Distribution of effective strain along the C-D section of the sheet for three different die outer corner angles [19]

2.4.3.6 Forming Speed

Thermal behavior of the DCAP processed materials show different characteristic with different processing speeds during DCAP. Yamaguchi et al. [20] compared the thermal histories of the samples obtained from their ECAP trials at forming speeds of 18mm/s and 0.18 mm/s. They observed an abrupt increase in the temperature from ~11°C to ~90°C for Al-3%Mg alloy and ~11°C to ~40°C for pure aluminum at a speed of 18 mm/s. But they did not observe an increase in the temperature of the pure aluminum pressed at a speed of 0.18 mm/s. Lee et al. [14] also measured the temperature increase during DCAP at higher forming speeds (~83 mm/s) than the forming speeds observed in literature studies of ECAP. They found the temperature imposed on the samples as ranging from 100 to 300^0C depending on the channel angle. They ended up with the result that although the exposure duration is short, high temperatures obtained with the extensive strain can accelerate the UFG formation but growth of these grains occurs resulting in softening behavior. However, it is known that low forming speed does not significantly affect the final microstructure of the sample during ECAP [1].

2.4.3.7 Forming Temperature

Temperature of the process during SPD is an important parameter in terms of the mechanism behind UFG formation and further evolution of the microstructure. During hot deformation of the metals, flow rates of the plastic flow or creep are governed by diffusion-controlled processes associated by intragranular processes such as dislocation climb, dislocation glide and grain boundary processes including grain boundary sliding and vacancy flow [1].

In the literature, microstructural evolution of the samples deformed by different forming temperatures is studied by many researchers [16,1,21,22]. Jining et al. [16] studied on DCAP of 6061 alloy at four different forming temperatures of RT (298 K), 353 K, 433 K and 513 K. Figure 2.19 illustrates the TEM images obtained by their study showing that forming up to 513 K does not lead a substantial growth in grain size and a decrease in misorientation meanwhile having similar microstructures

formed at RT, 353 K and 433 K basically consisting of thick and waved non-equilibrium grain boundaries and high dislocation density within the cells and subgrains. Whereas, thin and regular shaped cell boundaries with lower misorientations and a decreased dislocation density due to dynamic recovery is mentioned to be observed in DCAP process at 513 K.

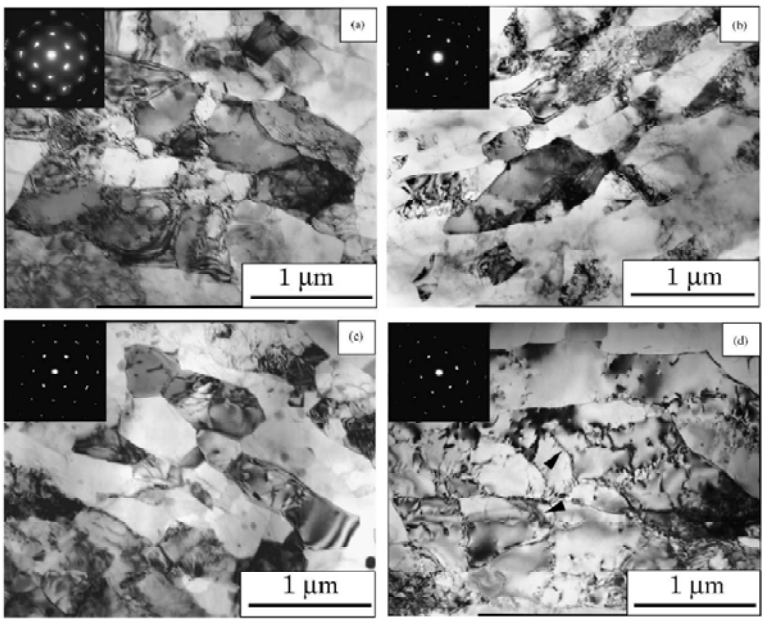

Figure 2.19: TEM photographs and SAED patterns of DCAPed 6061 Al alloy sheet at (a) RT (b) 353 K (c) 433 K (d) 513 K [16]

A similar study is held by Wang et al. [22] at four different temperatures of RT, 373, 473 and 523K with 12 ECAP passes of AA1050 alloy (commercial purity Al) and further quenching into water. The average subgrain sizes and fractions of High Angle Grain Boundaries (HAB) with different forming temperatures obtained by their study are shown in Table 2.1. It can be seen that there is no any significant change both in subgrain size values and fraction of HAB from 298 to 473 K but there is a sharp increase in grain size and a decrease in fraction of HAB at 523K.

Table 2-1: HAB% and subgrain sizes obtained at various ECAP processing temperatures [22]

Temperature, K	HAB%	Subgrain size, μm
298	68	0.55
373	66	0.59
473	69	0.9
523	49	2.2

These results show that after a critical forming temperature, characteristics of the deformation microstructure changes dramatically which inevitably results in differences in mechanical properties of the deformed sample. Tensile properties of severely deformed materials are known to be deteriorated with increasing forming temperatures [21].

2.4.3.8 Initial Material Properties

Initial material properties such as hardness, ductility and strength directly affect the applicability of DCAP process. It is inherently hard to pass harder and high strength materials through the DCAP die. These properties are also important for the life cycle of DCAP die, rolls and other parts contacting directly to the pressed material.

Some material properties does not have a direct effect to the DCAP process but important in determining the final properties. In the literature there are some studies about these material properties affecting the final properties of UFG materials deformed by different SPD methods. These effects can also be considered for DCAP process.

It is known that Stacking Fault Energy (SFE) determines the degree of mobility of dislocations in terms of cross-slip. Zhilyaev and Langdon [23] mentioned that narrower separation of partial dislocations and an easy cross slip which provides higher recovery rates was observed for materials having high stacking fault energies such as aluminum. In contrast, slower recovery rates were observed for materials

having lower stacking fault energies suggesting slower evolution rate of microstructure and requirement of higher strain rates.

Valiev and Langdon [1] dealt the effect of second phases or arrays of precipitates in the material to the high temperature stability of ultrafine grains. They illustrated the change in grain size of many aluminum based alloys which are ECAPed, as a function of annealing temperatures as shown in Figure 2.20. They observed that the grain growth is rapid at temperatures above 500K for pure aluminum and Al-3%Mg solid solution alloy. Introduction of fine Al_3Sc precipitates in Al-3%Mg alloy by the addition of 0.2%Sc provide a stability of submicrometer ultrafine grains up to temperatures of 700K. Also, the presence of $CuMgAl_2$ precipitates in Al 2024 alloy and the presence of Al_3Zr and $MgZn_2$ precipitates in the Al-7034 alloy shows the same effect in order to be good candidate materials for achieving superplastic ductilities at high temperatures [1]. Wang et al. [22] also studied the effect of Mg addition to aluminum alloys which results in finer subgrain sizes at elevated temperatures higher than 373K for ECAP processes. They correlated this result to the explanations of Iwashashi et al. [24] related to the decreasing rate of recovery by the addition of Mg which leads a decrease in grain size and requirement of higher accumulative strain to establish a homogeneous microstructure. These effects of second phases and precipitates to the final thermal and mechanical properties of ECAPed materials are considered to be the similar for DCAPed materials.

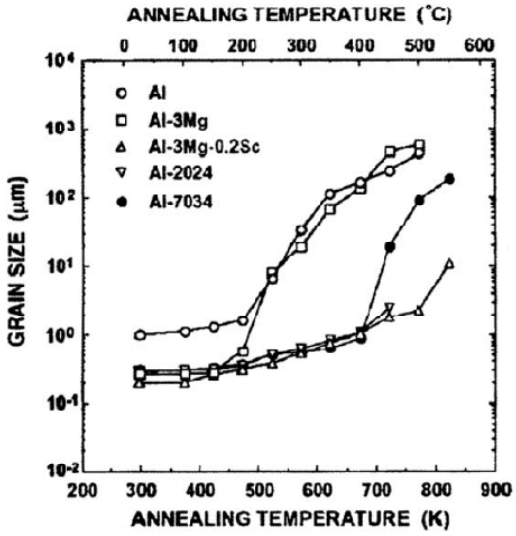

Figure 2.20: Variation in the grain size of different aluminum based alloys as a function of annealing temperatures after ECAP process [1]

2.4.4 Industrial Potential of DCAP

SPD techniques have a great potential for industrial processes due to their advantages over conventional methods such as introducing advanced mechanical and physical properties by imposing very high strains without changing the material geometry. Literature studies shows that DCAP is a very effective technique to provide these requirements for sheet or strip products and also it is very advantageous because of being a continuous process. Although many developments are required to be able to be used in industrial processes, there is a huge potential of DCAP technique as an alternative method for rolling operations and a strengthening method for sheet products obtained by thin slab casting.

2.5 Formation of Ultra Fine Grained Al by DCAP – ECAP

Mechanism of grain refinement by severe plastic deformation is generally discussed in Part 2.1. Grain refinement particularly in Al alloys and examples from literature will be discussed in this part. Grain refinement by severe plastic deformation is related to the evolution of subgrain boundaries. Actually the grain refinement mechanisms are not fully understood yet [25]. A detailed analysis of microstructure,

grain and subgrain evolution, microscopic deformation behavior and dislocation behaviors etc. during severe plastic deformation should be made in order to understand this mechanism.

2.5.1 Microstructural Investigation of Al alloys

Evolution of initial grain structure of Al alloys by severe plastic deformation give important data about the deformation behavior and the texture evolution. Many researchers include microstructural inspection to their studies about ECAP and DCAP.

Tham, Fu, Hng, Pei and Lim [26] studied ECAP of Al-6061 alloy billets which had been annealed at 415°C for 3 hours before ECAP and the microstructures of Al-6061 hot extruded billets before and after 4 passes of ECAP are shown in Figure 2.21. Flow lines and elongated grains with an average grain size of ~80 μm and flow marks can be seen in hot extruded samples as shown in Figure 2.21 (a). After 4 passes of ECAP with a strain value of ε~4, the flow lines are disappeared and elongated grains become more uniformly distributed with an average grain size of about 10 μm shown in Figure 2.21 (b).

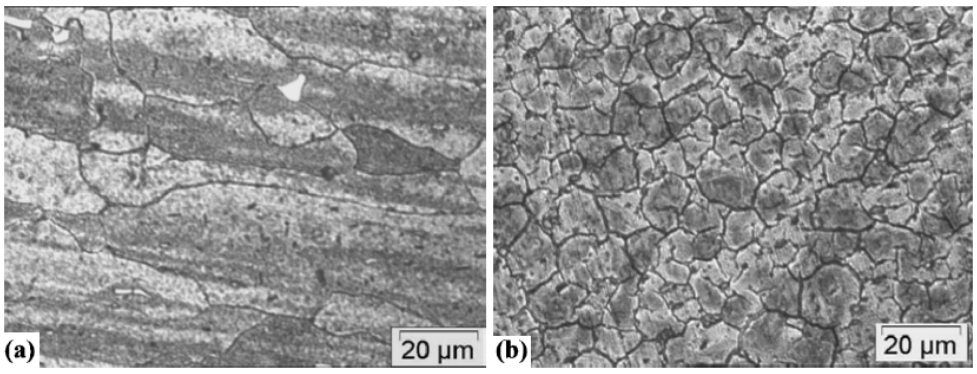

Figure 2.21: Microstructure of Al 6061 Alloy (a) before ECAP and (b) after 4 ECAP passes [26]

Evolution of grain structure and deformation shearing during DCAP with a 120° die angle is studied by Lee, Seok and Suh [14] by numerical analysis and experimental

observations of Al 1050 alloy. Figure 2.22 shows both the optical micrograph taken from the side surface of sample deformed by DCAP and the numerical analysis results by finite element modeling (FEM). They concluded from the results that the simple shear is the dominant mode of deformation during DCAP and a relatively uniform shear deformation was observed throughout the thickness direction except in regions close to the bottom surface due to curvature angle. Figure 2.23 shows the optical micrographs taken from the side surfaces of the strips that are objected to different DCAP passes. As seen in these micrographs, relatively uniform and equiaxed grains observed from specimens prior to DCAP were aligned along the direction of shearing after DCAP. It is also observed that as the number of passes increases, extent of the shear deformation is increased such that, a fibrous microstructure similar to a heavily rolled metal is observed after 3 passes of DCAP.

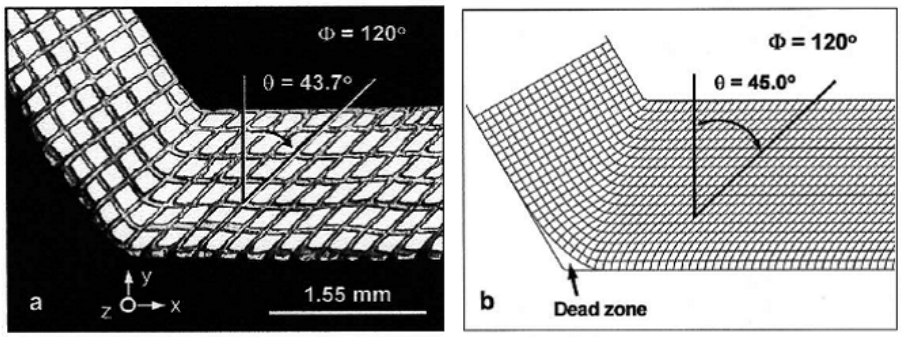

Figure 2.22: The shear deformation patterns obtained from (a) the experiment and (b) the FEM calculation [14]

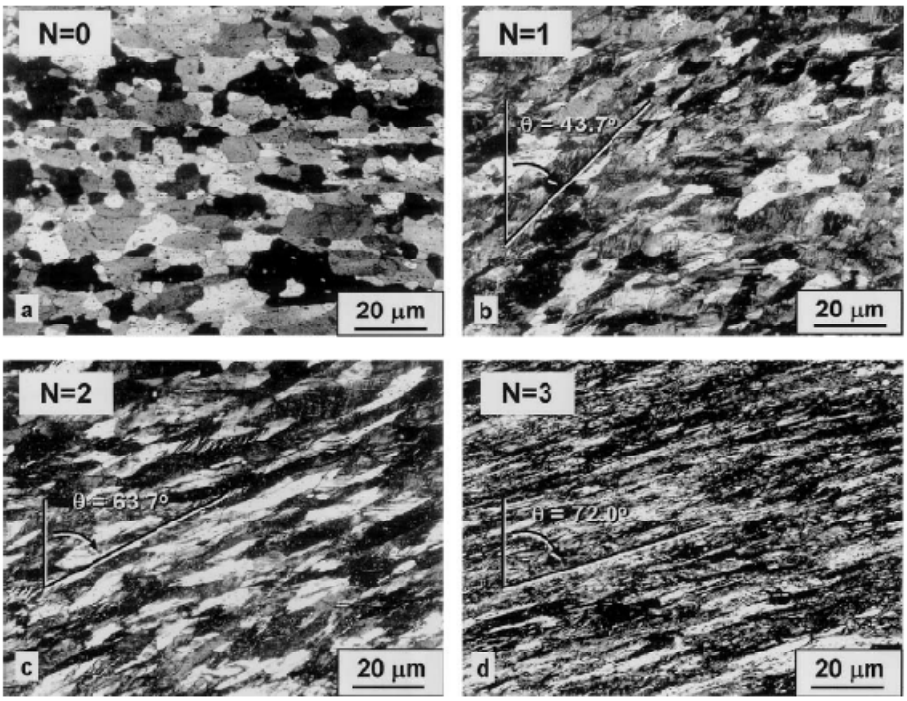

Figure 2.23: Optical micrographs of the 1050 Al before and after DCAP (a) N =0, (b) N = 1, (c) N = 2, and (d) N = 3. [14]

As seen from the results in the literature; observing the microstructural changes occurred during ECAP and DCAP with higher magnifications should be needed in order to understand the mechanism of deformation. Thus, observation of UFG evolution and grain refinement would be possible by using high resolution devices such as transmission electron microscopy (TEM), X-ray structural analysis, Mossbauer spectroscopy, differential scanning calorimetry etc. Related studies which are made about the microstructural evolution of Al alloys during DCAP and ECAP processes in ultra fine size will be represented in the following part:

2.5.2 Description of Dislocation Boundaries and Grain Boundaries

Before giving the results obtained by TEM studies about ECAP and DCAP in the literature, it would be helpful to introduce the description and types of grains, subgrains, boundaries and other substructures. These definitions are discussed in this part:

“It is found that if the dislocations have a low mobility at the temperature of deformation, they appear as a fairly random array in the deformed metal. However, if the dislocations are able to cross slip (high stacking fault energy), they immediately begin to condense into tangles so that the metal contains regions of high and low dislocation density. The regions of low dislocation density are called variously cells or subgrains. Aluminum deformed at room temperature forms a distinct subgrain or cell structure because its high stacking-fault energy does not inhibit cross slip.” [27] Boundaries between these subgrains are called as subgrain boundaries, cell boundaries or dislocation boundaries.

Wilsdorf and Hansen [28] suggested three types of boundaries formed by glide dislocations; namely domain boundaries, cell block boundaries and cell boundaries. They typed cell block boundaries and domain boundaries such as microbands and cell band walls as ‘Geometrically Necessary Boundaries’ (GNB) of which their average angular misorientation increases with strain at the start of deformation and saturating at larger strains. On the other hand, cell boundaries are typed as ‘Incidental Dislocation Boundaries’ (IDB) which are occurred by statistical mutual trapping of glide dislocations. Because misorientation of GNBs is thought to increase with strain at a higher rate than the misorientation of IDBs, GNBs are assumed to play a key role in obtaining UFG structure with high misorientations under severe plastic deformation [29].

Chang, Sun and Kao [30] have studied ECAP of pure aluminum to be able to see whether or not the boundaries of ultrafine-grained structure generated by severe plastic deformation are grain boundaries or dense dislocation boundaries. “A grain boundary is a two-dimensional planar defect, while a dislocation boundary consists of one-dimensional line defects.” [30] They have observed the development of fine-grained structure in the equivalent strain levels of 2, 4 and 8 with apparent grain sizes of 0.61, 0.57 and 0.35 μm respectively shown in Figure 2.24 and revealed that elongated shape of the grains have turned into an equiaxed shape, meanwhile the grain size and the dislocation density in the grain interiors are decreased with increasing strain level. They have also concluded that there have been dislocation

loop debris in some of the grain interiors (Figure 2.25) indicating that massive dislocation annihilations have occurred. They have introduced three types of boundaries generated at different strains according to their studies; polygonized dislocation walls (PDW), partially transformed boundary (PTB) and grain boundary as shown in Figure 2.26. They described PDW as a conventional subgrain boundary consisting perfect lattice dislocations and having very low misorientation which is typically less than 1º. They defined the misorientation of PTBs in the range of about 1-5º, where the thickness fringes can be seen on these boundaries. Grain boundaries have misorientations larger than 10 º that they can be classified as high angle boundaries. After a strain level of e=4; it is observed by the study of Chang et al. [30] that 85% of the boundaries and after e=8; 95% of the boundaries have been observed to be transformed into grain boundaries.

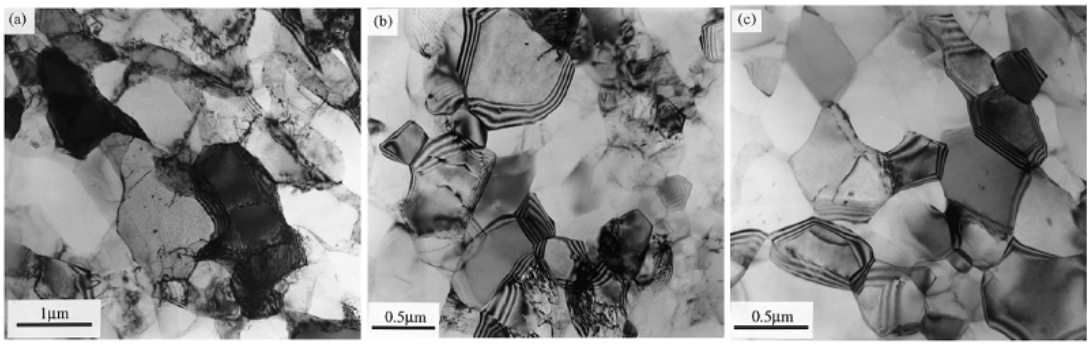

Figure 2.24: TEM micrographs of pure Al ECAPed at an equivalent strain of (a) 2, (b) 4 and (c) 8 [30]

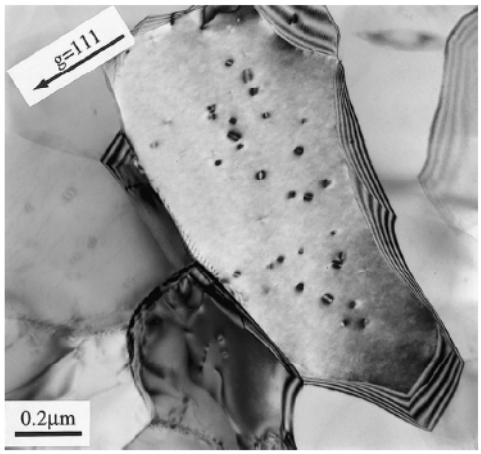

Figure 2.25: TEM micrograph showing dislocation loop debris [30]

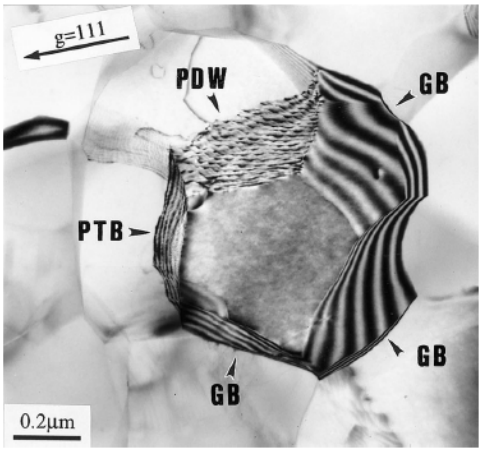

Figure 2.26: TEM micrographs showing a grain surrounded by different boundary types at an equivalent strain of 8 [30]

2.5.3 Evolution or Transformation of Substructures during ECAP/DCAP

It is known that UFG structure can be produced by severe plastic deformation methods such as ECAP and DCAP for Al alloys. Besides grain reduction, some other changes occur in the grain structure during these processes such as nucleation and growth of new grains, 'conversion of cells to grains' [25], misorientation increase in boundaries and dislocation density changes in grain interiors. There are many studies in the literature about these changes:

Tham, Fu, Hng, Pei and Lim [26] studied on ECAP of Al-6061 alloy at room temperature with a die angle of 90°. Grain size was reduced to 1μm after 8 ECAP passes (ε=8) as shown in Figure 2.27 where as the grain size of the undeformed sample was ~80 μm (Figure 2.21(a)). After 12 and 16 ECAP passes of the alloy, 0.8 μm grain sizes were obtained as shown in Figures 2.28 (a) and (b) respectively, whereas the grains are relatively more equiaxed and uniform in 16 passes of ECAP.

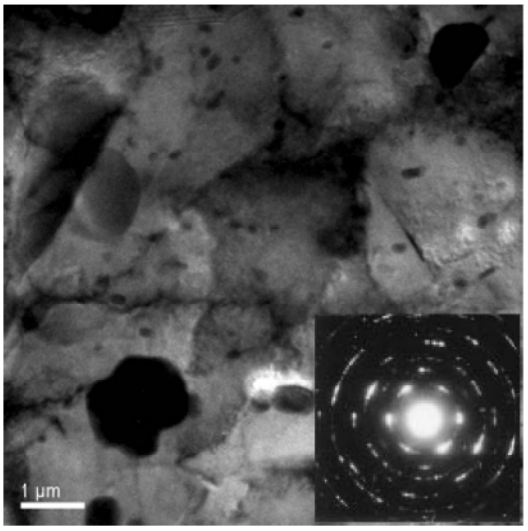

Figure 2.27: TEM micrograph of Al-6061 after 8 ECAP passes [26]

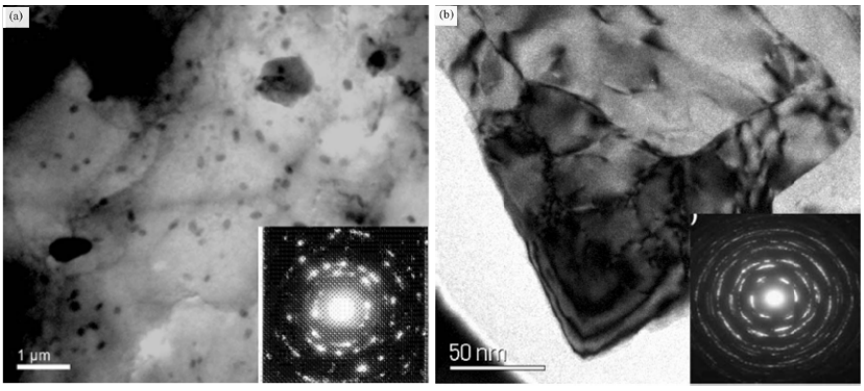

Figure 2.28: TEM micrograph of Al 6061 after (a) 12 and (b) 16 ECAP passes [26]

Also the corresponding SAED patterns shows that the diffracted beams scattering is more uniform around the rings in 16 passes of ECAP than lower number of passes as seen in Figures 2.27, 2.28. It can be said that increasing number of ECAP passes and so the strain level increases the misorientation angle between boundaries and number of subgrains [26]. In another study of Chang et al. [30] which supports this idea shows the misorientation angles measured from grain boundaries is increased with increasing strain levels that at e=4, 85% and at e=8, 95% of the grain boundaries have misorientations larger than 10° as shown in Figure 2.29, meaning; that much of the boundaries are transformed into the grain boundaries.

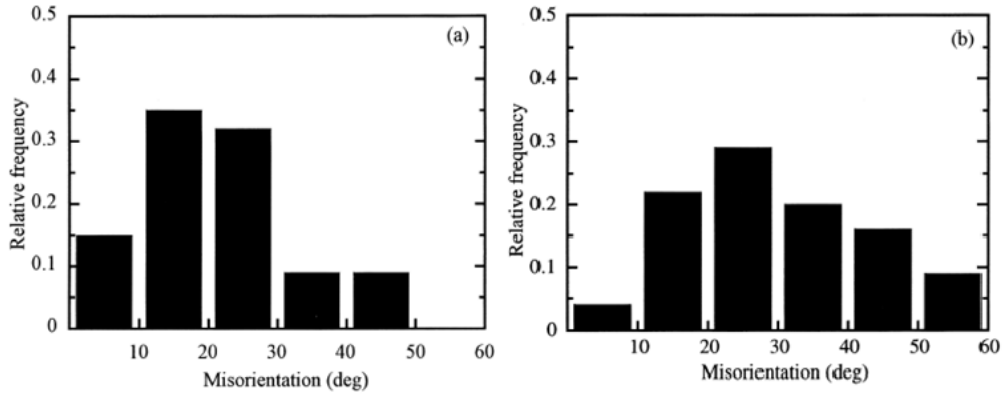

Figure 2.29: Graph showing the misorientation frequency of generated boundaries at equivalent strains of (a) 4 and (b) 8 [30]

Kim et al. [21] observed a grain size reduction of 6061 alloy from 60 μm to 1 μm after 2 passes, 0.5 μm after 4 passes and 0.3 – 0.4 μm after 12 passes of ECAP as shown in Figure 2.30 with increasing misorientation angles and equiaxed subgrains. Also Kang et al. [31] studied DCAP with Al – Mn alloy AA 3103 and obtained an inhomogeneous grain size distribution ranging from 0.5 – 10 μm for different DCAP passes as seen in Figure 2.31.

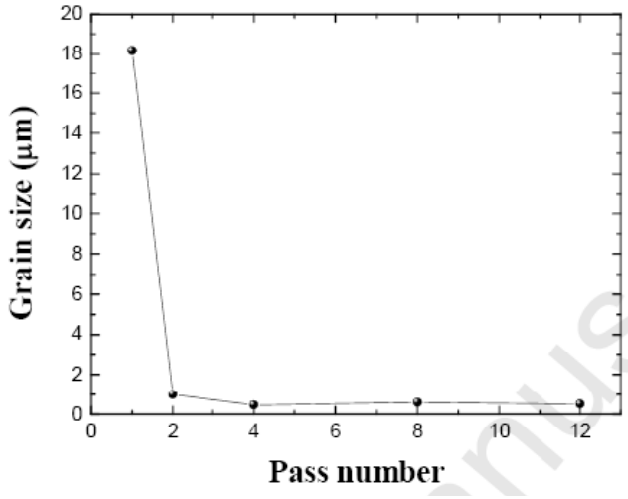

Figure 2.30: Variation of grain size with ECAP passes [21]

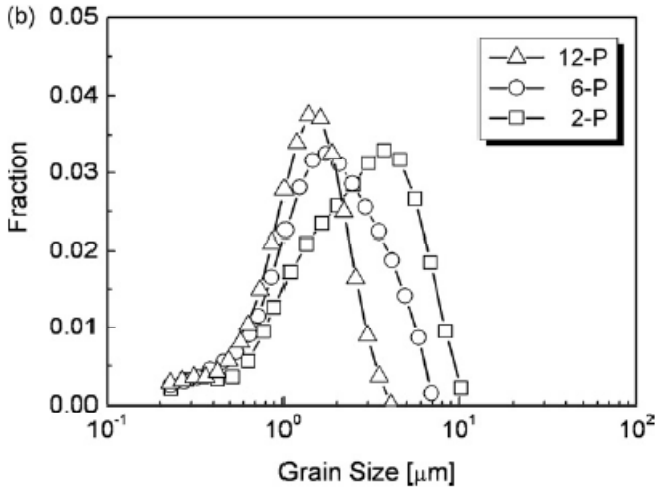

Figure 2.31: Distribution of grain size for 2, 6 and 12 DCAP passes [31]

In the study of Tham et al. [26] it is appeared that the rapid decrease in the grain size slows down after 8 ECAP passes and there is no difference in the grain size of the 12 and 16 ECAP passed Al alloy. This result leads that the subgrain size decreases rapidly and approaches saturation after a critical strain level. This is also correlated with the decrease of strain hardening level. [25] The critical strain level mentioned is

related to the alloy type, parameters of deformation and some environmental effects like temperature.

In the study of Lee, Seok and Suh [14] about DCAP of 1050 Al alloy with 120° die angle, observations are classified in two different regions of strain levels representing different hardening characteristics that the region A is where an abrupt increase in the hardness is seen, while region B is where the hardness either saturates or slightly decreases. Figure 2.32 shows the TEM images of 1050 Al alloy at different strain levels deformed by DCAP by their study. In the first DCAP pass (ε=0.6), dislocation tangling to form cell structures with many interior dislocations are observed in the microstructure as shown in Figure 2.32 (a). After 2 passes of DCAP (ε=1.2), a decrease in the cell size is observed with increased misorientation across the boundaries (Figure 2.32 (b)). After 3 passes of DCAP at a strain level of ε=1.8 which is mentioned as critical strain level where the hardening characteristics starts to change (boundary between region A and region B); new types of cell boundaries begin to appear which are thinner, more regular and well developed than the cell boundaries in region A and a decreased interior dislocation density is observed as shown in Figure 2.32 (c). At 5 passes of DCAP (ε=2.9), grains with very thin and regular boundaries and grains with a low dislocation density and high angle boundaries were observed. It is also pointed by the writers that further straining in region B does not change the microstructural features significantly, except a gradual increase in the grain size with a slightly decreased dislocation density is observed with increasing strain which is also correlated with work softening in region B [14].

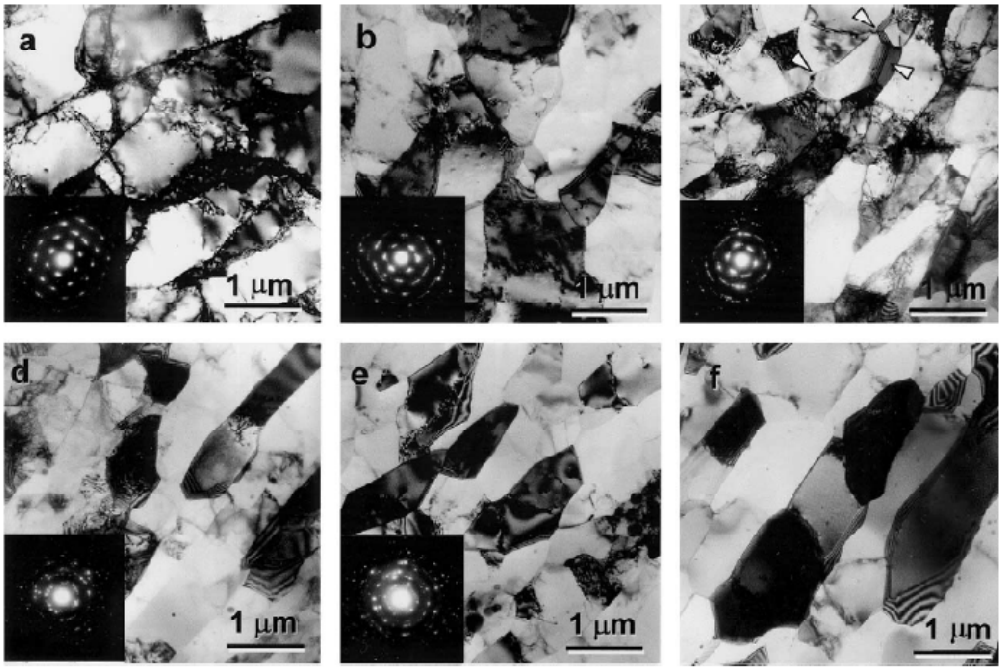

Figure 2.32: TEM micrographs showing the evolution of the grain structures with different number of DCAP passes (a) N=1 (ε=0.6), (b) N=2 (ε=1.2), (c) N=3 (ε=1.7), (d) N=5 (ε=2.9), (e) N=9 (ε=5.2), (f) N=50 (ε=29) [14]

A similar study is held by Lee, Suh and Ahn [32] that the microstructural features observed are related with the data obtained by Valiev et al. [5] proposing that a transformation of a cellular structure to a granular one and with further deformation, transformation to the UFG structure by the partial annihilation of dislocations of opposite signs at the cell boundaries and by Chang et al. [30] regarding the structural evolution sequence of dislocation cells→ PDWs→ PTBs→ Ultra-fine grains as mentioned earlier. In their studies, at lower accumulative strain levels than ε=~2 (region A), it is said to be observed that generated dislocations are concentrated at cell walls with low angles of misorientations. At ε=~1.2, generated dislocations are observed to rearrange to form PDWs and also limited number of PTBs were also observed as seen in Figure 2.33 (b). After reaching the strain level of ε=~2 (boundary between region A and region B) some PDWs are observed to transform into PTBs and some PTBs transformed into grain boundaries with more regular-shaped and thinner boundaries as shown in Figure 2.33 (c-d). When strains larger than ε=~3

(region B) reached, most of the grains are observed to be separated with high angles of misorientation which are mainly characterized by either thickness fringes or regular-shaped walls. Transformation of cell structure to grain boundary structure is thought to be occurred at region B as seen in Figure 2.34. Misorientation distribution of boundaries was also graphed by using EBSD data for various strain levels as shown in Figure 2.35. It is observed that boundaries with high angles of misorientation were observed to increase as the number of DCAP passes and so the strain level increases. [32]

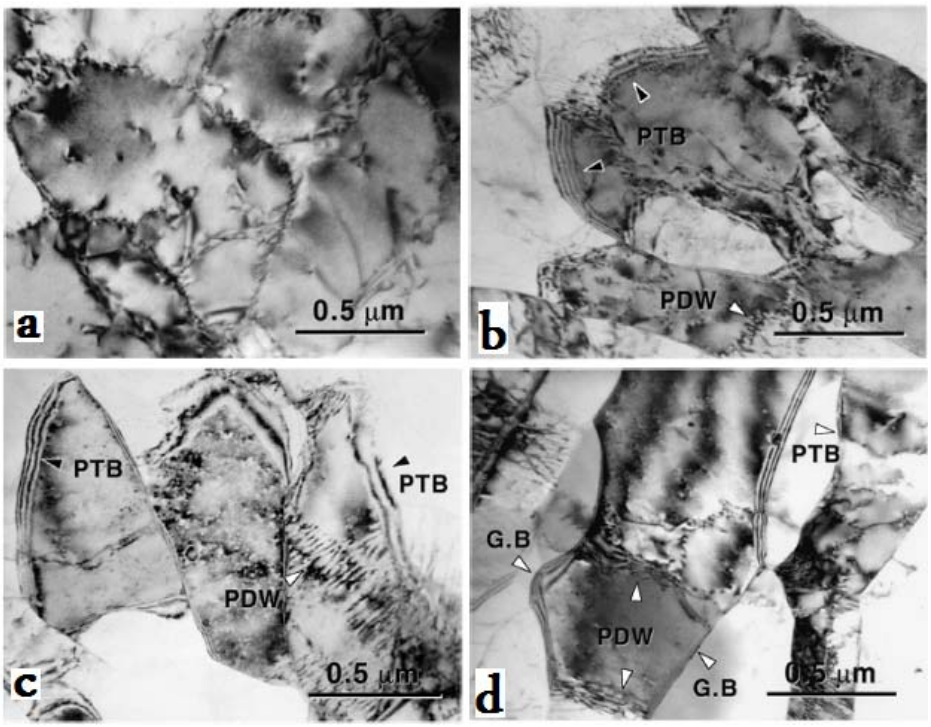

Figure 2.33: TEM micrographs showing evolution of the grain structures with different numbers of DCAP passes (a) N=1 (ε=0.6), (b) N=2 (ε=1.2), (c) N=3 (ε=1.7), (d) N=4 (ε=2.3) [32]

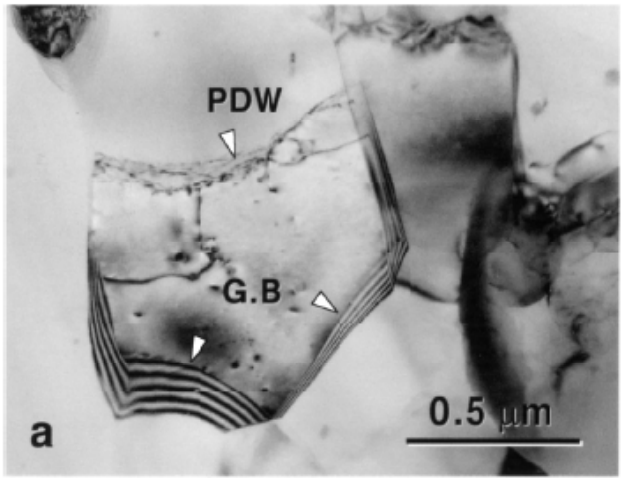

Figure 2.34: Transformation to a grain boundary structure at N=5 (ε=2.9) [32]

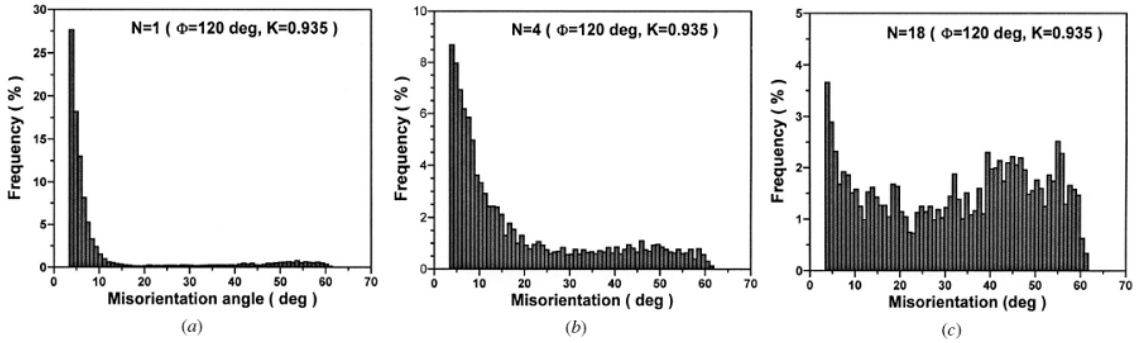

Figure 2.35: Misorientation distribution of Al 1050 alloy with different numbers of DCAP passes (a) N=1, (b) N=4, (c) N=18 [32]

The mechanism of the transformation from PDW into a grain boundary structure is thought to be caused by an increase of dislocation density inside these boundaries during straining. According to Chang et al. [30] massive annihilation between traveling dislocations and deposition of glide dislocations onto the boundaries is expected and deposition of dislocations would reduce dislocation spacing causing the interaction energy between lattice and dislocations would become so high that the dislocations starts to dissociate. Finally, it is explained that as the deposition of dislocations onto the boundaries and so the reduction of dislocation spacing continues and these dislocations eventually lose the identity of individual dislocation,

and they become grain boundary structure. Increase of grain boundary misorientation at higher strains is explained as the rotation of the grains. [30]

According to Zhilyaev, Swisher, Oh-ishi, Langdon and McNelley [33]; the formation and evolution of lamellar boundaries (LBs), microbands (MBs) and dense dislocation walls (DDWs) is also included in the grain subdivision process as well as subgrains and cellular structures. It is explained that they elongate as the prior grains deform and the LBs and MBs become band-like structures with high misorientation boundaries aligned with the rolling direction. "These features generally separate regions within prior grains that have experienced lattice rotation in opposite senses away from the original grain orientation." [33]

2.5.4 Recrystallization Mechanism During Plastic Deformation

Static or dynamic recrystallization is the primary mechanism for grain refinement in metals at a certain elevated temperature, but it is a surprising result to achieve grain refinement by plastic deformation at room temperature [30]. It is necessary to know the types of recrystallization mechanisms to find out the reason of grain refinement by plastic deformation. Static recrystallization occurs after annealing of a hot deformed metal whereas dynamic recrystallization generally takes place during hot deformation of ordered alloys where large amount of stored energy is preserved [34].

Humphreys and Hatherly [34] classified dynamic recrystallization into two types namely; Discontinuous Dynamic Recrystallization (DDRX) and Continuous Dynamic Recrystallization (CDRX). DDRX has clear nucleation and growth stages where new grains originate at the old grain boundaries, as the material continues to deform, dislocation density of the new grains increases which reduces the driving force for further growth and stops the growth of recrsytallizing grains. In CDRX process; a microstructure of high-angle grain boundaries may evolve during hot deformation in other ways than the nucleation and growth process as in discontinuous process. A fine grained microstructure consisting of crystallites having high-angle boundaries are resulted by minor boundary movements either during the deformation or on subsequent annealing without any recognizable nucleation or

growth process in continuous recrystallization. Geometric Dynamic Recrystallization (GDRX) is one of these ways of CDRX mentioned which have many similarities between continuous recrystallization occurring on annealing alloys that are largely strained. Although, GDRX has been recognized to occur during high temperature deformation, many researches has shown that a microstructure consisting of high-angle boundaries is resulted in a metal severely cold-worked and it may undergo continuous recrystallization with annealing. [34]

According to Montheillet and Coze cited by Skrotzki et al. [35] with increasing purity of the material, the recrystallization temperature may become lower than the processing temperature leading to dynamic recrystallization. Skrotzki et al. [35] studied ECAP of 5N purity Al and realized that recrystallization has taken place at room temperature assuming no significant temperature increase is expected to have taken place by adiabatic heating due to high thermal conductivity of pure aluminum. They introduced many indications suggesting that DDRX is the prevalent mechanism of recrystallization which is characterized by nucleation and growth.

However; according to Chang et al. [30] since very large strain is induced by ECAP, generation of a fine-grained structure during ECAP was said to be caused by GDRX due to flattening of original grains as similar in the GDRX process which is regarded in the literature to takes place in conventional methods and it is described as “the original grains are flattened at large strain, the original grain boundaries become serrations due to dynamic recovery and when the grain boundary spacing is reduced to a certain distance about twice the subgrain size, these grain boundaries will pinch-off and fine equiaxed grains are formed” [30]. On the other hand; Lee et al. [14] suggested that GDRX is not necessarily true to explain grain refining mechanism in ECAP or DCAP due to independency of UFG formation to the process routes which is effective in the grain shape where as the flattening of the original grains are considered in GDRX.

2.5.5 Modeling of Dislocation Density Based Strain Hardening

It is told previously that the grain refinement by severe plastic deformation is arised from the evolution of subgrain (dislocation cell) boundaries. This is related with the subgrain size and the dislocation density evolution during SPD. In this manner; Baik, Estrin, Kim and Hellmig [25] developed a 'dislocation density-based strain-hardening model' including cell size and dislocation density calculations to analyse the deformation behavior of polycrystalline aluminum under ECAP by FEM.

According to this model:

The total dislocations are composed of the dislocations in the cell walls and the dislocations inside the cell interiors, by the rule of mixtures total dislocation density (ρ_t) is obtained by:

$$\rho_t = f\rho_w + (1-f).\rho_c \qquad (2.7)\ [25]$$

Where:

ρ_c : Cell interior with a relatively low dislocation density
ρ_w : Cell walls with a higher dislocation density
w : Width of the cell wall
ρ_t : Total dislocation density
f : Volume fraction of the cell walls

Volume fraction is approximated by:

$$f = f_\infty + (f_0 + f_\infty)\exp\left(-\frac{\gamma^r}{\tilde{\gamma}^r}\right) \qquad (2.8)\ [25]$$

Where:

f_0 : Initial value of f
f_∞ : Saturation value of f at large strains
γ_r : Resolved shear strain

$\tilde{\gamma}^r$: Rate of variation of f with γ_r

The average cell size (d) is obtained by the equation:

$$d = \frac{K}{\sqrt{\rho_t}} \quad (2.9)\ [25]$$

Where;

d : Average cell size

K : Proportionality constant (Decreases with the accumulation of total dislocation density)

The (scalar) stresses in the cell interiors (τ_c^r) and in the cell walls (τ_w^r) are increased by the dislocation densities inside by;

$$\tau_c^r = \alpha G b \sqrt{\rho_c} \left(\frac{\dot{\gamma}_c^r}{\dot{\gamma}_0}\right)^{1/m} \quad (2.10)\ [25]$$

$$\tau_w^r = \alpha G b \sqrt{\rho_w} \left(\frac{\dot{\gamma}_w^r}{\dot{\gamma}_0}\right)^{1/m} \quad (2.11)\ [25]$$

where;

τ_c^r : Stress in the cell interiors

τ_w^r : Stress in the cell walls

$\dot{\gamma}_c^r$: Shear rates in cell interiors

$\dot{\gamma}_w^r$: Shear rates in cell walls

G : Shear Modulus

b : Magnitude of burgers vector

$\dot{\gamma}_0$: Reference strain rate

1/m : Strain rate sensitivity parameter

α : Constant (~0.25)

The overall stress (τ^r) behavior of the composite structure is obtained by rule of mixtures:

$$\tau^r = f\tau_w^r + (1-f)\tau_c^r \qquad (2.12)\ [25]$$

where;

τ_r : The overall stress

Finally the evolution of the dislocation density in the cell interior is given by the equation:

$$\dot{\rho}_c = \alpha^* \frac{1}{\sqrt{3}} \frac{\sqrt{\rho_w}}{b} \dot{\gamma}_w - \beta^* \frac{6\dot{\gamma}_c}{bd(1-f)^{1/3}} - k_0 \left(\frac{\dot{\gamma}_c}{\dot{\gamma}_0}\right)^{-1/n} \dot{\gamma}_c \rho_c \qquad (2.13)\ [25]$$

where;

α^*, β^*, k_0 : Constants

n : Strain rate sensitivity of the annihilation process

First term : Rate of generation of cell interior dislocations generated by Frank-Read sources at the interface

Second term : The loss of the cell interior dislocations that move into the walls

Third term : Mutual annihilation of cell interior dislocations governed by cross-slip

The evolution of the dislocation density in the cell walls is governed by the equation:

$$\dot{\rho}_w = \frac{6\beta^* \dot{\gamma}_c (1-f)^{2/3}}{bdf} + \frac{\sqrt{3}\beta^* \dot{\gamma}_c (1-f)\sqrt{\rho_w}}{fb} - k_0 \left(\frac{\dot{\gamma}_w}{\dot{\gamma}_0}\right)^{-1/n} \dot{\gamma}_w \rho_w \qquad (2.14)\ [25]$$

where;

First term : The dislocation density gained in the walls corresponding to the loss of cell interior dislocations

Second term : The increase of dislocation density in the wall due to the activation of Frank-Read sources at the interface by dislocations coming from the cell interior

Third term : Annihilation of cell wall dislocations involving cross-slip

2.6 Effect of DCAP – ECAP to the Mechanical Properties of Aluminum

It is known that severe plastic deformation enables superior mechanical properties in metals. Small grain sizes and high defect densities [1] attained by severe plastic deformation lead to higher hardness and strength values comparing with coarse grained metals. This has been attracted many researchers that there are many studies in the literature about the development of mechanical properties of Al alloys by Dissimilar Channel Angular Pressing or Equal Channel Angular Pressing methods. Besides high strength of the material, better fatigue and superplastic properties can be obtained without decreasing the ductility so much as compared to conventional deformation techniques. Also fracture toughness of the materials can be considered to be increased by grain size refinement which makes crack propagation more difficult [36]. These properties can be achieved by assuring some requirements such as obtaining optimum microstructural parameters (cell size, dislocation density, texture etc.), optimum processing conditions and regimes, selecting appropriate material, etc.

2.6.1 Strengthening Mechanisms

Strengthening is obtained during severe plastic deformation mainly as a result of strain hardening caused by dislocation behavior and Hall-Petch effect of subgrains. Strain hardening is achieved by increasing dislocation density inside grains where this hardening can be empirically formulized by Hollomon's equation (Eq. 2.15):

$$\sigma = K\varepsilon^{n} \qquad (2.15)$$

where;

σ is the stress

K is the strength index

ε is the plastic strain
n is the strain hardening coefficient

Grain size is also constitutive in determining the strength of the materials. Strengthening of Al alloys during severe plastic deformation can be considered to be caused by Hall-Petch effect of ultra-fine grains in this manner. According to the Hall-Petch equation (Eq. 2.16) a relationship between the yield stress and grain size is proposed:

$$\sigma_0 = \sigma_i + k.D^{-1/2} \qquad (2.16)$$

where;
σ_0 is the yield stress
σ_i is the friction stress (resistance to dislocation movement)
k is the strengthening coefficient
D is the grain size

However, Hall-Petch effect is not necessarily valid for nanostructured materials due to the change in mechanisms of plastic deformation since initiation and movement of dislocations may be prohibited in grains of a nanometric size [5]. Strength and hardness may show different characteristics with Hall-Petch relationship due to new possible mechanisms for nanostructured materials which are grain boundary sliding, diffusional creep along grain boundary and serving of grain boundaries as sources of dislocations [36]. According to Valiev et al. [5] the defect structure of the grain boundaries has also an important role in determining the yield strength with constant grain sizes.

Sedlacek et al. [37] suggested that the formation of subgrains lead to hardening as their boundaries induce long-range internal back stresses in the interior of the subgrains by forcing the mobile dislocations to take a bowed configuration and because smaller subgrains are stronger, they described the phenomenon as size-dependent subgrain hardening.

Kim, Sa, Kim and Yoon [21] used Deformation Mechanism Maps (DMM) represented by grain size vs. strain rate (σ/E) for aluminum to determine the dominant deformation mechanism of ECAP processed and as received aluminum at 523 K. Figure 2.36 shows the Deformation Mechanism Map of Aluminum at 523 K where data points of the unECAPed and ECAPed Al is pointed. They came up with the result that pipe-diffusion controlled by grain boundary sliding is dominant at low strain rates whereas pipe-diffusion controlled dislocation climb creep is the dominant mechanism at higher strain rates. On the other hand; they compared the results with coarse grained unECAPed Al alloy of which the deformation mechanism is pipe-diffusion controlled climb creep at even low strain rates as shown in Figure 2.36. They concluded that the reason of ECAPed alloy having larger ductility values than the unECAPed alloy is due to their deformation mechanism difference between ultra-fine grained and large grained microstructure.

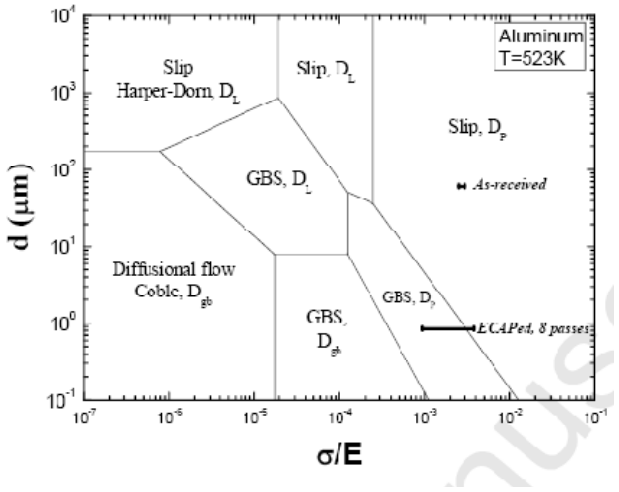

Figure 2.36: Deformation Mechanism Map (DMM) for Al at 523K [21]

2.6.2 Strain Softening

Strength of the metals is known to increase with severe plastic deformation and at a critical strain level it reaches saturation. It is observed in the literature that

[26,14,21,38] further plastic straining results with a decrease in the flow stress introducing the term strain softening. According to Wei et al. [38], this softening behavior is known to occur during hot deformation as a result of dynamic recovery and dynamic recrystallization and they regarded that ultra-fine grains with high angle grain boundaries are more sensitive to temperature at large strains than large grains. Estrin, Toth, Molinari and Brachet [39] developed a hardening model considering this softening behavior as stage III and stage IV hardening where the strain hardening coefficient shows a gradual decrease signifying a saturation of stress at large strains. This decrease is said to be caused by dynamic recovery related to change of the total dislocation density representing a competition between dislocation generation and annihilation processes.

2.6.3 Hardness and Strength

Hardness and strength of the materials is related with the grain size by Hall-Petch equation (Eq. 2.16) and the dislocation density as mentioned previously. Change in the hardness and strength of the materials processed by ECAP and DCAP is represented in the literature in many studies. Examples of these changes will be given in this part:

Tham et al. [26] examined the changes in the hardness of Al-6061 alloy with different ECAP passes (90° die angle, route C) as shown in Figure 2.37. It is seen that there was an increase in hardness of Al-6061 alloy from 40HV to 79 HV of about 95% increase within the first 4 passes of ECAP. After 8 passes of ECAP the hardness increased to 98HV of about 145% of increase and it is related by the authors to the decrease in grain size from 10μm to 1 μm. With further straining with ECAP of 16 passes, a saturation of strengthening and an even decrease in the hardness value with 88HV is observed as seen from the Figure 2.37. Although the grain size is decreased to 1μm to 0.8μm with further ECAP passes after 8 passes, this decrease in hardness after reaching the peak value is thought by the authors to be a result of decreasing density of dislocations inside the subgrains.

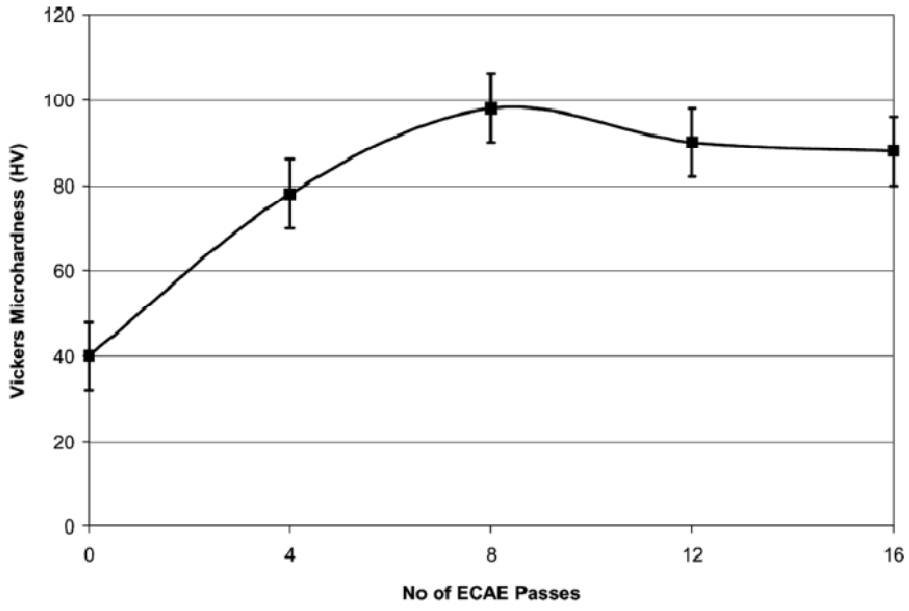

Figure 2.37: Hardness vs. number of ECAP passes [26]

Tensile properties also show a similar trend with hardness values with ECAP passes in their studies. Figure 2.38 and Figure 2.39 illustrate the strain-stress curves of the 6061 alloy and UTS changes of Al-6061 alloy with different ECAP passes respectively. The UTS values of the sample show an increase from 120 MPa to 260 MPa with a 116% increase after 4 passes of ECAP but a decrease in the ductility from 35% to 10% as seen in Figures 2.38 and 2.39. Decrease in ductility is thought by the authors to be caused by the decrease in hardening exponent with increase in accumulated strain. The UTS reaches a peak value of 340 MPa of 183% increase with a ductility of 5% at 8 ECAP passes. Similar to the hardness results UTS values of the alloy with 12 passes of ECAP is decreased to 280 MPa but an increase of the ductility is observed. Finally; researchers obtained an UTS value of 300 MPa and a ductility of 5% in the 16^{th} pass of ECAP.

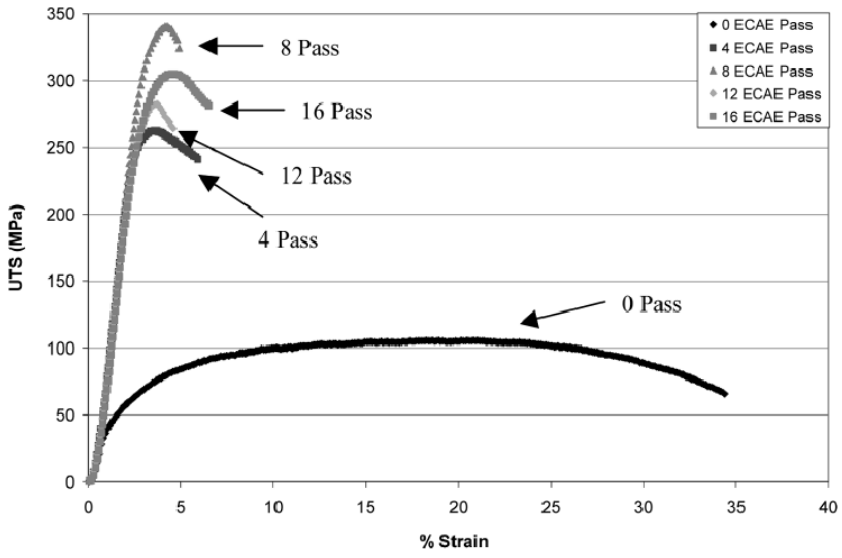

Figure 2.38: Stress-Strain curves with different ECAP passes [26]

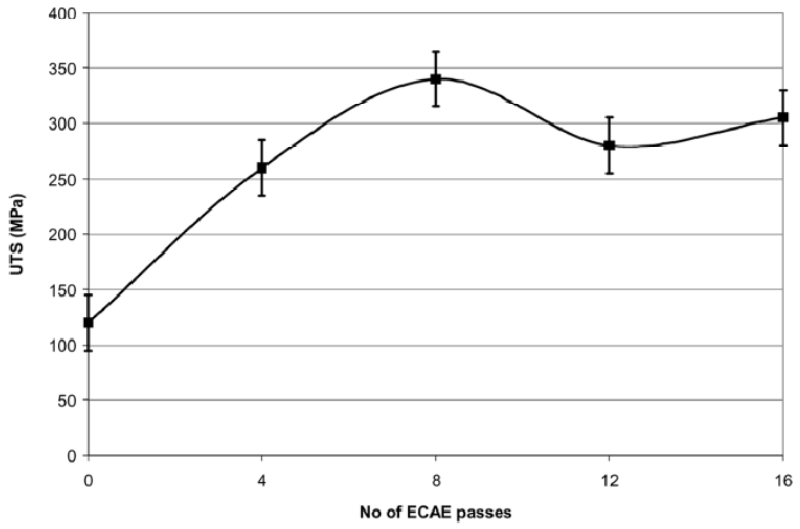

Figure 2.39: UTS vs. number of ECAP passes [26]

Lee et al. [14] had similar results with DCAP processed (120° die angle) Al 1050 alloy. They investigated the variation of microhardness values measured from the side surface of the 1050 alloy strips with increasing DCAP passes up to 12 passes as shown in Figure 2.40. They obtained nearly a 100% increase in microhardness from

~23HV to ~46HV in the first 2 DCAP passes and they observed that the hardness reaches a peak value of ~48HV with 4 DCAP passes. This accumulative strain level is accepted by the authors as critical strain level where the hardness is either saturates or slightly decreases with further straining depending on the processes which can also be seen by the Figure 2.40.

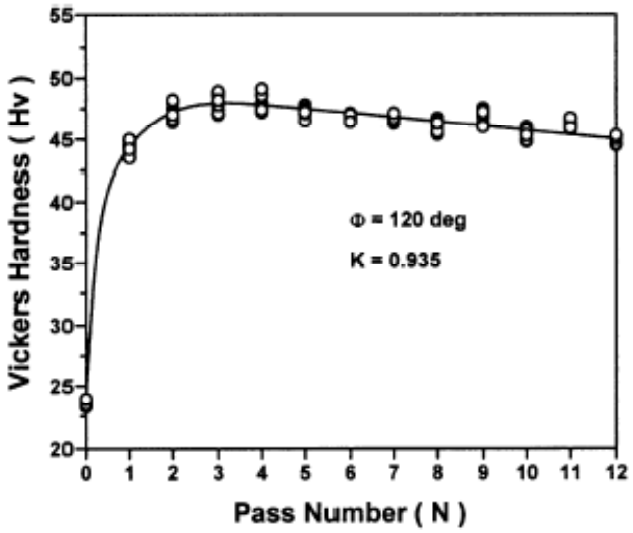

Figure 2.40: Hardness vs. number of DCAP passes of 1050 Al alloy sheets [14]

In another study, a good linear correlation between the yield stress and the hardness of the ECAP processed Al 6061 alloy with different number of passes is observed by Kim et al. [21] as shown in Figure 2.41. Similar trend of an increase in the hardness and the yield strength up to 6 ECAP passes and a decrease after 6 passes up to 12 passes is observed in this study.

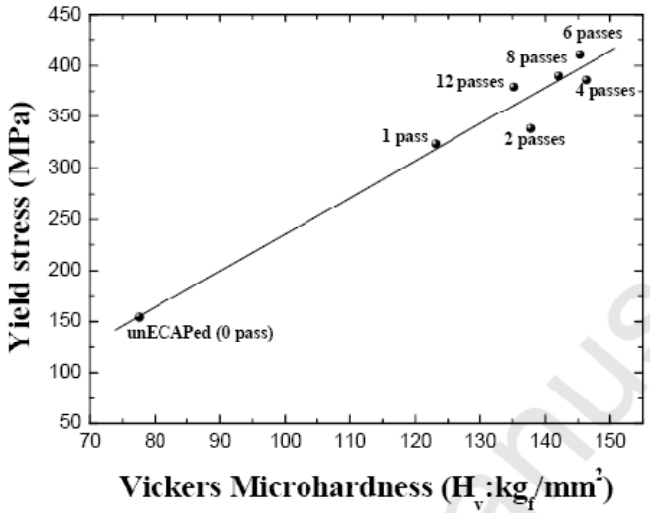

Figure 2.41: Relationship between yield stress and hardness in ECAPed 6061 Al alloy [21]

2.6.4 Ductility

Strength and ductility are important mechanical properties of materials but they have opposing characteristics. Both strong and ductile materials are desired to be produced but it is not so simple. Ductility of the materials is known to decrease with conventional plastic deformation techniques such as rolling and extrusion. It is also mentioned before that with severe plastic deformation processes such as ECAP and DCAP besides the significant increase in strength and hardness of the materials, a decrease in the ductility is observed. But this reduction in the ductility is considered to be less than the conventionally deformed materials [1].

Valiev and Langdon [1] conducted experiments to compare the strength and the ductility of the 3004 Al alloy processed by ECAP and cold-rolling and they showed that these two processes shows different trends in this manner as seen in Figure 2.42. It can be seen that the strength of both processed alloys increases with increasing equivalent strain but the ductility of cold rolled specimen is continually decreases with strain whereas the ductility of the ECAP processed alloy shows no additional reduction after a critical strain level. According to the researchers; the reason behind this phenomenon is regarded as an increase in the fraction of high-angle grain

boundaries with increasing straining causing the change of dominant deformation mechanism which is based on the grain boundary sliding and grain rotation as mentioned previously. Kim et al. [21] also explained this phenomenon as the ductility enhancement is obtained by the contribution of superplastic flow to total deformation due to an increase in subgrain boundary area with subgrain refinement by severe plastic deformation.

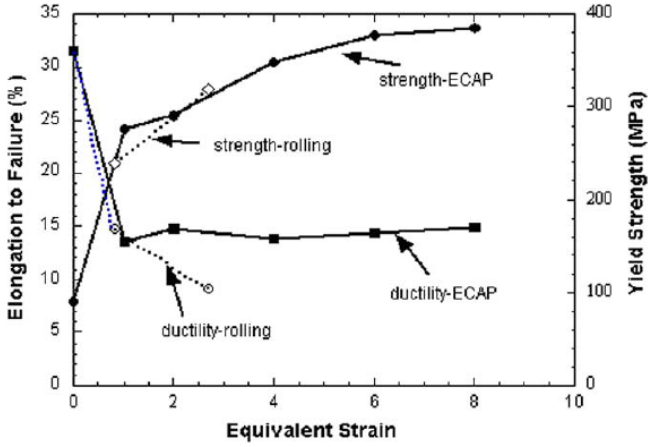

Figure 2.42: Comparison of yield strength and ductility of cold-rolled and ECAPed Al 3004 alloy [1]

2.6.5 Superplasticity

Langdon [40] suggested that the grain boundary sliding is the dominant deformation mechanism process in superplasticity. Superplastic flow of microcrystalline materials is described by the Equation 2.17 [40]:

$$\dot{\varepsilon}_{gbs} = \frac{A_{gbs} D_{gbs} Gb}{kT} \left(\frac{b}{d}\right)^{p_{gbs}} \left(\frac{\sigma}{G}\right)^{n_{gbs}} \qquad (2.17)\ [40]$$

Where $\dot{\varepsilon}_{gbs}$ is the rate of grain boundary sliding (representing the superplasticity), A_{gbs} is a dimensionless constant, D_{gbs} is the coefficient of grain boundary sliding, G is the shear modulus, b is the Burger's vector, k is the Boltzman constant, T is the

testing temperature, d is the grain size, p_{gbs} is the grain size exponent, σ is the flow stress and n_{gbs} is the stress exponent.

According to this equation; Valiev et al. [5] suggested that the superplasticity can be increased at relatively low temperatures and/or high strain rates by decreasing the grain size. In this manner they considered that severe plastic deformation methods for processing nanostructured materials can provide good superplastic properties which can show very high ductilities at definite temperature-strain rate intervals in metallic materials. Komura et al. [41] show that more than 2000% elongations to failure by tensile testing at temperatures of 623 and 723 K can be obtained at a strain rate of $10^{-2}s^{-1}$ with 8 ECAP passed Al–3%Mg–0.2%Sc alloy whereas only 400% tensile elongations can be obtained by cold rolling at those temperatures.

2.6.6 Fatigue

The fatigue life can be divided into two regions of time that crack nucleation time of which the material requires high strength and crack propagation time of which the material requires good ductility to resist them [1]. In this manner, materials processed by SPD techniques such as ECAP and DCAP would possibly have good fatigue properties as a result of having both high strength and good ductility properties in SPD materials as mentioned in previous parts. Valiev and Langdon [1] suggested that the fatigue limit of SPD materials follow the standard Hall-Petch relationship in many alloys and pure metals, so they considered UFG materials should generally show a great potential for an enhancement of the high cycle fatigue life when compared to coarse grained materials. Valiev, Islamgaliev and Alexandrov [5] show this enhancement of fatigue limit as a result of a considerable increase in strength and having good ductility by their study of ECAP processed VT1-0 alloy (Commercial Pure Ti). As shown in the Table 2.2 that includes their data, the fatigue limit of the VT1-0 alloy is increased from 252 MPa to 403 MPa after ECAP with a definite route.

Table 2-2: Mechanical and Fatigue properties of VT1-0 alloy in the as-received state and after ECAP process with two different routes. [5]

No	State	Tensile mechanical properties				Fatigue limit σ_{-1}, MPa	Cyclic endurance, N
		σ_s, MPA	$\sigma_{0,2}$ MPa	δ, %	ψ, %		
1.	As-received state	460	400	27	60	252	4.211
2.	After ECA pressing by route 1	816	800	15,5	60	403	34.504
3.	After ECA pressing by route 2	772	732	14	59	354	17.504

2.6.7 Modeling of Strain Hardening and Softening

Change in the average subgrain size and the evolution of dislocation density both in the cell interiors and cell walls are modeled by Baik, Estrin, Kim and Hellmig [25] which were mentioned in previous section (2.6). A model including both the strain hardening and softening was proposed by combining a similar model called Estrin-Mecking Model and an Avrami-type equation by Wei et al. [38] to compare their experimental results of ECAP or DCAP processed pure Aluminum and Copper. They proposed an alternative approach to UFG metals at large strains by correlating the Estrin-Mecking Model:

According to Estrin-Mecking Model relationship of macroscopic strain and stress is expressed as:

$$\frac{\sigma^2-\hat{\sigma}_s^2}{\sigma_o^2-\hat{\sigma}_s^2} = \exp\left(-\frac{\varepsilon}{\varepsilon_c}\right) \qquad (2.18)\ [38]$$

Where σ_s is the saturation stress, σ_0 is the friction stress, and ε_c is the critical strain at σ_s.

The authors used the expression of saturation stress in the Kocks-Mecking Model as;

$$\hat{\sigma}_s^2 = \alpha G b (k/k_2)^{1/2} \qquad (2.19)\ [38]$$

Where α is a numerical factor, G is the shear modulus, b is the Burger's vector and $k=(bL)^{-1}$ where L is determined by mean free path of dislocations and k_2 is associated with dynamic recovery.

According to the authors; Estrin-Mecking model considers that the dislocation interactions are predominant mechanism but the actions of grain boundaries in UFG materials are also important in establishing hardening-softening models. So they proposed a universal equation of stress and strain characterizing hardening and softening behaviors (Eq. 2.20) at large strains by adopting softening kinetic equations obtained by their literature researches:

$$\sigma = \sigma_s + (\sigma_f - \sigma_s)\exp\left(-r\left(\frac{\varepsilon}{\varepsilon_p}\right)^q\right) \qquad (2.20)\ [38]$$

Where r and q are constants, ε_p is close to the peak strain determined experimentally, σ_f is flow stress predicted by Estrin-Mecking model.

Wei et al. [38] correlated the results of the model proposed with the experimental data obtained in the literature. Figure 2.43 shows that there is a good correlation between the theoretical results with the stress-strain curve representing the softening behavior obtained by Lee et al. [14] who studied DCAP with 1050 Al alloy.

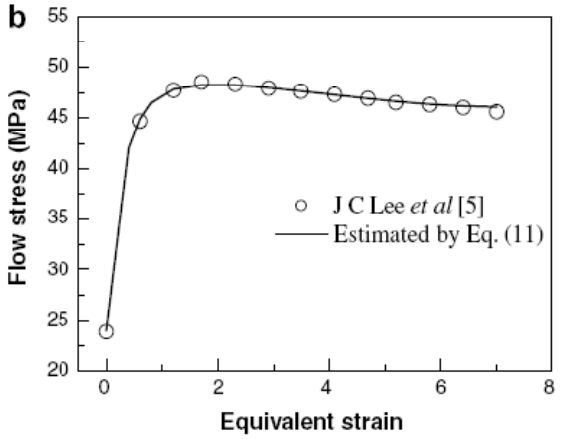

Figure 2.43: Stress-Strain curve estimated by Equation 2.20 and experimental data of Lee et al. [14,38]

2.7 Effect of Post Annealing

Ultra Fine Grained and Nanostructured Materials are non-stable and prone to grain growth at high temperatures of ~$0.4T_m$. Valiev et al. [5] illustrates the stages of structural changes during heating of nanostructured materials by copper example shown in Figure 2.44, including firstly; recovery from non-equilibrium structure by partial annihilation of defects and relaxation of internal elastic stresses, secondly; migration of non-equilibrium grain boundaries resulting in an abnormal grain growth and finally; subsequent normal grain growth of which all these stages are depending on the rate of heating and annealing time.

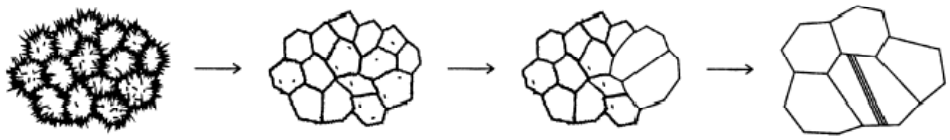

Figure 2.44: Structural evolution during heating of nanostructured copper [5]

Thermal stability of the UFG materials meaning the resistance of the microstructure against grain growth upon annealing becomes important when considering the annealing operations after DCAP or ECAP. Extend of the resistance against grain growth is directly interpreted by the mechanism of the grain growth phenomena in a continuous or discontinuous manner. Continuous grain growth is beneficial for thermal stability which is characterized by a rather slow increase in average subgrain size whereas in discontinuous processes, nucleation and subsequent growth of new strain-free grains is involved which is detrimental for thermal stability [31]. Considering the UFG materials having a microstructure with high angles of misorientations, it can be inferred that the misorientation is very important in terms of thermal stability for ECAP and DCAP processes. Humphreys [42] suggested that the thermal stability of the microstructure is based on the orientation dependence of subgrain boundary energies and mobilities and his analysis showed that the high

angle grain boundaries are much more stable against coarsening than the low angle grain boundaries. Study of Kang et al. [31] about DCAP of AA3103 Al-Mn alloy supports this theory that the higher DCAP passes results in a higher stability during annealing at 300 and 350 C° exhibiting continuous growth whereas lower DCAP passes undergo the discontinuous processes of nucleation and growth similar to the conventionally cold-rolled sheet. This is illustrated in Figure 2.45 showing the evolution of the microhardness of the AA3103 alloy with different numbers of DCAP passes that 6-passes DCAPed and especially 12-passes DCAPed alloys show a slower and more continuous decrease in hardness (by the slopes of the lines) with annealing time at 350 C° than 2-passes DCAPed alloy which is similar to cold rolled specimen.

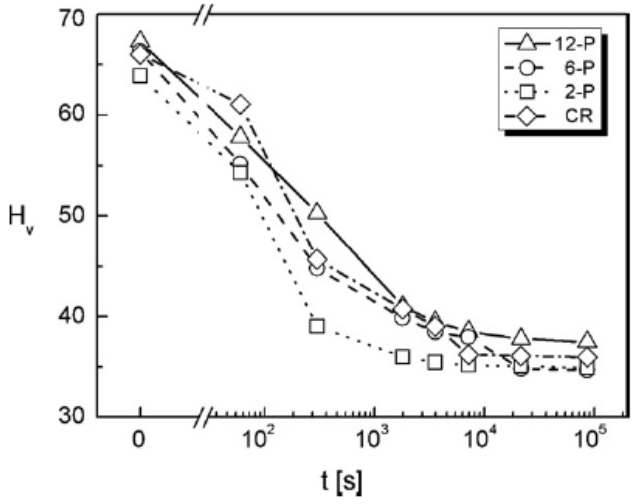

Figure 2.45: Evolution of the hardness values with annealing time t at 350 °C [31]

In contrast, some studies [21,31] indicates that Al alloys with ultra fine grain size may also display discontinuous grain coarsening upon annealing besides continuous process meaning worse thermal stability. This is illustrated by Kim et al. [21] by lower flow stresses obtained with ECAP processed Al 6061 alloy than as pressed Al 6061 alloy at elevated temperatures as seen in Figure 2.46.

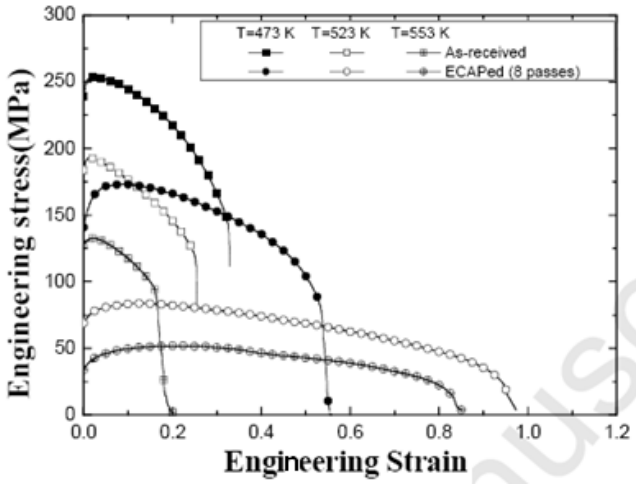

Figure 2.46: Stress-Strain curves for as received and ECAP processed Al 6061 alloy at 473, 523 and 553 K

It is also known that grain growth in pure metals occurs more easily than alloys having precipitates due to restriction effect of precipitates against movement of the grain boundaries [1]. Figure 2.47 and 2.48 obtained from the study of Valiev et al. [1] shows the grain growth effect during annealing of ECAP processed pure Al and Al-1%Mg alloy respectively at temperatures from 423 K to 573K for 1 hour. Both materials show a gradual grain growth with increasing annealing temperatures but it is obvious that the grain sizes are smaller in Al-1%Mg alloy than pure Al at each annealing temperatures. However it is important to note that the pre-annealed grain sizes are ~1.3 μm for pure Al and ~0.45 μm for Al-1%Mg alloy.

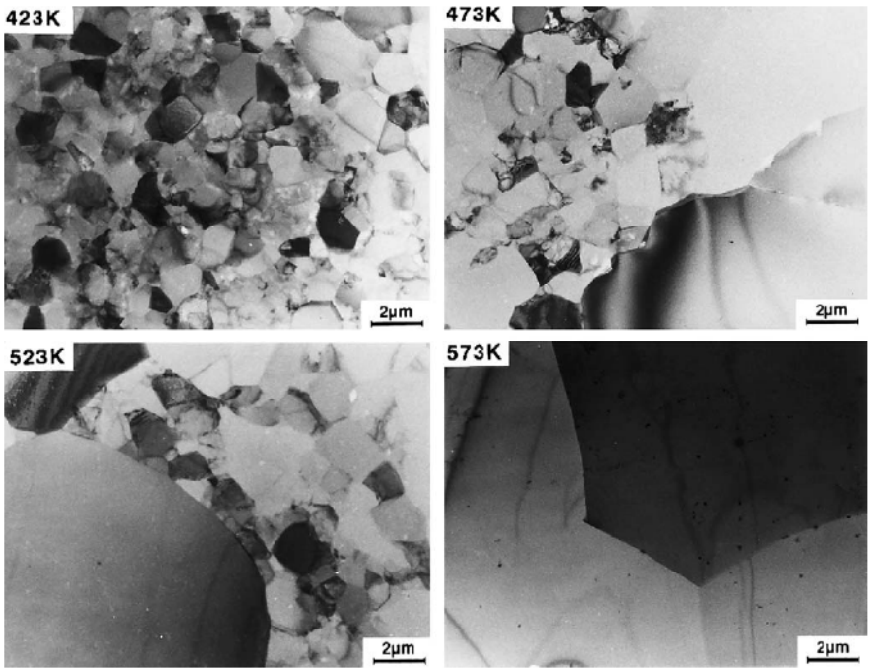

Figure 2.47: Microstructures of pure Al after ECAP and annealing for 1 hour at 423, 473, 523 and 573K [1]

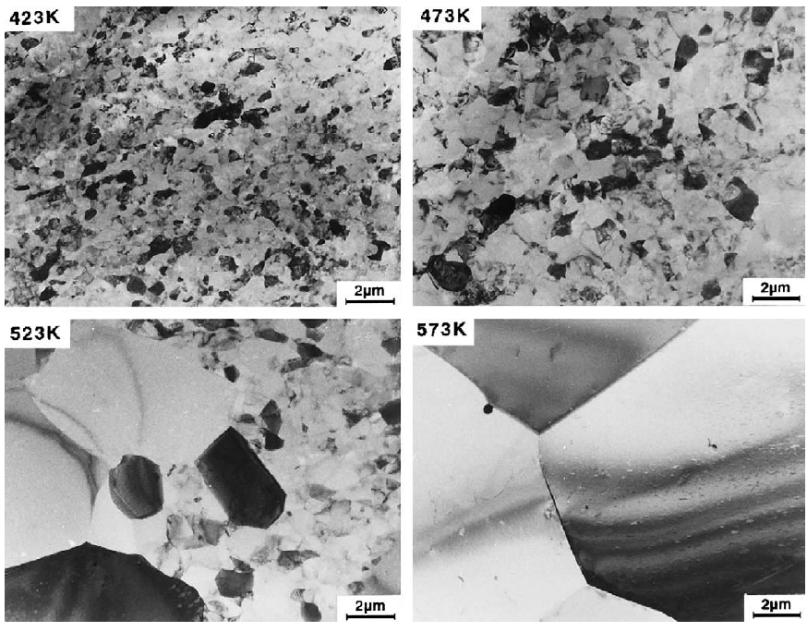

Figure 2.48: Microstructures of Al-1%Mg after ECAP and annealing for 1 hour at 423, 473, 523 and 573K [1]

2.8 Differences between SPD and Conventional Methods

Identical subgrain sizes can be obtained by SPD methods and conventional cold-working techniques like rolling and extrusion. However, SPD techniques have some advantages over conventional methods. The most important characteristics of the SPD methods like ECAP and DCAP are that the geometry of the deformed sample does not change after deformation which provides repetitive pressings and imparting very high strains on the material. This characteristic of the SPD methods brings some differences in the final microstructure of the material between conventionally deformed and severely deformed samples. Subgrain boundaries of severely deformed material evolve into high-angle boundaries by the introduction of very high strains. Finally; arrays of ultrafine grains separated by high-angle boundaries [1] and different subgrain types are produced. This difference in the microstructure between SPD and conventional methods also affect the final mechanical properties of the deformed materials.

Kang et al. [31] compared the microstructural features of conventionally cold rolled and DCAP processed Al-Mn alloy AA 3103 with further annealing. They obtained the TEM micrographs of only cold rolled specimens (58% thickness reduction), 2-passes DCAPed and 12-passes DCAPed specimens after cold rolling are shown in Figure 2.49. It is seen that cold rolled samples have a microstructure with elongated dislocation cells with a high dislocation density in the interiors (Figure 2.49 (a)) and a microstructure of heterogeneously distributed dislocation cells with irregular size and shape exist in 2-passes DCAPed samples (Figure 2.49 (b)) and finally 12-passes DCAPed samples have very fine grains with lower dislocation density in the grain interiors (Figure 2.49 (c)). Also it is observed that the misorientation angle of the 12-passes DCAPed sample is much higher than the 2-passes DCAPed specimen which has slightly higher misorientations than the cold rolled one as shown in Figure 2.50.

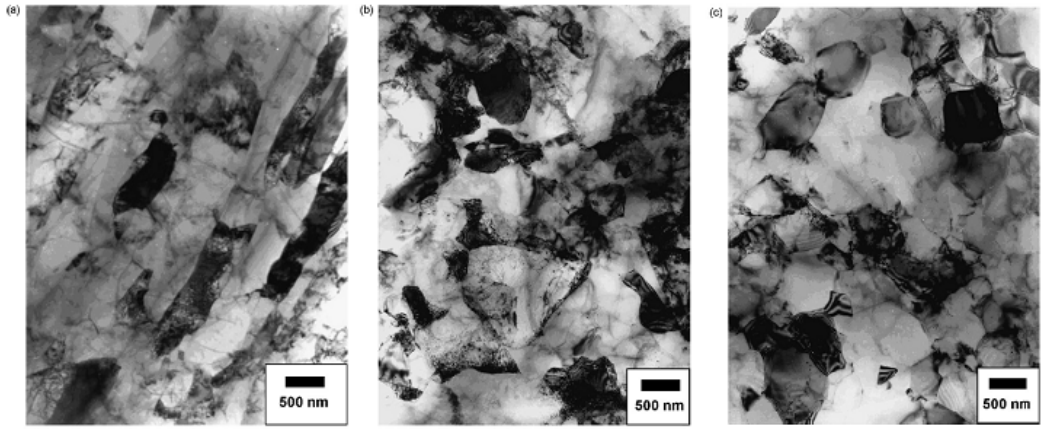

Figure 2.49: TEM micrographs of (a) cold rolled, (b) 2-passes DCAPed, (c) 12-passes DCAPed sample [31]

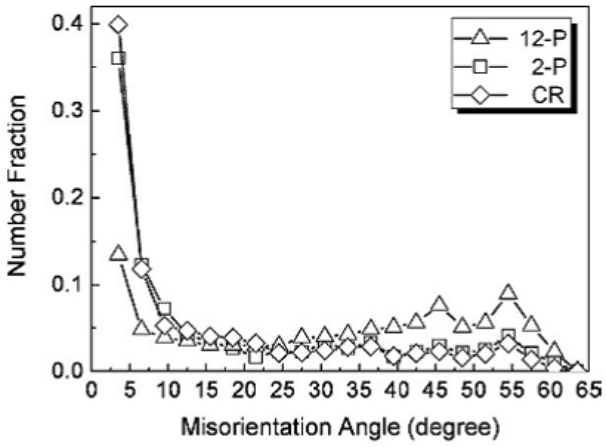

Figure 2.50: Distribution of misorientation angles of cold rolled and DCAP processed samples [31]

As stated above Kang et al. [31] compared the cold rolled samples with cold rolled and further DCAPed samples. As a result, the total strain for cold rolled and DCAPed samples are accumulated for both processes. To make a distinct comparison between DCAP and cold rolling process it would be better to investigate samples that are subjected to annealing operation in order to obtain fully recrystallized grains prior to both processes. In this manner, Lee et al. [14] compared the microstructural

features of the samples as a function of total accumulated strain calculated both for cold rolling and DCAP processes as given in Table 2.3.

Table 2-3: Reduction in thickness for cold rolling and the number of DCAP passages with related strain values [14]

Rolling	57% (1.0)	77% (1.7)	83% (2.1)	90% (2.7)	94% (3.2)
DCAP	$N = 1$ (0.6)	$N = 2$ (1.2)	$N = 3$ (1.7)	$N = 5$ (2.9)	$N = 50$ (29.0)

According to their study, microstructural features of cold rolled and DCAPed specimens do not show significant differences up to a critical accumulative strain value of ε=~2. After this critical strain value, cells with new type of boundaries begin to appear, UFG structure with boundaries of high angles of misorientations and a decreased dislocation density inside the grains are observed in DCAPed samples as explained in Section 2.5 in detail. In addition, cell sizes are observed to be gradually increased at high strains of ε=~30 in DCAPed samples. Cold rolled specimens are observed to have a microstructure of cells having relatively thick boundaries with irregular shapes and a decreased dislocation density inside the grains. Also the misorientation of the boundaries are observed to remained low when compared with the cell boundaries of the DCAPed sample supporting the idea of producing UFG structure by cold rolling is not possible.

Authors also compared the hardness variations as a function of effective strains of DCAPed and cold rolled samples. To make a direct comparison of the hardening behaviors exhibited via cold rolling and DCAP, hardness vs. effective strain of two techniques were graphed as seen in Figure 2.51. According to their study; two different regions were observed in terms of hardening behaviors; region A where an abrupt increase in the hardness takes place and region B where the hardness either saturates or slightly decreases depending on the processes. Both processes show a

similar trend of increasing hardness with increasing strain up to ε=~2 in the region A and maximum hardness obtained by DCAP was measured to be ~94% of the cold rolling process. In the region B where the strains are larger than ε=~2, hardness of the DCAPed sample is observed to be gradually decreased to ~83% of the cold rolled one up to a strain of ε=~58 which is correlated with the increase in the grain size observed in region B by the authors. Hardness of the cold rolled sample was observed to remain constant which is considered by the authors to be due to the equal rates of dynamic recovery and work hardening.

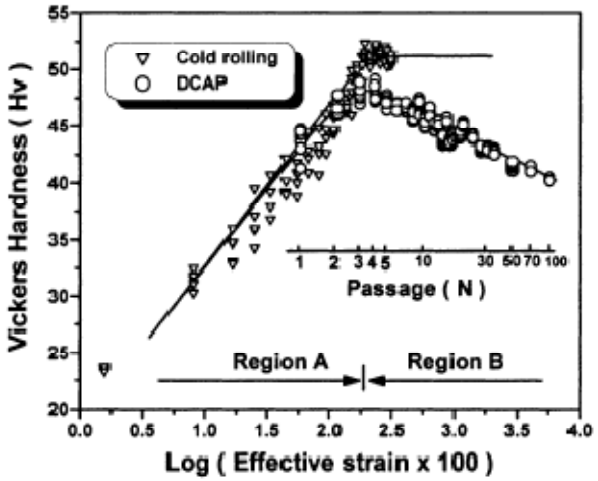

Figure 2.51: Variations in the hardness as a function of the effective strain [14]

2.9 Texture Evolution of Al after ECAP – DCAP

It is known that the texture evolution during deformation is strongly dependent on the type of the deformation. As a result SPD techniques like ECAP and DCAP are very significant in controlling of texture evolution of Aluminum alloys and other metals when considering that the texture has an important effect on many properties of metals like formability. There are many studies [16,18,43,44,45] about the texture evolution of Aluminum alloys during ECAP and DCAP.

Han et al. [43] studied the effect of initial textures on texture evolution of 1050 Al alloy during DCAP. According to their texture data obtained by X-Ray diffractometry and simulations; DCAP promoted a simultaneous formation of <111>//ND texture and the {001}<110> rotated cube texture regardless of the initial texture, but major texture types formed during DCAP were observed to be affected by initial textures where <110>//ND texture promoted the formation of the <111>//ND texture and {100}<100> cube texture promoted the formation of the {100}<110> rotated cube texture. Formation of <111>//ND textures by shear deformation in Al alloys are very important in terms of formability because it exhibits the highest plastic strain ratio while the planar anisotropy of these textures is the lowest. However, {100}<110> rotated cube texture exhibits a low plastic strain ratio and high planar anisotropy so DCAP of Al sheets with the {100}<100> cube texture which transforms to {100}<110> rotated cube texture should be avoided [43].

Effect of accumulative strain by DCAP on texture evolution of Al 1050 alloy is investigated by Han, Oh, Lee [45] up to $\varepsilon=\sim 19$ (N=32). They obtained {111} pole figures of Al samples before and after DCAP up to 32 passes as shown in Figure 2.52 with X-Ray diffractometer by using Schultz Reflection Method. It is observed that the overall intensity of the textures gradually decreases with increasing pass number and after 10 DCAP passes no significant change in the texture intensity is observed. They ended up with the result that the intensities of the texture depend on the accumulative strain imposed on the alloy for low applied strain values ($\varepsilon < 5.8$).

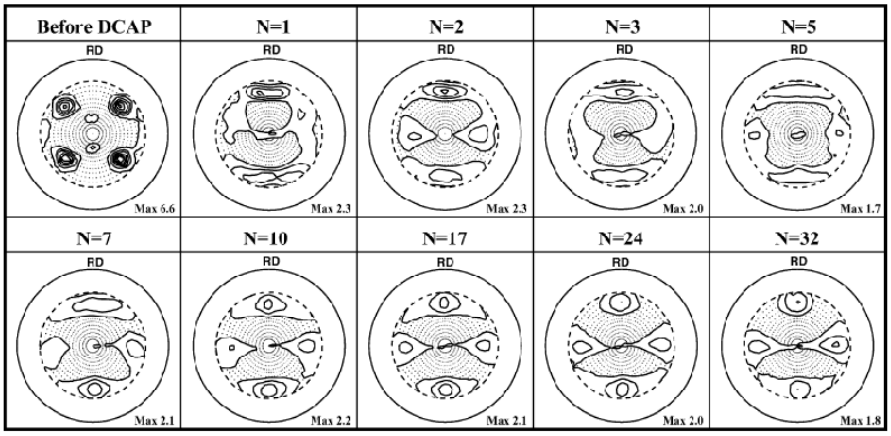

Figure 2.52: {111} pole figures obtained from the sample before and after DCAP (N=1-32) [45]

Lee, Seok, Han, Chung [44] recorded the XRD results obtained from the annealed and DCAPed samples as shown in Figure 2.53. It can be seen that {200} was the dominant peak in the annealed raw sample, while a strong {111} peak was observed in DCAPed sample showing the change in texture caused mainly by slip band formation inside the grains.

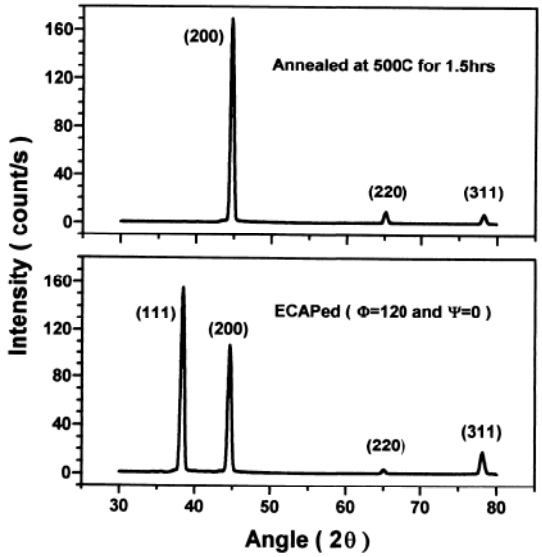

Figure 2.53: XRD results of annealed (above) and DCAPed (below) 1050 Al alloy strip [44]

The R-value (Lankford Parameter) is also an important parameter in terms of measuring the formability which controls the strain between the strain in plane and the strain normal to the plane that larger R value is desired for achieving optimum formability [16]. It is known that BCC metals have high R values whereas FCC metals have R values less than 1 and R values of most commercial Al alloys lies between 0.7 and 0.8 [44] which is a big disadvantage for forming operations. R-values are calculated by popLA program [16,44] using the data of pole figures obtained by X-Ray texture goniometer and average R-values ($\bar{R}$) are calculated by Equation 2.21 to make a comparison between deformed and annealed samples. Jining et al. [16] showed the effect of temperature in texture formation of 6061 Aluminum sheet during DCAP by evaluating the R-values of samples DCAPed at RT, 353K, 433K and 513 K as shown in Figure 2.54. It can be seen that the sample DCAPed at 513K have higher R-value of 1.5 than other samples due to <111>//ND fiber formation [16]. Lee et al. [44] calculated the average R-values of DCAPed and annealed 1050 Al alloy and they graphed the results as a function of angle to the rolling direction as seen in Figure 2.55. The R-values of the DCAPed sample is observed to be relatively higher than the annealed one. Both studies show that the DCAP process can be used to control the texture of aluminum sheet to enhance the formability.

$$\bar{R} = \frac{R_0+2R_{45}+R_{90}}{4} \qquad (2.21)$$

Where $\bar{R}$ is the average R-value and R_0, R_{45}, R_{90} are the R values calculated by popLA program in directions of 0°, 45° and 90° respectively with respect to the longitudinal direction of DCAP sample.

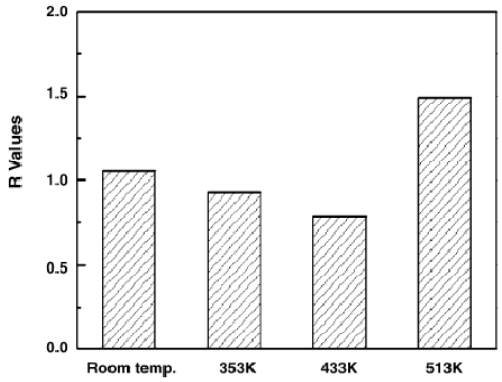

Figure 2.54: Variation of R-values as a function of DCAP temperatures [16]

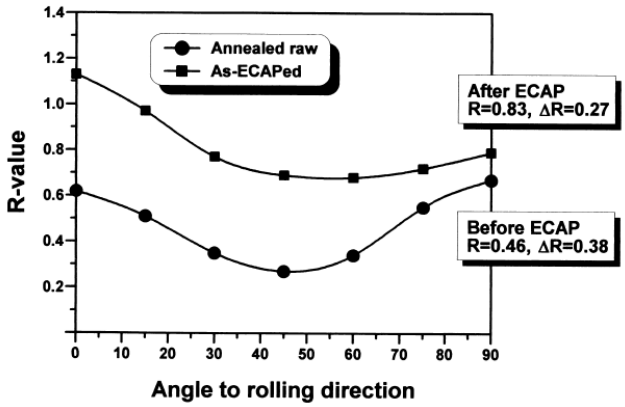

Figure 2.55: Variations of R-values as a function of the angle to the rolling direction [44].

2.10 FEM analysis of DCAP

Optimal processing parameters in DCAP can be determined by making many experimental studies. However, it is not possible to take extensive information about the material flow properties, deformation modes, texture evolution and process parameters. Therefore, numerical simulations by Finite Element Modeling (FEM) are used to predict these parameters and properties with less effort and money. In this context, many FEM studies about DCAP are made [17,18,19].

Zu et al. [19] simulated DCAP process for pure aluminum of which the finite element model is shown in Figure 2.56 (a). Effect of DCAP process parameters such as die channel angle, die outer channel angle and friction to the material properties is predicted by finding the effective strain distribution for different parts of the material as shown in Figure 2.56 (b) and for different process times. These topics were mentioned in Part 2.4 in detail.

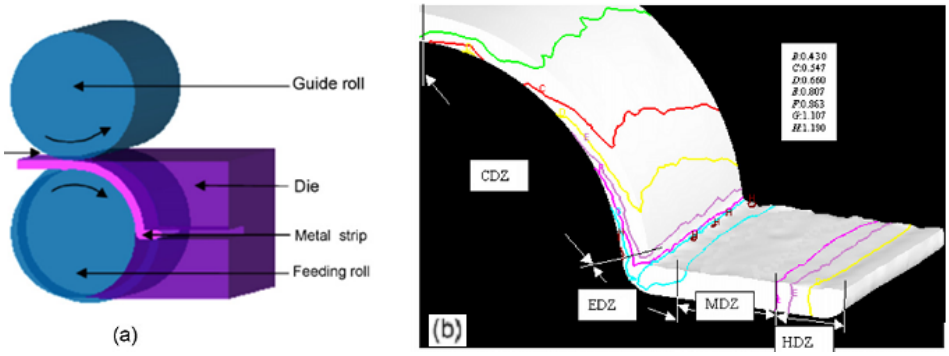

Figure 2.56: (a) The FEM for the simulation of the DCAP Process (b) Effective strain distribution for different parts of the sheet during DCAP Process [19]

It is also mentioned in Part 2.4 that the deformation history of the DCAP process is based on a complex mode of deformation consisting of tension, compression as well as shear and the reason behind why the thicknesses of the inlet and outlet channels are not similar to each other is explained by the FEM results. Suh et al. [18] and Han et al. [17] obtained many FEM data about DCAP and ECAP which provide a basis of these explanations. They investigated the shape change of a tracer element selected from the middle of the specimen thickness during DCAP as shown in Figure 2.57. Deformation period is considered to start at point A, continue at deformation region marked as point B and is completed at point C. An example is shown in Figure 2.58 that how the shape changes of the tracer element occurs during DCAP and ECAP at different time steps of their FEM analysis.

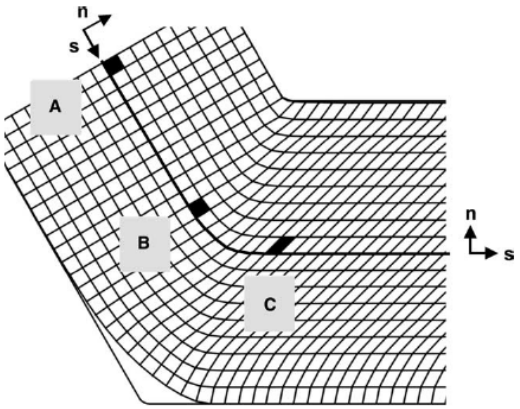

Figure 2.57: Evolution of the shape of a tracer element during DCAP [17]

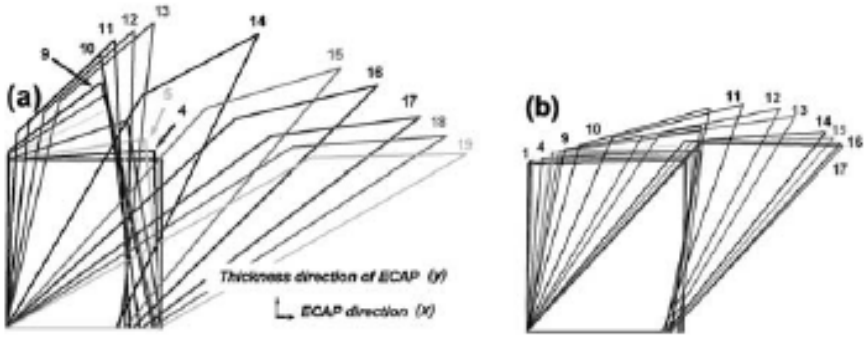

Figure 2.58: Evolution of an initially square cell grid during (a) ECAP (Φ=90°) and (b) DCAP (Φ =120°) by increasing time steps [18]

During these FEM studies in literature some assumptions is made in order to simplify and speed up the analysis. First of all, two dimensional problem was considered in those studies because plane strain condition is satisfied in DCAP process. The sheet material is considered as elasto-plastic [17,18] or rigid-plastic [19] with an equivalent relationship between stress and effective strain. The DCAP die is assumed to be rigid and with a constant friction factor or frictionless. Other parameters such as strain rate sensitivity, temperature, strain hardening exponent is considered as constant.

2.11 Other Property Changes During DCAP

It is shown in many studies that Severe Plastic Deformation techniques have an improving effect to the conventional mechanical properties such as strength, hardness and fatigue life. However, there are not many detailed studies about the effect of SPD techniques to other physical properties in the literature. It is known that some physical properties such as magnetic properties, diffusivity, optical properties, corrosion properties and electrical properties of metallic materials may show different characteristics after severe plastic deformation [5].

Valiev et al. [5] investigated these differences of coarse-grained and nanostructured materials. According to their studies; magnetic characteristics of nanostructured magnetic materials show dissimilarities with coarse grained materials. They also investigated a contributing effect of SPD to optical properties of semiconductors in terms of to luminescence observed in the visible area of spectrum. Finally; they observed from the literature that different corrosion characteristics are obtained in UFG or nanostructured materials and they ended up with the result by their studies that a better and more homogeneous corrosion behavior is obtained in UFG materials when compared to conventional materials for practical applications. It is also stated in some articles [3,26] that enhanced electrical properties can be obtained in UFG or nanostructured materials although it is thought that electrical conductivity is decreased by conventional cold deformation of Aluminum due to hindering of the passage of electrons through the distorted lattice structure [46]. By the production of UFG structure, DCAP can be considered to be effective on these properties.

CHAPTER III

EXPERIMENTAL PROCEDURE

3.1 General

The effect of severe plastic deformation by Dissimilar Channel Angular Pressing (DCAP) method to the mechanical and physical properties of 6061 Al alloy was investigated in this experimental study. In this context; hardness and tensile tests, characterization tests by SEM, TEM, Optical microscope and XRD investigations and electrical resistivity tests were made.

3.2 Material Used

Usage of aluminum alloys is widely spreading in many fields of structural applications like; automotive and aerospace industries and aluminum alloys are even started to be replaced with steel in many fields of these applications. One of the aims of this study is to expand the potential usage of aluminum alloys in these applications by improving the properties of aluminum alloys by strengthening mechanisms of severe plastic deformation. This is why aluminum was selected for severe plastic deformation trials in this thesis study.

Commercially available 6061 aluminum alloy, a typical Al-Mg-Si alloy, was used as deforming material in this study. 6xxx series aluminum alloys have been extensively used in deformation applications such as extrusion, rolling or drawing because of their high ductility and formability properties besides their medium strength, weldability, corrosion resistance and low cost when compared to other aluminum alloys [47]. The 6061 aluminum alloy was used in this study for its high ductility and heat treating capacity. It is most commonly available; precipitation hardening aluminum alloy in different pre-tempering grades such as 6061-O (solutionized),

6061-T6 (solutionized and artificially aged), 6061-T4 (solutionized and naturally aged). The chemical composition of the 6061 aluminum alloy is given in Table 3.1:

Table 3-1: Chemical composition of the 6061 aluminum alloy

Si	Mg	Fe	Cu	Mn	Cr	Zn	Ti	Al
0.4 – 0.8	0.8-1.2	0.7 (Max)	0.15-0.4	0.15 (Max)	0.04 – 0.35	0.25 (Max)	0.15 (Max)	Remains

6061 Al alloy sheets were delivered in T6 condition with 1000 x 600 x 2 mm dimensions from Turkish Aerospace Industry (TAI) Inc.

3.3 Mechanical and Thermal Preparation of Samples Before DCAP

Samples were cut into strips of different configurations with 300 mm – 120 mm – 2 mm dimensions as seen in Figure 3.1 and 155mm x 27.5mm x 2mm dimensions to be able to feed into DCAP die.

Figure 3.1: Al 6061 Specimen before DCAP

The strips were annealed at 415˚C for 3 hours in order to have a homogeneous and fully recrystallized microstructure. Softening of the alloy is also important for easy passage from DCAP die and in order to have larger numbers of passes.

Each sample was marked with different designation indicating the sample and trial numbers for discerning that the specimens are objected how many passes and DCAPed at which trial. Also two different surfaces of each sample were marked as ‘a side’ and ‘b side’ to determine the homogeneity of the deformation by observing the property changes between the lower and upper parts of the samples.

Some of the DCAP processed samples were also annealed at 200°C and 350°C for 1 hour to see the effect of post-annealing to mechanical properties with hardness tests.

3.4 Dissimilar Channel Angular Pressing (DCAP) Process

A laboratory scale DCAP system had been designed and improved (Figure 3.2) by the thesis studies of Göktürk Emre Uzunçakmak [2] and Evren TAN in Metallurgical and Materials Engineering Department – METU in the scope of a TÜBİTAK project - 105M174.

Figure 3.2: Present DCAP Device in METU

This device was used for Dissimilar Channel Angular Pressing of Al-6061 specimens in this thesis study. The thickness of the specimens were 2.0 mm whereas the inlet channel thickness of the DCAP die was 1.9 mm in order to prevent material to escape from the roll gap and due to the increase in the final thickness after deformation. The specimens were fed through the rolls, then they pass through the die and finally taken from the channel. The rolls had been designed by Uzunçakmak, Tan and Gür [48] with different characteristics and after many trials they were taken the final condition with patterned parts of 14 mm wide in the middle part and of 17 mm at the sides as shown in Figure 3.3 to be able to push the specimen and to create sufficient frictional force on the surface of specimen to enable easy passage through the die. After specimens leave the die, they have patterned parts as expected as seen in Figure 3.4.

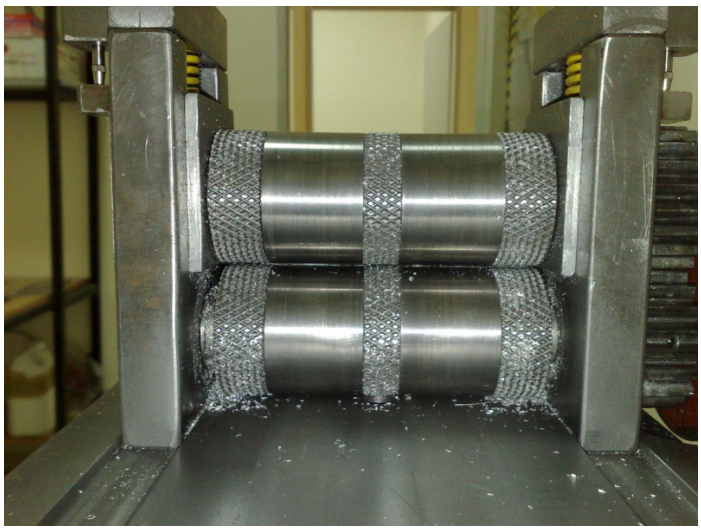

Figure 3.3: Rolls of the DCAP Device

Figure 3.4: Specimens after DCAP Process

The technical drawing of the side cross-section of DCAP device is shown in Figure 3.5. The DCAP process parameters are as follows:

- Roll diameter: 50 mm
- Thickness of the sheet material: 2 mm
- Thickness of the inlet channel: 1.9 mm
- Thickness of the outlet channel: 2.0 mm
- Die Channel Angle: 120°
- Die Outer Corner Angle: 0°
- Feeding speed: 20 cm/min
- Forming Temperature: Room Temperature

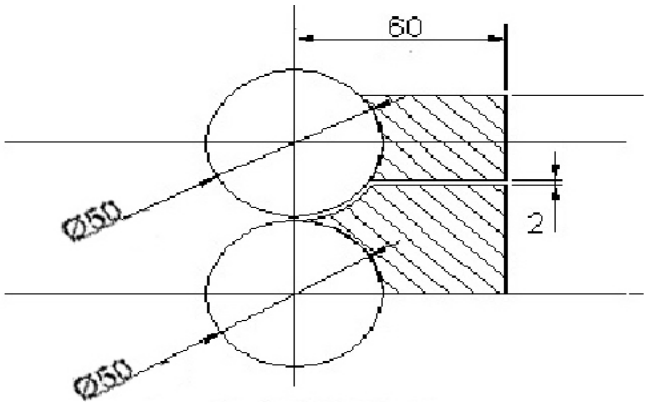

Figure 3.5: Side cross-section of the DCAP device [48]

Many different trials were made by using DCAP device. Samples with different numbers of DCAP passes obtained by those trials up to 5 passes. Samples were fed through the rolls with route A, without changing the feeding direction between subsequent passes and with route C for once with 2-passes DCAPed alloy; changing the feeding direction before 2nd DCAP pass.

3.5 Characterization Tests

Different characterization tests have been undertaken for the as-received (No DCAP pass) and DCAPed samples for different numbers of DCAP passes from different parts of the DCAPed strips as shown in Figure 3.6.

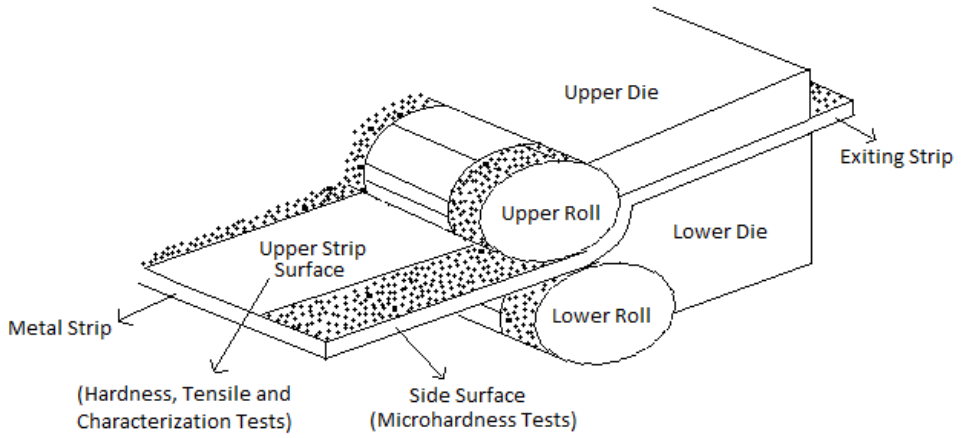

Figure 3.6: Schematic of the strip showing where the mechanical tests applied

As-received and DCAPed samples with different numbers of passes were cut into small pieces and mounted together that the side surfaces parallel to the deformation direction of each specimen stayed at the surface of the mounted sample as shown in Figure 3.7 for microhardness measurements, optical and SEM investigations to be able to observe the grain shape change.

Figure 3.7: Mounted Specimens

3.5.1 Hardness Tests

Macrohardness measurements were made from as-received samples and from the upper and lower strip surfaces of DCAPed samples for different numbers of passes. The measurements were performed with HB 2.5 tip at 15.6 kg by Struers hardness testing device. Hardness results of the samples were obtained by taking average values of at least four different hardness measurements from each specimen.

Microhardness tests were performed with HV tip at 500 gr by Schimadzu microhardness testing device from side surfaces of the samples. Measurements were taken through at least two different profiles along the side thickness (close to upper surface, from the middle and close to lower surface) of each specimen to be able to see the change in hardness values at different parts of the specimen and the average microhardness of each specimen by taking average of all these hardness values.

All hardness test results were converted into MPa unit.

3.5.2 Tensile Tests

Tensile specimens of the as-received and DCAPed samples were machined parallel to the rolling direction in the dimensions shown in Figure 3.8 according to ASTM

B557M-02a standards. Tensile tests were performed with Schimadzu Digital mechanical testing machine at a strain rate of 1.0 mm/min with a load cell of 30 kN at room temperature. Related stress-strain diagrams of each specimen were obtained by the conversion of the load-displacement data. Two tensile tests were conducted for each DCAP passes and the average values were taken for discussions.

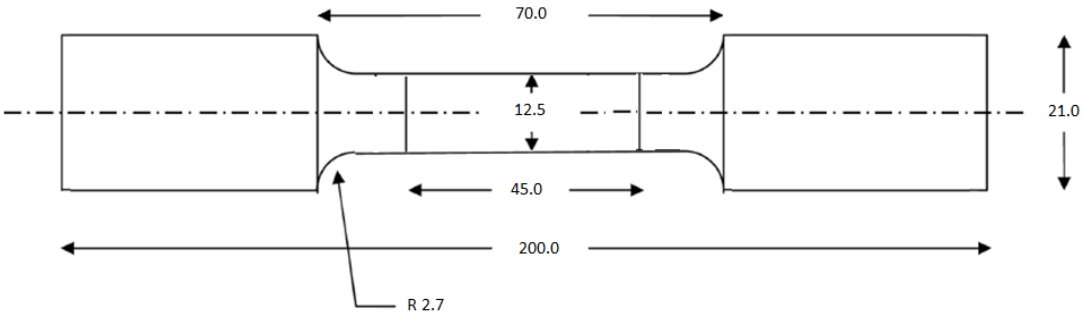

Figure 3.8: Dimensions of the tensile specimen (mm)

3.5.3 Microstructural Investigations

To take optical images from the side surfaces of the samples, they were mechanically grinded, polished and etched by different types of etchants such as Weck's double reagent ($KMnO_4$ - NaOH), Keller's reagent (HF-HCl-HNO_3) and Barker's solution (HBF_4, Electrolytic Etching) and finally they were investigated under optical microscope.

SEM (Scanning Electron Microscope) images were taken by 'JEOL JSM 6400 Electron Microscope with equipped with EDS analysis system' located in Metallurgical and Materials Engineering Department – METU as shown in Figure 3.9. The images were taken from the side surfaces of the as-received and DCAPed samples (2 and 4 passed) which were etched with Weck's Double Reagent. The chemical compositions of the matrixes and the intermetallics were also analyzed by the EDS analysis of the samples.

Figure 3.9: Scanning Electron Microscope Laboratory in METU

For preparation of TEM (Transmission Electron Microscope) investigations from the as-received and DCAPed samples (1, 2 and 5 passed), some of the samples were annealed at two different temperatures of 200°C and 350°C for 1 hour in order to observe clear images free from dislocations. The specimens were then cut into small strips and thinned from 2 mm to ~500 μm by grinding and then punched into 3mm diameter discs and finally mechanically thinned to ~200 μm by further grinding. Resting sample preparation and TEM investigation processes were conducted in TÜBİTAK Marmara Research Center (MAM) – Materials Institude – Gebze. The samples were electrolytically polished with an electrolyte of 25% nitric acid + 75% methanol solution at about –33°C with 15-20V in Struers-Tenupol-5 Double Jet Electropolisher. Then the disks having 3 mm diameter were thinned down to ~60 μm and then the center was further thinned to ~5μm with Gatan 656 Dimple Grinder. Finally, samples were ion polished at 5kV and 3kV until the transparent area is obtained. JEOL 2100 Transmission Electron Microscope 2100 (LaB6 filament) operated at 200 kV was used for analysis.

Firstly, TEM investigations were made from the 2-passes DCAPed samples which are as deformed, annealed at 200°C and annealed at 300°C. 2-passes DCAPed samples which were annealed at 350°C gives the clearest TEM images although a little grain growth was observed. Remaining TEM investigations were conducted with the 1 and 5-passes DCAPed samples annealed only at 350°C.

3.5.4 XRD Analysis

XRD measurements were made with as-received and DCAPed samples to evaluate the subgrain sizes and observe the differences between the intensities of the samples. The measurements are conducted by Rigaku 2200/PC X-Ray Diffractometer located in Metallurgical and Materials Engineering Department - METU from 0° to 90° of 2θ angles with a scanning speed of 2 degrees per minute and Cu target with a wavelength of $\lambda_{Cu\ K\alpha}$ = 1.54056 Å. The subgrain sizes were evaluated by using Scherrer Formula (Equation 3.1):

$$t = \frac{0.9\lambda}{B\cos\theta} \qquad (3.1)\ [49]$$

Where t is the subgrain size, λ is the wavelength of the radiation, B is the structural broadening value obtained by Full Width at Half Maximum intensity (FWHM) values in radians and finally θ is the half of the diffraction angle.

Structural Broadening (B) was obtained by subtracting the instrumental broadening of the reference specimen (coarse grained as-received sample) (B_S) from measured breadth including structural and instrumental broadening (B_M) (DCAPed samples) by Equation 3.2:

$$B^2 = B_M^2 - B_S^2 \qquad (3.2)$$

Subgrain size and intensity change determinations were made for each peak obtained by XRD diffractogrammes.

3.5.5 Electrical Resistivity Tests

Electrical resistivity measurements of the samples were conducted by nano-voltmeter device located in Central Laboratory – METU with wire shaped specimens of ~1 mm to ~2 mm cross-section as shown in Figure 3.10. This geometric form was obtained by wire-erosion device in 'Mensan Kalıp & Tel Erezyon San. Tic. Ltd. Şti.' – Ostim/ANKARA.

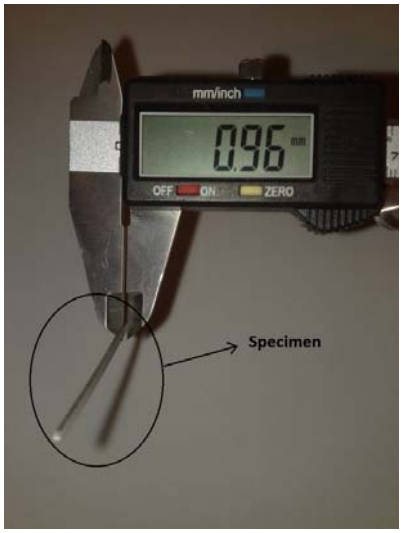

Figure 3.10: Electrical resistivity specimen obtained by wire-erosion technique

Electrical resistivity values (ρ) were calculated by Equation 3.3; where R is the electrical resistance (Ohm), A is the cross-sectional area (m^2) and L is the length (m). Because nano-voltmeter device gives resistance values in micro-ohm measure it was required to have very small cross-sections and long wires in order to obtain accurate results. Also producing the wire form by mechanical cutting could damage the microstructural features affecting the final properties. This is why wire-erosion technique was used for obtaining wires.

$$\rho = R\frac{A}{L} \qquad (3.3)$$

CHAPTER IV

RESULTS AND DISCUSSION

4.1 General

Changes in the mechanical and physical properties as a function of DCAP passes were examined in order to observe the effect of strain accumulated on the 6061 Al alloy strip. The values of the accumulated effective strain were calculated by Equation 2.5 [14] and the values are given in Table 4.1 with DCAP parameters used in this study.

Table 4-1: Effective strain values corresponding to different DCAP passes

N	1	2	3	4	5
ε	0.6	1.2	1.8	2.4	3.0

4.2 Hardness results

Average macrohardness results of the samples which were taken from the upper and lower strip surfaces and the microhardness results which were taken from side surfaces of the samples versus number of DCAP passes and effective strain values are given in Figure 4.1. Macrohardness of the samples showed an increase from ~395 MPa to ~551 MPa after the first DCAP pass and reached the highest value of ~558 MPa after second DCAP pass which corresponds to ~41 % increase. The hardness of the samples did not show any increase, and even slightly decreased up to 5 DCAP passes. The microhardness of the samples increased from ~390 MPa to ~461 MPa

after first DCAP passage and increased to ~477 MPa after second pass (~22% increase). However, after the third DCAP passage, the hardness decreased to ~467 MPa and did not change with further passes.

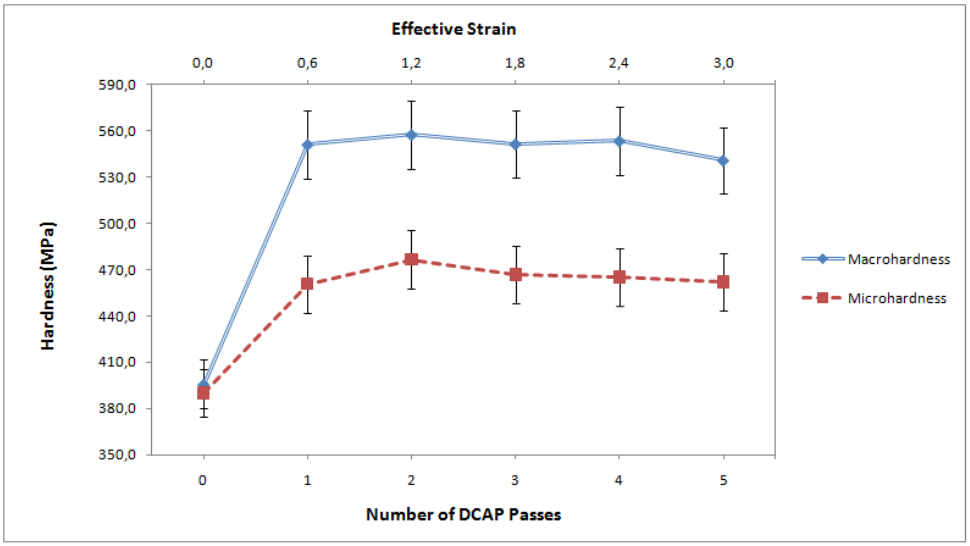

Figure 4.1: Change in the hardness values with DCAP passes

Both macrohardness and microhardness results show a similar trend with DCAP passes. Hardness of the samples reaches the highest values after the second DCAP pass and reaches saturation at this strain level of 1.2. This increase in the hardness is considered to be caused by the formation of the Ultra Fine Grain (UFG) structure and increase in the dislocation density. With further straining, hardness of the strip remains constant due to the saturation of the strengthening and even decreases due to the softening caused by the annihilation of the dislocations inside the subgrains. Those results are consistent with literature results mentioned in section 2.6 [14,26,39]. The accumulative strain value of 1.2 with corresponding 2 DCAP passes is accepted as the critical strain level of which Lee et al. [14] suggested where the hardness saturates or slightly decreases with further straining.

Differences between hardness values of the upper and lower strip surfaces were also determined by macrohardness and microhardness measurements to predict the strain

distribution along the thickness of the strip. Hardness results taken from the upper and lower surfaces of the strips and microhardness measurements taken from the side surface of the strips at regions close to the upper and lower surfaces as a function of DCAP pass numbers are given in Figure 4.2. It can be seen that average hardness of the lower surfaces is a bit higher than the upper strip surfaces from the first DCAP pass up to fourth DCAP pass. Reason of this difference is thought to be caused by the higher strain accumulation in the lower surface due to the die geometry. After fourth DCAP passes average hardness of the upper surface reaches and exceeds the average hardness of the lower surface due to the changes in the dislocation behaviors.

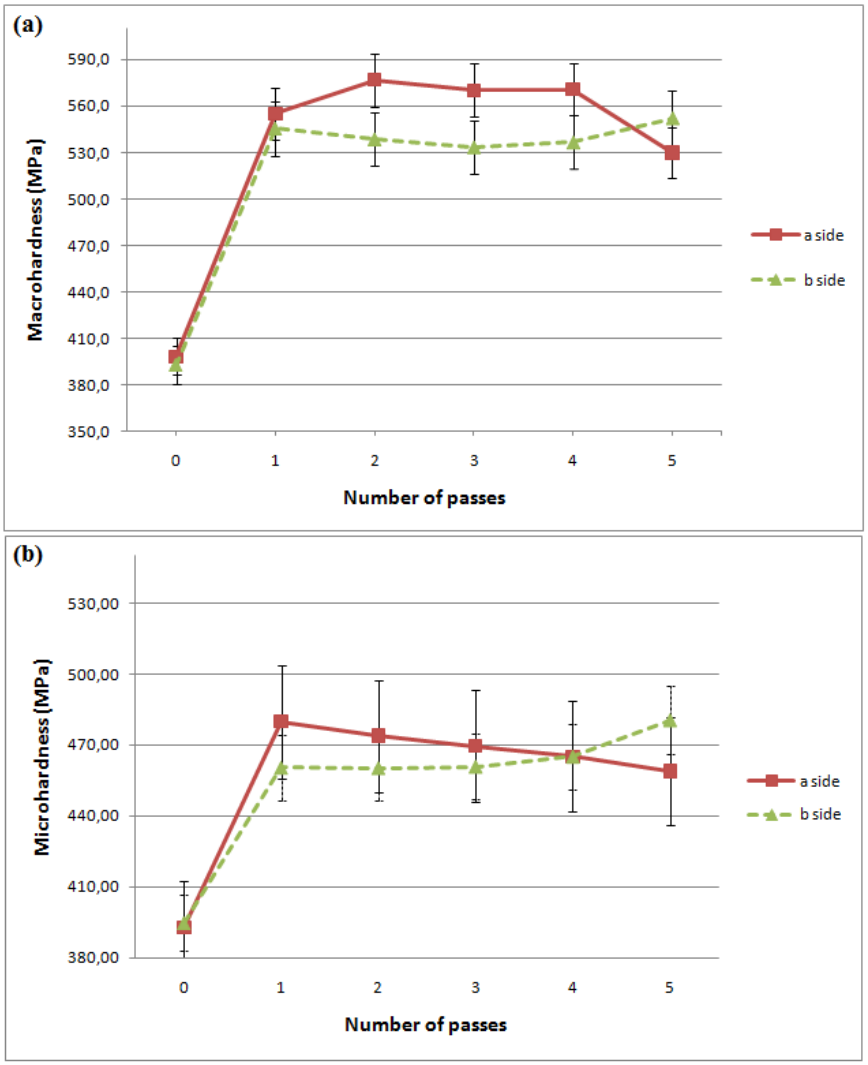

Figure 4.2: (a) Macrohardness values of the upper and lower surfaces (b) Microhardness values taken from the regions close to the upper and lower surfaces at the side surface

Although there seems a difference between the upper and lower strip surfaces, it would be wrong to say that there is a significant difference. Microhardness measurements taken from the side surface as a profile along the thickness as shown in Figure 4.3 indicates that the hardness does not change dramatically along the profile thickness. This result is consistent with the literature results obtained by Finite Element Modelling (FEM) studies of Xu, Zhao, Ren and Guan [19] indicating

that the distribution of the effective strain is uniform through the thickness of the DCAPed sheet as mentioned in Part 2.4.3.

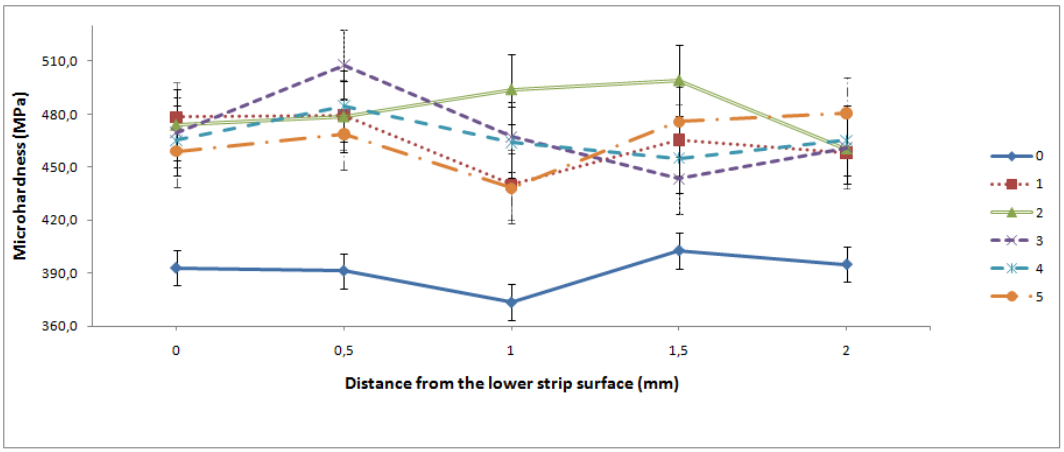

Figure 4.3: Microhardness measurements taken from the side surface as a profile along the thickness

Effect of passing route to the DCAP process was also investigated by macrohardness and microhardness measurements taken from two different samples with 2 DCAP passes of route A (no change in the direction of feeding in the second DCAP pass) and route C (changing the direction of feeding by 180 ^{0} in the second DCAP pass). Figure 4.4 shows the results of the hardness measurements taken from the upper and lower surfaces (macrohardness) and regions close to the upper and lower surfaces on the side surfaces (microhardness) of samples of sample no '3' and sample no '7' that processed by route A and route C respectively. Although; sample '7' shows a more homogeneous distribution along thickness, there is no significant difference between the upper and lower surfaces of the sample '3' which is also obvious by the error percentages shown. These data lead the result that the passing route of DCAP process has no considerable effect on the mechanical properties of the samples in consistence with literature.

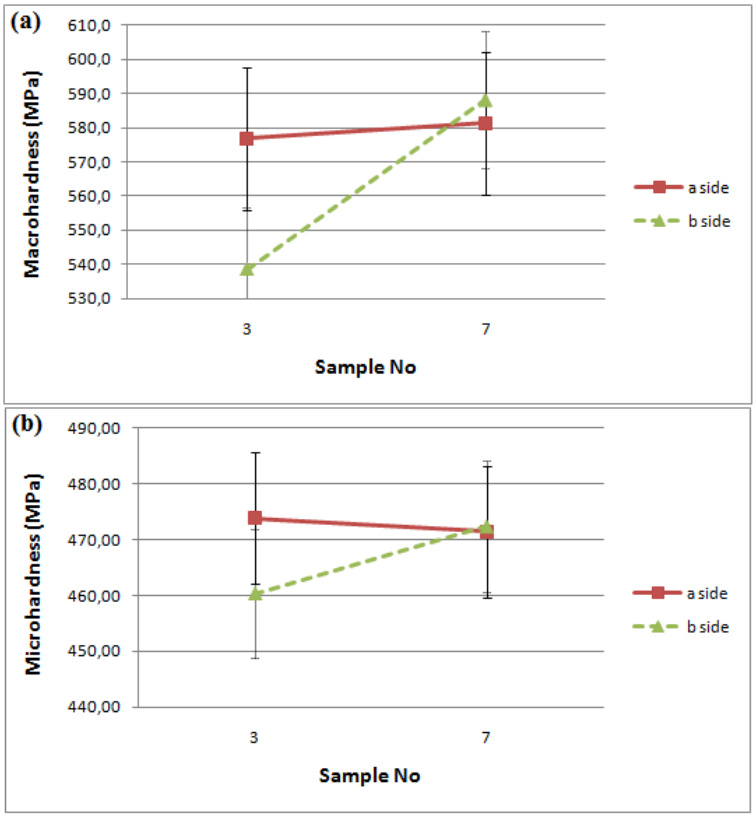

Figure 4.4: (a) Macrohardness measurements taken from the upper and lower surfaces (b) Microhardness measurements taken from the regions close to the upper and lower surfaces on the side surfaces of samples with sample no '3' and sample no '7' that processed by route A and route C respectively

Effect of post annealing was also investigated by macrohardness tests with 1, 2 and 5-passes DCAPed samples. The results are shown in Figure 4.5. Annealing at 200°C for 1 hour does not make any difference in the hardness values of any sample. It is thought that there is no any recrystallization or grain growth at this annealing temperature but only there may be a little decrease in the dislocation density as a result of dynamic recovery. However, annealing at 350°C for 1 hour resulted with a decrease in the hardness of the DCAPed samples due to the grain growth besides the decrease in the dislocation density. Hardness of the single pass DCAPed strips decreased by ~15% whereas the hardness of the 2 and 5-passes DCAPed strips decreased by ~20%. It was mentioned in Section 2.7 that there are two different approaches in the literature about the thermal stability of the UFG materials. Results

obtained by this study are consistent with the study of Kim et al. [21]. Kang et al. [31] also suggests that the Al alloys with ultra fine grain size may also display discontinuous grain coarsening upon annealing besides continuous process meaning worse thermal stability than coarse grained materials. The increased driving force due to the increased dislocation density might possibly leads to more grain coarsening when the boundary structure has not totally converted to UFG boundary.

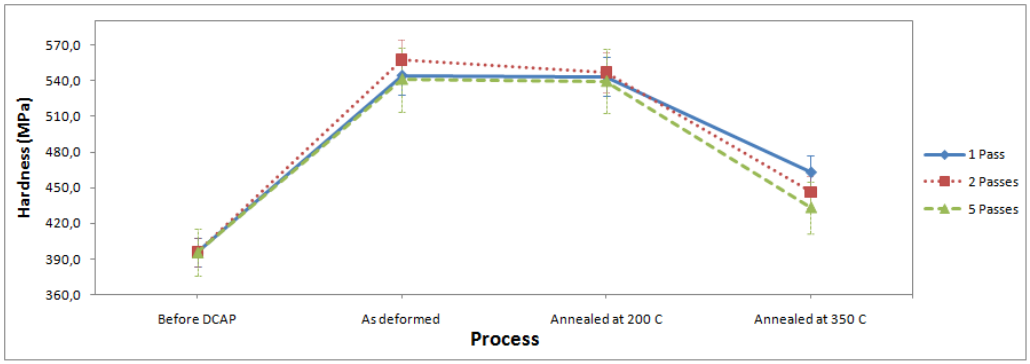

Figure 4.5: Macrohardness results of the 1, 2 and 5-passes DCAPed samples after two different annealing temperatures

4.3 Tensile Results

Stress and strain relationship of the as-received and DCAPed samples were obtained by tensile testing. Stress-strain diagrams of one of the samples from different trials for each DCAP pass number are given in Figure 4.6. It can be roughly seen that the as-received sample shows a more ductile behavior when compared with DCAP processed samples and the strength of the samples were observed to be increased with DCAP process.

Yield strength of the as-received sample was increased by ~52% from 114 MPa to 173 MPa in the first DCAP pass and increased by ~65% to 189 MPa after the second DCAP pass as seen in figure 4.7. Also it can be seen that the yield strength remained at the neighborhood of 180 MPa and even decreased a little after 3rd pass up to 5 passes. Finally, it can be said that the yield strength reaches its maximum at about

189 MPa for the strain level of 1.2 after the second DCAP pass. These results are consistent with hardness test results in terms of the changes in mechanical behaviors. Similar to hardness results, the reason of this behavior is caused from the decrease in the grain size due to the formation of the Ultra Fine Grain (UFG) structure and increase in the dislocation density. These results are also consistent with literature results [14,21,26] mentioned in part 2.6.3.

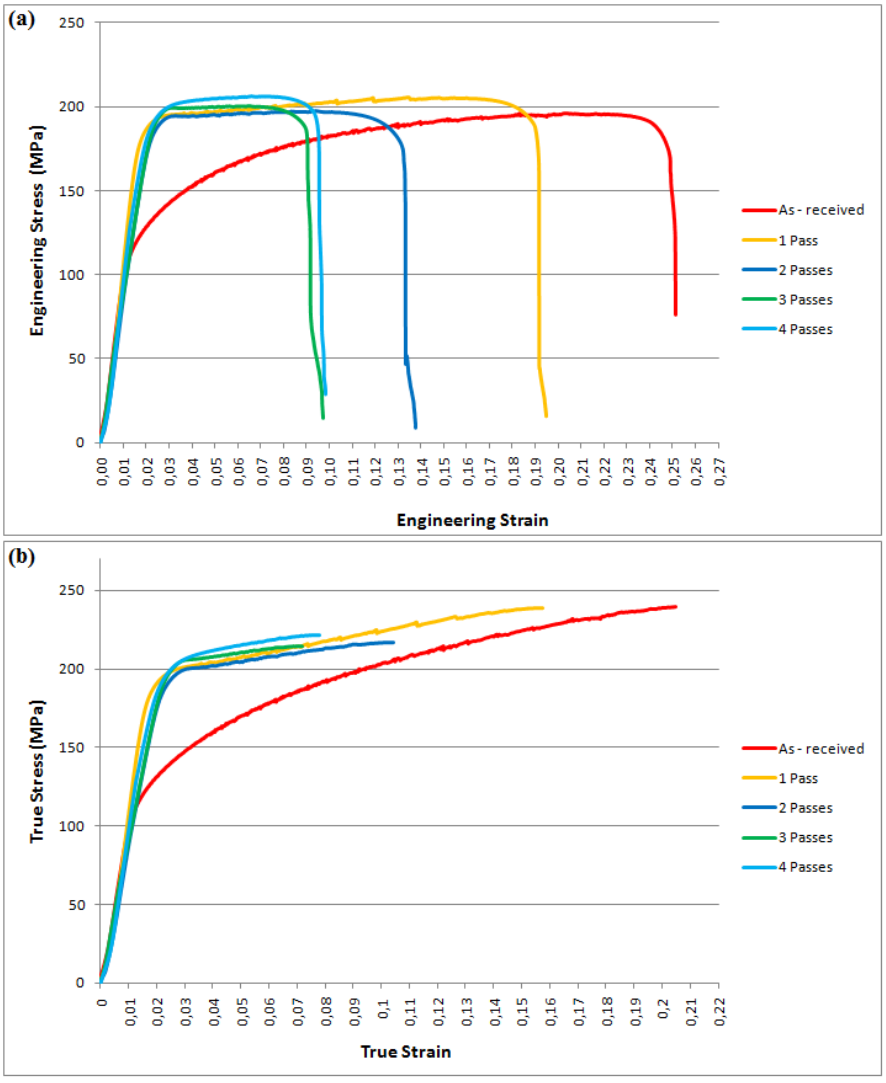

Figure 4.6: (a) Engineering (b) True Stress – Strain diagrams of the as-received and DCAPed samples

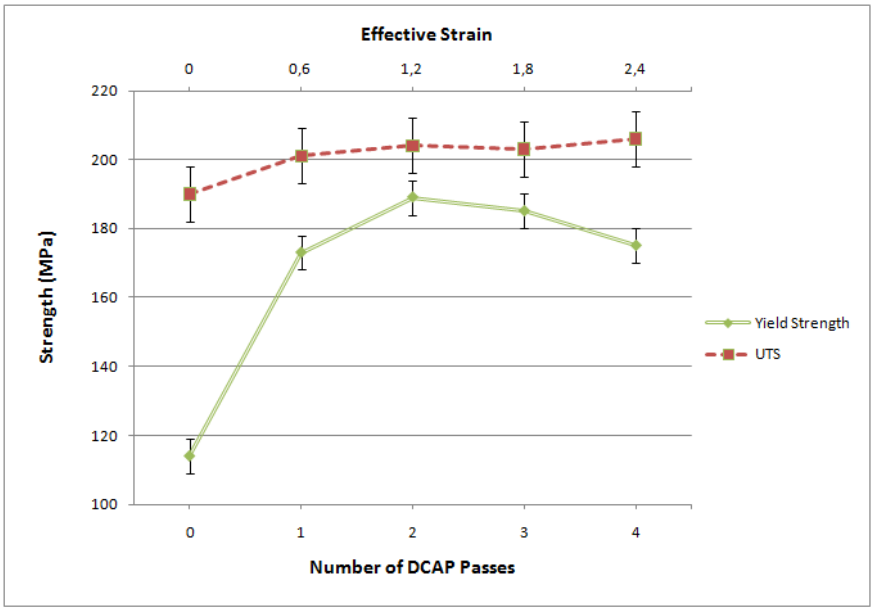

Figure 4.7: Variation of the Yield Strength and UTS values of the as-received and DCAPed samples

UTS of the samples shows similar behavior with yield strength but have lower increasing rates as seen in Figure 4.7. UTS increase in the first two passes is ~7 % whereas it was ~65 % in yield strength as an indication of little work hardening as a result of saturation of the dislocation density at small strains and observing the stress peaks at low strains. This is caused by the fast dynamic recovery rate which increases with dislocation density as Uzunçakmak [2] explained in his study.

Ductility of the metals is known to be decreased with plastic deformation but literature results [1,21] show that the ductility of severely deformed materials decreases less when compared with conventional materials. Results obtained by this study shows that the ductility values were decreased with increasing DCAP passes up to 3 passes with inversely proportional by strength values as seen by the stress – strain diagrams of the samples in Figure 4.6. However, it is required to obtain much more equivalent strain values by higher DCAP passes in order to compare the ductility-strength relationship of conventional deformation methods and DCAP method.

4.4 XRD Results

By the X-Ray Diffraction (XRD) analysis of the as-received and DCAP processed samples peaks from (111), (200), (220), (311) and (222) planes of Aluminum were obtained. It was observed that the (200) plane is the dominant peak in the diffraction pattern of the samples. It is stated in the literature that the selection of the peaks at higher diffraction angles provides more precise results about the stress condition and (311) plane is recommended for observations about aluminum alloys [50].

When comparing the intensities and broadenings of the (200) peaks and the (311) peaks of the samples; it was observed that the as-received sample have the highest intensity as seen in Figure 4.8. The intensity of the single pass DCAPed sample decreased, and the 2-passes DCAPed sample had the lowest intensity. The intensity values in the XRD results of the samples with further DCAP passes was observed to fluctuate between the intensity values of the as-received and 2-passes DCAPed sample. This fluctuation in the peak intensity of (200) peak is related with the changes in the peak broadening caused from the fluctuations in the dislocation densities of the samples, UFG production and other parameters. It is known that the material parameters like dislocation density, grain size, defects and local stresses affect the X-Ray structural analysis in terms peak broadening, peak position and integral intensity of the background [5,49,51,52]. As a result, the dislocation density of the DCAP processed samples are thought to be increased up to 2 passes, and then, has a fluctuating trend up to 5 DCAP passes.

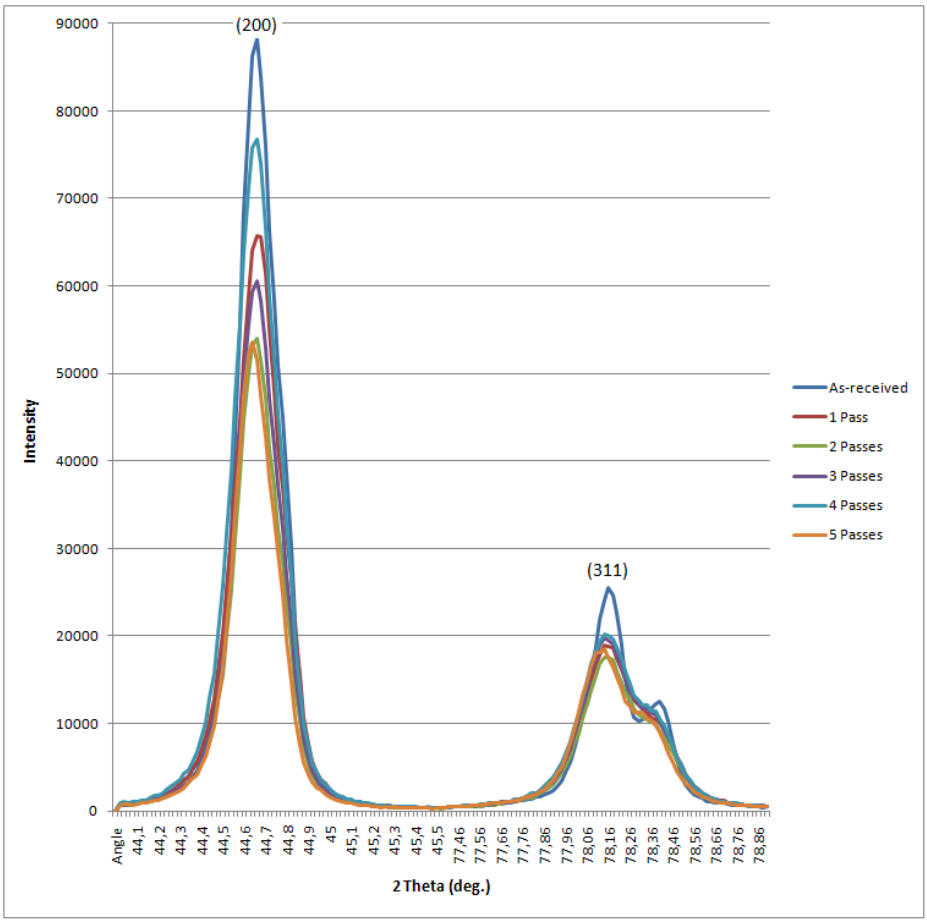

Figure 4.8: XRD Pattern of the samples from (200) and (311) peaks

Intensity and the broadening values of some peaks does not show the similar behavior with (200) and (311) peaks. For example, the intensity of the (111) peak for the 3-passes DCAPed sample is the highest whereas the intensity is lower for the as-received and 1 pass DCAPed sample as shown in Figure 4.9. It was mentioned in section 2.9 that the Severe Plastic Deformation affects the texture evolution. This is why DCAP processed samples have higher intensities in some peaks and it is thought that the DCAP process can be used for texture control. It is also possible to say that increase in the (111) peak intensity by DCAP process indicates the crystallographic restructuring of {111} planes by considering the major slip plane of FCC metals is {111} as stated in the literature [44].

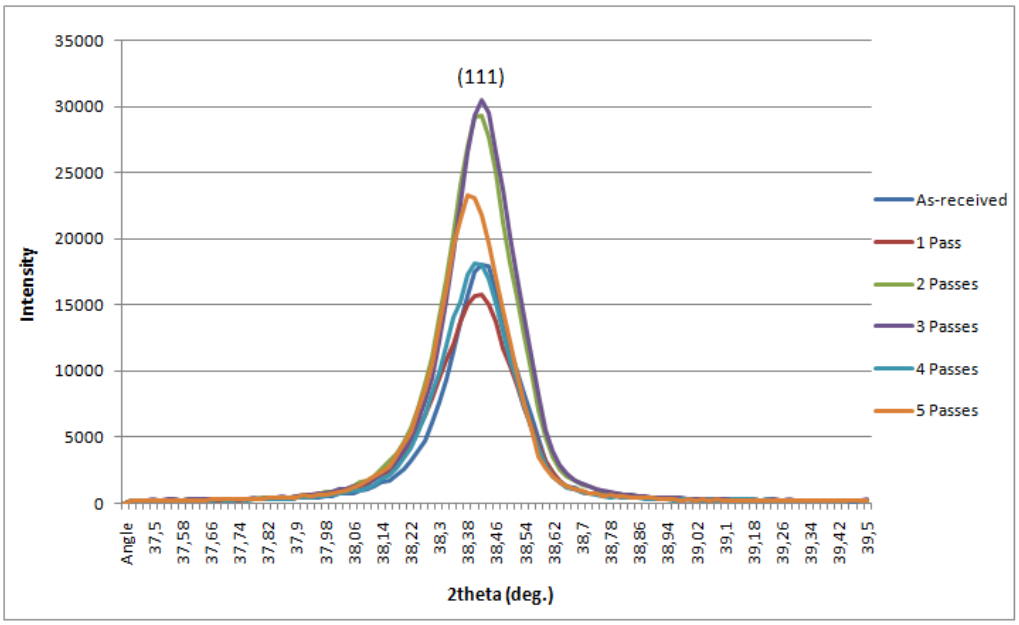

Figure 4.9: XRD Pattern of the samples from (111) peak

Another important data obtained by XRD analysis is the subgrain sizes of the deformed samples by taking the broadening value of the as-received sample as reference value. Subgrain sizes of the DCAP processed samples was calculated as 42 nm by Scherrer Formula for (311) peak. Broadening values and so the subgrain sizes was obtained as the same value for each DCAPed sample. However, those results were not accurate enough to talk about the correct grain sizes [5]. The accurate results can be obtained by TEM analysis which will be mentioned in the next part.

4.5 Microstructure Investigation Results

4.5.1 Optical Microscope

Optical images of the samples were taken in order to have an idea about the initial grain size of the as-received sample and to see the effect of deformation to the grain structure and direction of shearing in the DCAPed specimens. However, optical images of the grain structure could not be obtained although many types of etchants were tried. Figure 4.10 shows the optical image of the sample etched by Keller's reagent where the grains could not be distinguished.

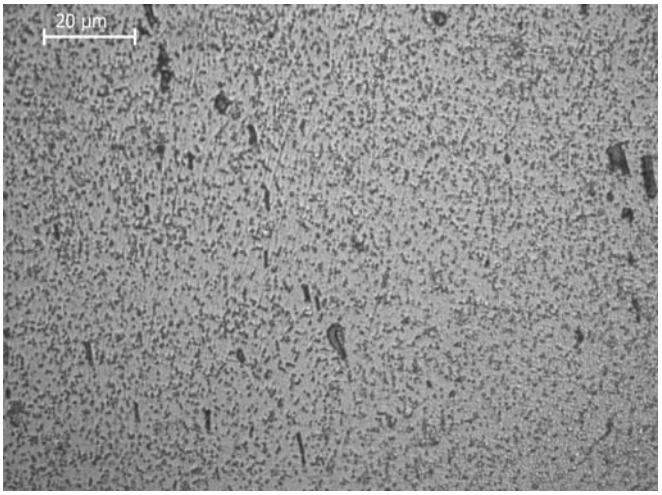

Figure 4.10: Optical image of the as-received sample etched by Keller's reagent

4.5.2 SEM

Grain structure of the as-received and DCAPed samples were observed by the SEM analysis even though the grains were not so clear. The microstructures of the samples are given in Figure 4.11. By the grain size measurements; it was obtained that the grain size of the as-received sample is ~5.2 µm. Grain size was decreased to ~4.2 µm after 2 DCAP passes and ~2.9 µm after 4 DCAP passes. This decrease in the grain size is caused by the deformation process but it is not possible to observe the ultra fine grain evolution by this magnification. To be able to observe the evolution of subgrains with high angle boundaries TEM investigations are needed.

Beside the decrease in the grain size of the DCAPed samples, it was also observed that the grains of DCAP processed samples are more equiaxed and homogeneous in terms of size and shape. The standard deviation of the grain sizes of the as-received sample was calculated as 2.1 µm whereas it was calculated for 2 and 4-passes DCAPed samples as 1.5 and 1.1 µm respectively indicating the degree of homogeneity.

The possible differences between the effect of DCAP routes to the deformation structure was also investigated by comparing the SEM images of the 2-passes

DCAPed samples with route A and route C as seen in Figure 4.11 (c) and (d) respectively. Although, the sample DCAPed by route C have more homogeneous grain size and shape (standard deviation of the grain size is 1.1 μm), there is no any significant difference between the deformation structures between these routes at this strain level observed by the images. This result also supports the idea that the passing route of DCAP process has no considerable effect on the final properties of the samples which is consistent with the hardness results.

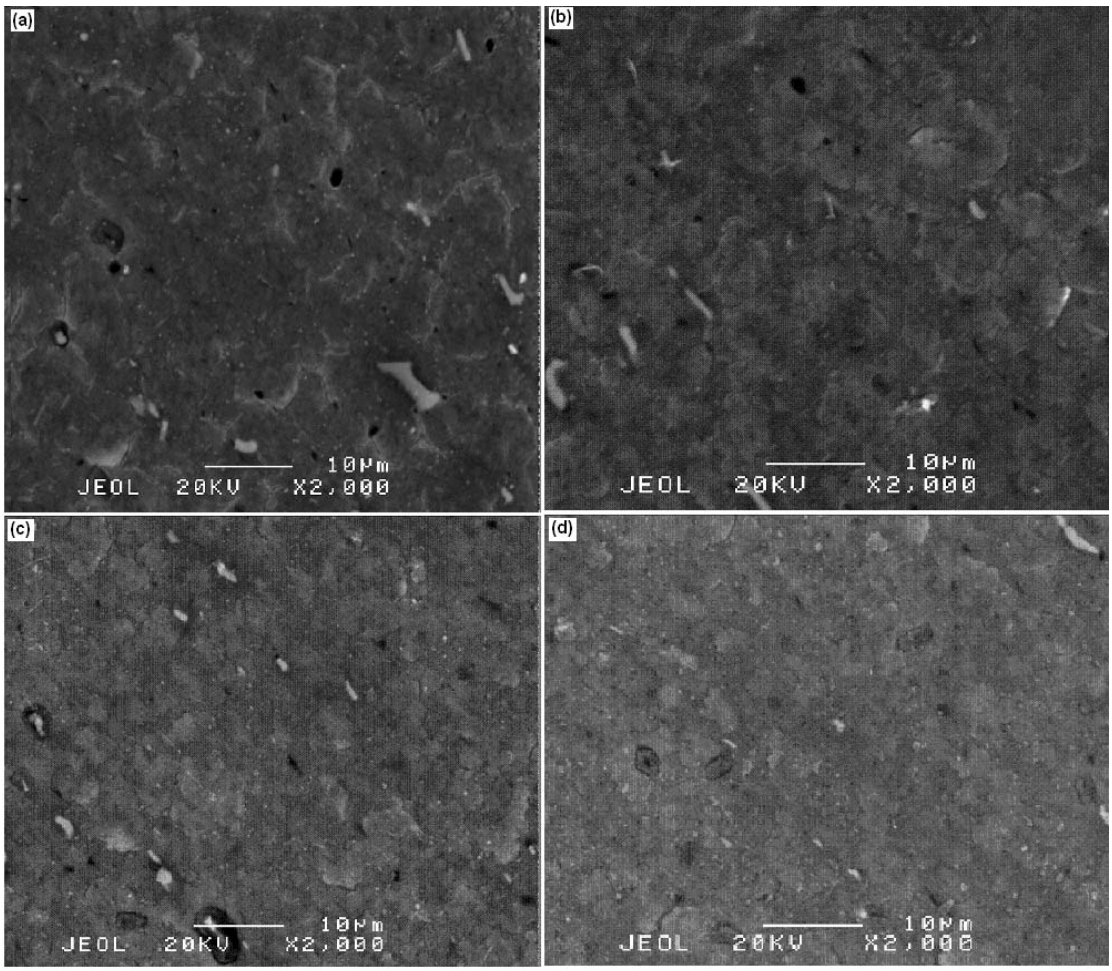

Figure 4.11: SEM Photographs of (a) as-received (b) 2-passes DCAPed (c) 4-passes DCAPed (d) 2-passes DCAPed with Route C

It can be seen by Figure 4.11 that there exists intermetallic particles in the microstructure of the 6061 alloy which differentiates with matrix phase by white and rod like appearance with 1-7 μm size. Results of the EDS/SEM analysis taken from these white regions are given in Figure 4.12 and the concentrations of the elements inside these regions are given in Table 4.2. It is concluded that the intermetallic regions mainly consist of Fe and Si based secondary particles such as Al-Fe, Al-Fe-Si, Al-Fe-Mn-Si intermetallic phases. These particles are probably the precipitates formed during casting operation of the alloy. It was not observed any evolution in the shapes of these intermetallic particles during DCAP process by the SEM images of the samples. However, it can be seen by Figure 4.11 (c) that the intermetallic regions of the 4-passes DCAPed sample is directed to the same direction which is along the shearing direction.

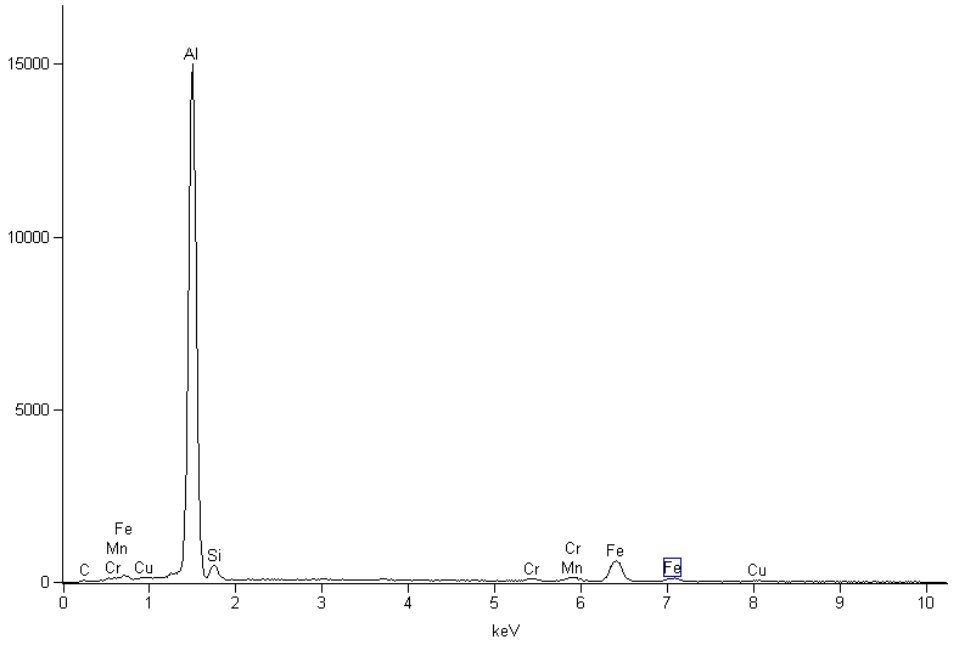

Figure 4.12: EDS/SEM analysis of the intermetallic white regions

Table 4-2: Elemental compositions of the intermetallic white regions obtained by EDS/SEM analysis

Element	*Weight Conc %*	*Atom Conc %*
Al	77.27	85.26
Si	5.06	5.37
Cr	0.95	0.54
Mn	1.82	0.98
Fe	13.51	7.20
Cu	1.39	0.65

4.5.3 TEM

It was tried to investigate grain and subgrain size evolution by TEM analysis. Figure 4.13 shows the TEM image of the as-received 6061 Al alloy. Dark regions in the photograph are the precipitates which were also seen in the SEM images. A clear image of the grain structure could not be obtained but it is seen in the figure that grains larger than 2 μm exist surrounded by darker lines indicating the grain boundaries which is also consistent with the results obtained by SEM analysis. It can be concluded by the images that the dislocation density of the as-received samples was very low due to annealing operation at 415°C for 3 hours.

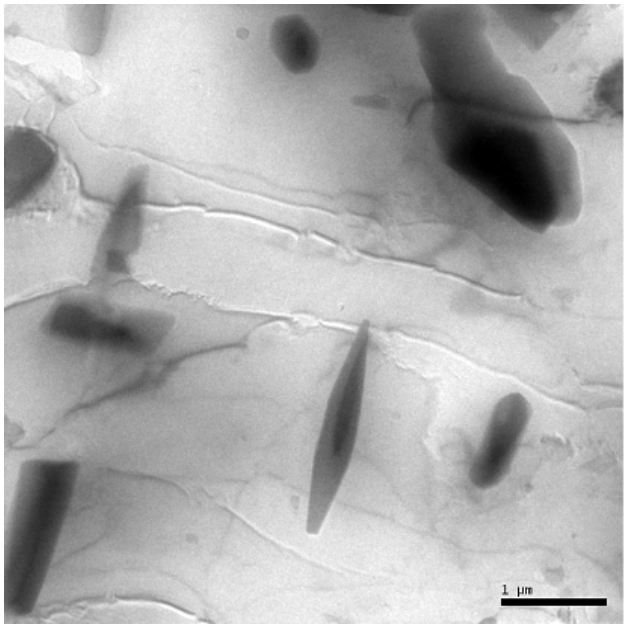

Figure 4.13: TEM image of the as-received 6061 Al alloy

Figure 4.14 presents the TEM photograph of the 2-passes DCAPed samples which were as-deformed (a), DCAPed and further annealed at 200°C (b), DCAPed and further annealed at 350°C (c). It was detected that the dislocation density of the DCAPed 6061 alloy is very high and it is decreased a little with further annealing operation at 200°C. However, in order to take clear TEM images of the grains, it was appeared that higher annealing temperatures were needed. Consequently, remaining TEM investigations were taken from the samples which had been annealed at 350°C after DCAP process. It is important to note that grain growth is expected in the annealed samples at 350°C but comparison of the grain structure and grain sizes can be made between DCAP passes by investigation of the samples subjected to same annealing operation.

It was also observed in the TEM images of the 2-passes DCAPed alloy in as-deformed condition that the dislocation bands which is considered to be due to the deformation shearing. These dislocation bands were observed only in the 2-passes DCAPed alloy which hadn't been annealed. Annealed samples show more homogeneous distribution of dislocations due to the annihilation process. It was also

observed that effect of annealing is not only on the dislocation density and grain size but also on the grain boundary structure. Samples annealed at 200°C and 350°C have more regular and thin boundaries as shown in Figure 4.14 (b-c).

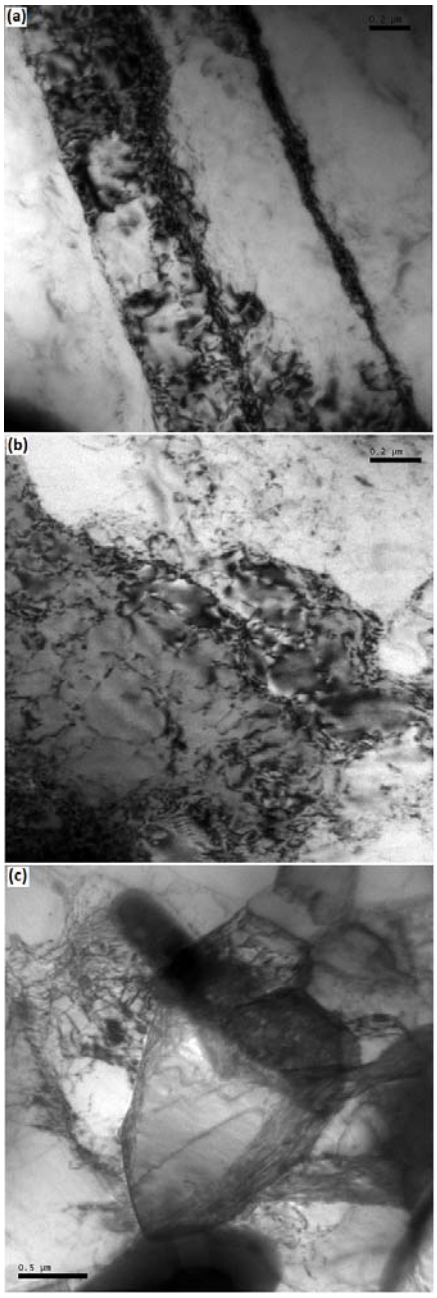

Figure 4.14: TEM images of the 2-passes DCAPed samples; (a) as-deformed (dislocation band structure), (b) further annealed at 200°C, (c) further annealed at 350°C

DCAPed and post annealed samples at 350°C shows different grain and cell structures. Grain size distribution was observed to be non-uniform by the TEM photographs of the deformed samples. Different types of grain structures of the deformed samples are shown in Figure 4.15 that some of the grains are free from dislocations, some of them have high dislocation density and some grains consist of smaller subgrains as Liu et al. [7] emphasized in their study about the deformation structures in FCC materials.

It was observed in the TEM images of the single passed DCAPed (ε=~0.6) sample that cell structures of different sizes ranging from ~50 nm to ~300 nm inside larger grains were observed in the sample after 1 DCAP pass as shown in Figure 4.15 (a) and grain sizes in the range of 300 nm to 1 μm was obtained as shown in Figure 4.15 (b-c). Equiaxed grains in the range of ~100 nm or even smaller was also detected as shown by black arrows which can be classified as Ultra Fine Grain (UFG) structure. 2-passes DCAPed (ε=~1.2) sample was observed to have similar grain sizes with 1 pass DCAPed sample as shown in Figure 4.15(d-e). Black arrows in the figures points the equiaxed ultra fine grains observed with similar sizes with 1 pass DCAPed alloy but with a higher fraction. It was also observed that higher fraction of subgrains or dislocation cells exist in grain interiors with similar sizes in the range of ~50 nm to ~300 nm.

Inherently, these grain/cell sizes might be increased by the effect of annealing at 350°C. It is shown in Figure 4.14(b) that the near initial grain sizes of the 2-passes DCAPed alloy with further annealing treatment at 200°C without any considerable grain growth effect although the image is not so clear due to high dislocation density. Dislocations were frequently observed to be accumulated near the grain boundaries as complex tangles and forests. It is seen that many ultra fine grains with an approximate size of 50 nm exist in the 2-passes DCAPed alloy. These results are consistent with the subgrain sizes obtained by XRD analysis which was mentioned in Part 4.4.

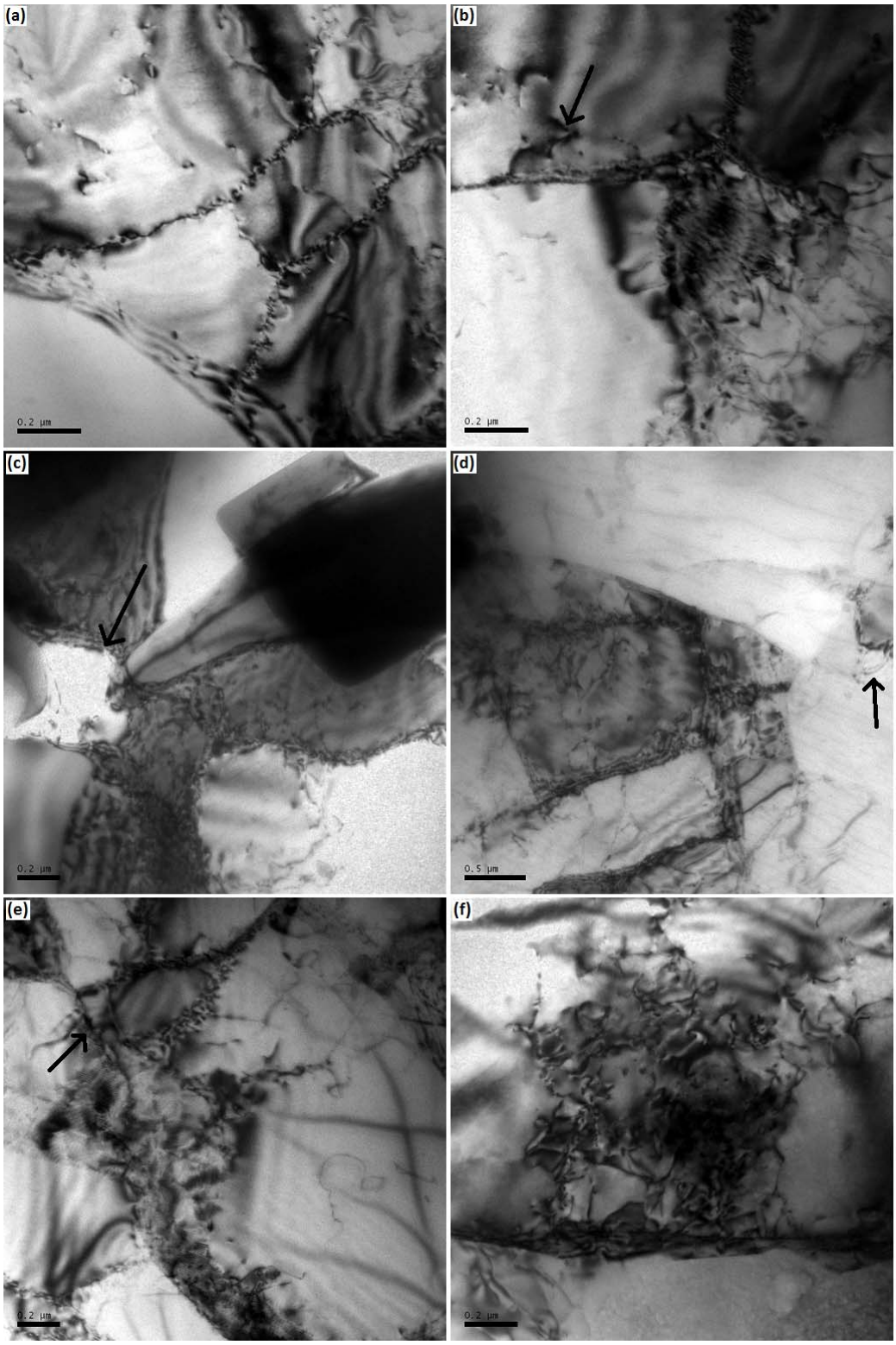

Figure 4.15: TEM images of the single pass DCAPed (a-b-c), 2-passes DCAPed (d-e) and 5-passes DCAPed (f) 6061 Al alloy further annealed at 350°C

Finally, effect of maximum strain by DCAP process to grain structure was desired to be investigated by TEM analysis of 5-passes DCAPed 6061 Al alloy but clear grain images could not be observed. Grain structure could be hardly detected in some photos as shown in Figure 4.15 (f). The reason of this difficulty is thought to be caused by the formation of complex dislocation loops and tangles. Also refining and sharpening of the boundaries made them hard to observe. Figure 4.16 illustrates a distinct and sharp boundary formed after 5 DCAP passes with an equivalent strain level of ~3.

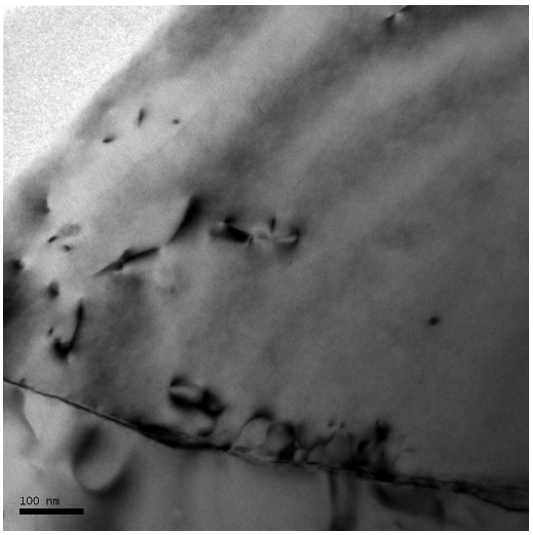

Figure 4.16: TEM images of the 5-passes DCAPed 6061 Al alloy further annealed at 350°C

Selected Area Diffraction (SAD) patterns of the as-received and 1 pass DCAPed alloy was obtained for determining the orientation differences between grains and subgrains with a ~50-100 μm selected area aperture. However, no orientation difference between the patterns was observed as obvious from the Figure 4.17. Consequently, there is no any satisfactory proof to be able to say that subgrains formed during DCAP process have high angle boundaries due to the lack of diffraction patterns of samples with higher DCAP passes. However, investigation of boundary types would give an idea about the misorientations in this manner.

Boundary types of the samples with different DCAP pass numbers and strain levels were observed to show different characteristics. It is mentioned in earlier chapters that a structural evolution sequence of dislocation cells→ PDWs → PTBs→ Ultra-fine grains is regarded by Chang et al. [30] where PDWs are Polygonized Dislocation Walls and PTBs are Partially Transformed Boundaries. There are supporting indications of this structural evolution in the TEM photographs of this study as shown in Figure 4.18. Grains of the 1 pass DCAPed alloy shows a boundary structure of dominantly having PDW structure as described in the literature. However, examples of a PTB structure was also detected for some grains as shown in Figure 4.18 (b) where the thickness fringes could be seen on these boundaries. Regular shaped and thinner grain boundaries (GB) and higher fraction of PTBs besides the PDW structure were observed in 2-passes DCAPed alloy as illustrated in Figure 4.18 (c) and (d). As mentioned before, 5-passes DCAPed alloy shows a boundary structure of having sharp grain boundaries as shown in Figure 4.16. It was mentioned in previous chapters that Chang et al. [30] suggested that the misorientation of PDWs is less than 1^0, PTBs is in the range of about 1-5^0 and GBs is larger than 10^0. This remark leads the result that high angles of misorientations could have been achieved by the background information of observing regular shaped grain boundaries at high strains.

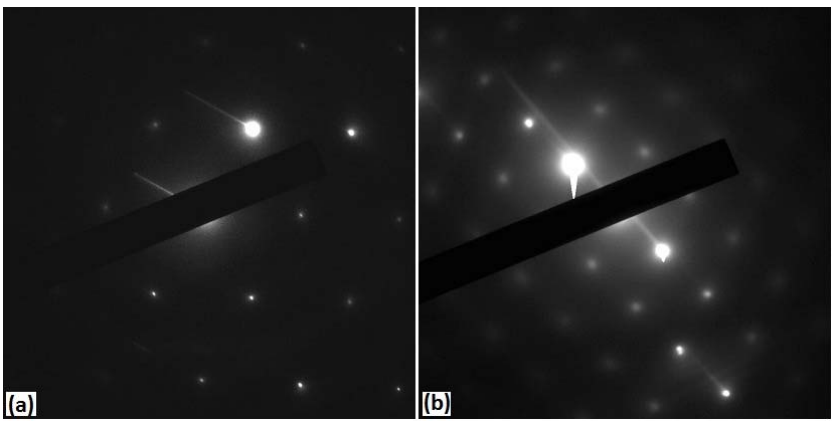

Figure 4.17: Selected Area Diffraction (SAD) pattern of the as-received (a) and single pass DCAPed 6061 Al alloy further annealed at 350°C

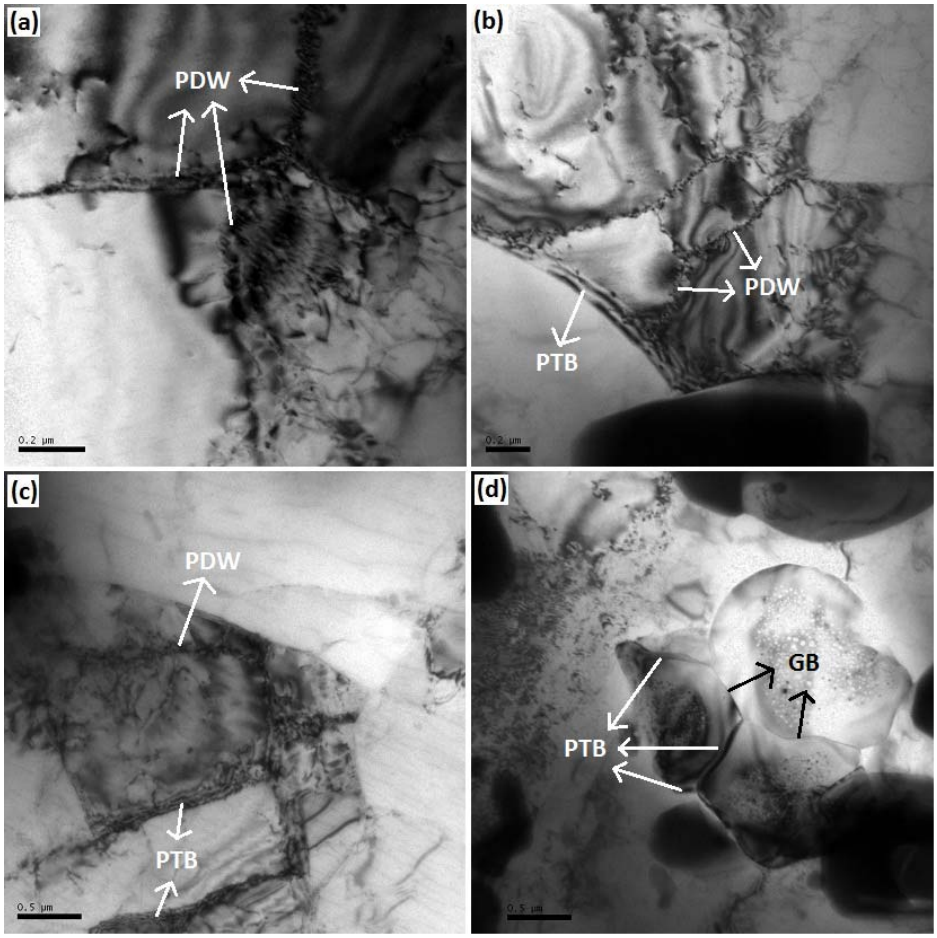

Figure 4.18: Different boundary types observed in 1 pass DCAPed (a and b) and 2-passes DCAPed (c and d) alloy

Finally, these results shows that ultra fine grained structure having boundaries with high angles of misorientations can be obtained at strain values higher than 1.2 (equivalent 2 DCAP Pass) in 6061 Al alloy by DCAP method undertaken in this study. The results are also consistent with literature data obtained by many studies [14,21,26,30,31,32].

It was stated in SEM analysis part of this thesis that intermetallic ceramic particles had been observed in the SEM images which differentiates with matrix phase by white colour and rod like appearance with 1-7 μm size. Similar observations of rod like precipitates along a definite direction were made by TEM analysis of the DCAPed alloy as shown in Figure 4.19. In addition, some spherical or hexagonal

particles were observed in the images with smaller sizes than observed by SEM analysis. Size of these precipitates lies between ~0,3 µm to ~2 µm. These fine precipitates constitutes similarities with the results obtained by the study of Lee et al. [47] about severe plastic deformation of 6061 Al alloy.

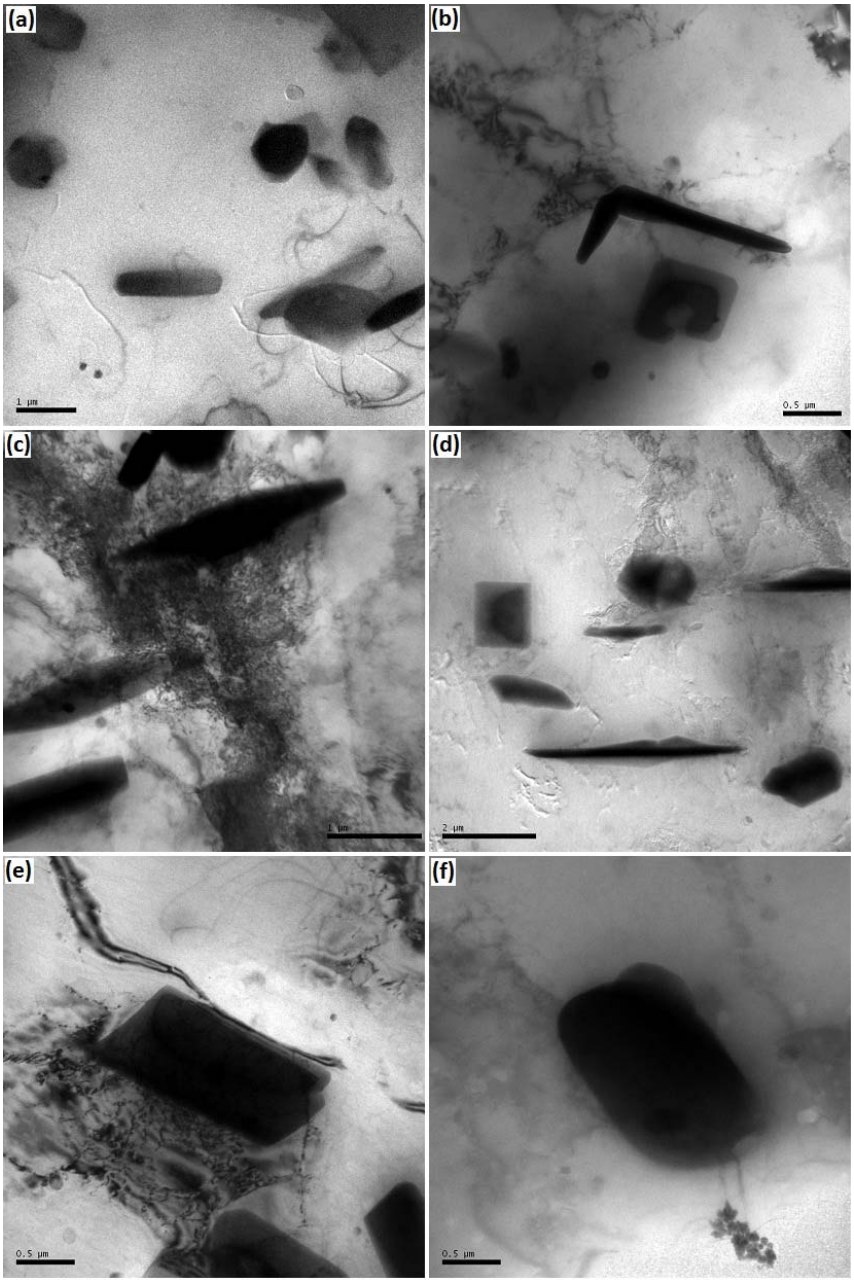

Figure 4.19: Precipitates observed in the as-received sample (a), 1 pass DCAPed sample (b), 2-passes DCAPed sample (c, d and e) and 5-passes DCAPed sample (f)

4.6 Electrical Resistivity

Electrical resistivity of the as-received and 2, 3 and 4-passes DCAPed samples are shown in Figure 4.20. There seems an increase in the resistivity of samples after deformation process up to 3 passes and a decrease after the 4th DCAP pass. This result can be related with the changes in the dislocation densities of the 6061 Al alloy with DCAP passes consistent with the literature studies [46] which reveal the resistivity of the aluminum alloys increases with conventional cold working methods. However, it would not be wrong to say that there is no any considerable effect of DCAP deformation to the electrical conductivity of the 6061 Al alloy when the error percentages of the resistivity values are considered as seen in Figure 4.20.

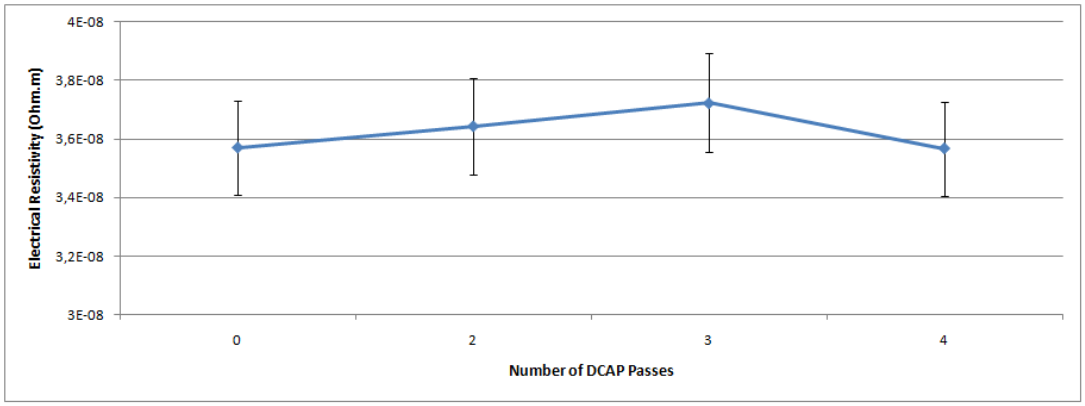

Figure 4.20: Change in the electrical resistivity of the as-received and DCAPed samples

4.7 General Discussion

Mechanical tests conducted by this study shows that the mechanical properties of the samples can be developed by the DCAP process. This development in the mechanical properties up to 2 passes of DCAP can be related with other findings like XRD data indicating an increase in the broadening and a decrease in the intensity of the peaks after DCAP process and electrical resistivity data indicating a slight increase in the resistivity values. All these findings lead the result that the grain

structure was refined and the dislocation density was increased up to 2 passes of DCAP which was confirmed by the microstructural analysis results obtained by SEM and TEM analysis. Different behaviors in the mechanical properties like hardness and strength, fluctuations in the broadening and intensity values of the peaks obtained by XRD analysis and the decrease in the resistivity values were observed after the critical strain value of 1.2 which corresponds to 2 passes DCAP. Those were caused by the changes in the dislocation density of the samples besides the continuing UFG production.

The obtained grain sizes and strength values were verified by Hall-Petch relationship which was given by the Equation 2.16. The linear relation of σ vs. $d^{-1/2}$ was constructed using the reference data of fully annealed 6061 Al alloy from the literature [26] with a grain size of 80μm and a yield strength of ~50MPa and the data of the DCAP passed sample obtained by this study with a grain size of 5.2 μm (by SEM analysis) and a yield strength of 114 MPa. By fitting the values, the Hall-Petch constants for 6061 Al alloy were obtained and the following Hall-Petch relation was obtained:

$$\sigma_0 = 28+195/d^{-1/2} \qquad (4.1)$$

Grains with different sizes in the range of 300nm to 1μm were observed by the TEM images of the single pass DCAPed samples. Because larger fraction of the grains have a size close to 1μm, average grain size of the single pass DCAPed sample used in calculations of Hall-Petch relation was assumed to be 0.8μm. 2-passes DCAPed samples were observed to have similar grain size range with higher fraction of smaller grains. So the average grain size was assumed to be 0.5μm for 2-passes DCAPed sample. When the above Hall-Petch equation was applied with these average grain sizes, it was observed that grain size and strength values did not fit with the Hall-Petch relation of σ vs. $d^{-1/2}$ as shown in Figure 4.21. The reason of this mismatch with the theoretical relationship was thought to be caused by the loss of the validity of the Hall-Petch relationship at small ranges of grain sizes and due to existence of the second phase particles which affects the strength of the material differently than the Hall-Patch relationship.

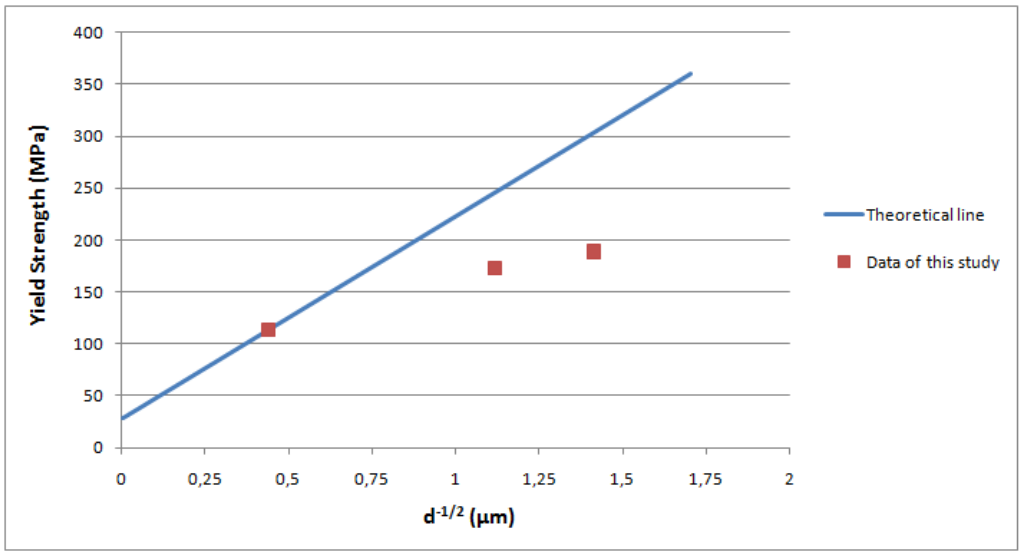

Figure 4.21: The Hall-Petch relation of σ vs. d-1/2 for the 6061 Al alloy which shows the correlation between the theoretical behavior and the data obtained by this study.

CHAPTER V

CONCLUSION

6061 Al Alloy strips were severely deformed by Dissimilar Channel Angular Pressing (DCAP) method with a 120° die angle at room temperature up to 5 passes which corresponds to an equivalent strain of ~3. Changes in the mechanical properties such as strength and hardness were observed, and the evolution of the microstructure was examined by XRD, SEM and TEM analysis.

It was observed that the mechanical properties were enhanced in terms of hardness, microhardness, UTS and yield strength due to the formation of the Ultra Fine Grain (UFG) structure and increase in the dislocation density. Hardness and the microhardness of the samples were observed to increase by ~41% and ~23% respectively within the first two DCAP passes and did not show an increase and even slightly decreased after second DCAP passes up to 5 DCAP passes. Yield strength showed a similar trend of increase by ~65% in the first two passes. Despite this huge increase in the yield strength, UTS showed much lower increase with a ~7% as an indication of little change in the work hardening behavior. Finally, it was observed that the mechanical properties of the samples showed the highest increase in the first DCAP pass and reached the highest values in the second DCAP pass where the critical strain value was considered to be obtained.

Macrohardness and microhardness measurements from the upper and lower strip surfaces shows that the hardness of the lower surfaces were a bit higher than the upper strip surfaces up to fourth DCAP pass caused by the higher strain accumulation in the lower surface due to the die geometry. However, this increase was considered to be negligible. It was also investigated that there was no any

significant difference between the microhardness values of the upper and lower strip surfaces of the 2 passed alloy with two different DCAP routes; route A and route C. These results lead the conclusion that the passing route of DCAP process has no considerable effect on the mechanical properties of the samples.

Effect of post annealing to mechanical properties was investigated by hardness tests. Annealing at 200°C for 1 hour did not make any difference in the hardness values of any samples but the hardness of the samples shows a decrease with annealing at 350°C for 1 hour by ~15% for single pass DCAPed alloy and ~20% for 2 and 5-passes DCAPed alloy. This difference in the softening ratios shows that the material having the UFG structure have sometimes worse thermal stability than coarse grained materials.

XRD patterns of the samples demonstrate decreasing intensities and increasing broadenings in some peaks caused by the increase in the dislocation density and UFG evolution. But, the intensity of the (111) peak showed different characteristics due to the texture formation as an indication of the crystallographic restructuring of {111} planes. Subgrain size of the deformed samples was also obtained by the XRD analysis as 42 nm.

SEM images of the samples illustrates the decrease in the grain size of the as-received sample up to 4 DCAP passes from ~5.2 μm to ~2.9 μm although the grain structure could not be distinguished clearly. It was also observed by the SEM photographs that there were intermetallic secondary particles with a rod like appearance and 1 - 7 μm size mainly consisting of Fe and Si based phases. These particles were also observed during the TEM analysis of the samples with additional data of existing smaller precipitates with sizes between ~0.3 μm to ~2 μm.

Different types of grain structures were detected by the TEM images of the deformed samples with further annealing at 350°C that some of the grains are free from dislocations, some of them have high dislocation density and some grains consist of smaller subgrains. Grain sizes in the range of 300 nm to 1 μm and even some equiaxed shape and ~100 nm sized Ultra Fine Grains were obtained in the single pass

DCAPed alloy. 2-passes DCAPed alloy represented similar grain sizes but with a higher fraction. Also cell structures inside larger grains were observed with sizes ranging from ~50 nm to ~300 nm for both single and twice-passes DCAPed alloy. 2-passes DCAPed samples were also investigated by TEM with further annealing operation at 200°C without any grain growth effect although the image was not so clear due to high dislocation density and ultra fine grains with an approximate size of 50 nm was observed to exist.

The structural evolution sequence of dislocation cells→ PDWs → PTBs→ Ultra-fine grains was detected by the changes in the grain structures of the samples through the increasing DCAP passes. These findings lead the result that misorientation angles of the subgrains might be increased with increasing DCAP passes.

Finally, electrical resistivity tests showed that there is no any considerable effect of DCAP deformation to the electrical conductivity of the 6061 Al alloy.

For further studies, these topics are recommended to be studied;

- Current DCAP system can be modified and improved that allows much higher DCAP passes enabling microstructural observations and investigation of the changes in the mechanical properties at very high strains.

- Effect of hot deformation to mechanical and microstructural properties of the metals can be investigated by adding a furnace ability near the DCAP system.

- Different aluminum alloy series can be studied to observe the effect of DCAP with different alloys and also for easier microstructural investigations.

- Different mechanical tests can be applied to DCAPed specimens to observe the effect of DCAP deformation to different mechanical properties like fatigue, fracture toughness etc.

- Effect of DCAP process to the planar anisotropy and textural evolution of the metals can be studied in detail.

- An extensive Finite Element Modelling (FEM) study can be undertaken in order to get detailed information about the material flow properties, deformation modes, texture evolution and process parameters.

REFERENCES

[1] Valiev R. Z., Langdon T.G., Progress in Materials Science, 2006, 881-981.

[2] Uzunçakmak G.E., Ms.C thesis, 2009, METU, Ankara.

[3] Viswanathan V., Laha T., Balani K. , Agarwal A., Seal S., Materials Science and Engineering, 2006, 121-285.

[4] Zhu Y.T., Lowe T.C., Langdon T.G., Scripta Materialia, 2004, 825-830.

[5] Valiev R.Z., Islamgaliev R.K., Alexandrov I.V., Progress in Materials Science 45, 2000, 103-189.

[6] Lowe T.C., Valiev R.Z. JOM Materials Researchs Center, 2004.

[7] Liu M., Roven H.J., Yu Y., Werenskiold J.C., Materials Science and Engineering A, 2007.

[8] Kozlov E.V., Zhdanov A.N., Koneva N.A., Physical Mesomechanics 11, 2008, 42-50.

[9] Utsunomiya H., Hatsuda K., Sakai T., Saito Y., Materials Science and Engineering A, 2004, 199-206.

[10] Fukuda Y., Oh-ishi K., Furukawa M., Horita Z., Langdon T.G., Acta Materialia 52, 2004, 1387–1395.

[11] Segal, Materials Science and Engineering A197, 1995, 157-164.

[12] Iwahashi Y., Wang J., HoritaZ., Nemoto M., Langdon T.G., Scripta Materialia Vol. 35, 1996, 143-146.

[13] Suo T., Li Y., Deng Q., Liu Y., Materials Science and Engineering A 466, 2007, 166–171.

[14] Lee J.C., Seok H.K., Suh J.Y., Acta Materialia 50, 2002, 4005–4019.

[15] Han J.H., Suh J.H., Jee K.K., Lee J.C., Materials Science and Engineering A 477, 2008, 107–120.

[16] Jining Q., Di Z., Guoding Z., Lee J.C., Materials Science and Engineering A 408, 2005, 79–84.

[17] Han J.H., Suh J.Y., Oh K.H., Lee J.C., Acta Materialia 52, 2004, 4907–4918.

[18] Suh J.Y., Han J.H., Oh K.H., Lee J.C., Scripta Materialia 49, 2003, 185–190.

[19] Xu S., Zhao G., Ren X., Guan Y., Materials Science and Engineering A 476, 2008, 281–289.

[20] Yamaguchi D., Horita Z., Nemoto M., Langdon T.G., Scripta Materialia, Vol. 41, 1999, 791-796.

[21] Kim W.J., Sa Y.K., Kim H.K., Yoon U.S., Materials Science and Engineering A, 2007.

[22] Wang Y.Y., Sun P.L., Kao P.W., Chang C.P., Scripta Materialia 50, 2004, 613–617.

[23] Zhilyaev A.P., Langdon T.G., Progress in Materials Science, Volume 53, 2008, 893-979.

[24] Iwahashi Y., Horita Z., Nemoto M., Langdon T.G., Metallurgical And Materials Transactions A, Volume 29A, 1998, 2503-2510.

[25] Baik S.C., Estrin Y., Kim H.S., Hellmig R.J., Materials Science and Engineering A351, 2003, 86-97.

[26] Tham Y.W., Fu M.W., Hng H. H., Pei Q.X., Lim K.B., Materials and Manufacturing Processes 22:7, 2007, 819-824.

[27] J.D. Verhoeven, Fundamentals of Physical Metallurgy, 328.

[28] Kuhlmann-Wilsdorf, Hansen N., Scripta Materialia 25, 1991, 1557 - 1562.

[29] Miyamoto H., Fushimi J., Mimaki T., Vinogradov A., Hashimoto S., Materials Science and Engineering A 405, 2005, 221–232.

[30] Chang C.P., Sun P.L., Kao P.W., Acta materials 48, 2000, 3377-3385.

[31] Kang H.G., Lee J.P., Huh M.Y., Engler O., Materials Science and Engineering A 486, 2008, 470–480.

[32] Lee J.C., Suh J.Y., Ahn J.P., Metallurgical And Materials Transactions A, Volume 34A, 2003, 625-632.

[33] Zhilyaev A.P., Swisher D.L., Oh-ishi K., Langdon T.G., McNelley T.R., Materials Science and Engineering A 429, 2006, 137–148.

[34] Humphreys F. J., Hatherly M., Recrystallization and Related Annealing Phenomena, 2004.

[35] Skrotzki W., Scheerbaum N., Oertel C.G., Brokmeier H.G., Suwas S., Toth L.S., Acta Materialia 55, 2007, 2211–2218.

[36] Özenbaş M., MNT 501 Nanoscience and Engineering Principles Course Notes, Mechanical Properties of Nanostructured Materials, 2009.

[37] Sedlacek R., Blum W., Kratochvil J., Forest S., Metallurgical And Materials Transactions A, Volume 33A, 2002, 319-327.

[38] Wei W., Wei K.X., Fan G.J., Acta Materialia 56, 2008, 4771–4779.

[39] Estrin Y., Toth L.S., Molinari A., Brechet Y., Acta mater. Vol. 46, 1998, 5509-5522.

[40] T.G. Langdon, Mechanism of Superplastic Flow, Superplasticity: 60 Years after Pearson.

[41] Komura S., Horita Z., Furukawa M., Nemoto M., Langdon T.G., Metallurgical And Materials Transactions A, Volume 32A, 2001, 707-716.

[42] J. Humphreys, Acta inater. Vol. 45, 1997, 4231-4240.

[43] Han J.H., Huh M.Y., Suh J.Y., Lee J.C., Materials Science and Engineering A 394, 2005, 60–65.

[44] Lee J.C., Seok H.K., Han J.H., Chung Y.H. Materials Research Bulletin 36, 2001, 997–1004.

[45] Han J.H., Oh K.H., Lee J.C., Materials Science and Engineering A 387–389, 2004, 240–243.

[46] C. Çetinarslan, Materials and Design 30, 2009, 671–673.

[47] Lee S.H., Saito Y., Sakai T., Utsunomiya H., Materials Science and Engineering A325, 2002, 228–235.

[48] Uzunçakmak G.E., Tan E., Gür C.H., 14th International Metallurgy & Materials Congress (IMMC 2009) Papers, 2009, p. 158.

[49] B.D. Cullity, Elements of X-Ray Diffraction, Addison-Wesley Publishing Company, 1956, 102

[50] ASM Metals HandBook Volume 10 - Materials Characterization, ASM internationa, 1986.

[51] Williamson G.K., Hall W.H., Acta Metallurgica Vol. 1, 1953, 22-31.

[52] Marinkovica B., Avilleza R.R., Saavedrab A., Assunçao F.C.R. Materials Research, Vol. 4, 2001, 71-76.